





# รายงานวิจัยฉบับสมบูรณ์

โครงการ การศึกษาเชิงทฤษฎีของการถ่ายโอนอิเล็กตรอนที่เหนี่ยวนำด้วยแสงในโปรตีน ฟลาวินโมโนนิวคลีโอไทด์ไบน์ดิงโปรตีน (เอฟบีพี) จากข้อมูลการจำลองพลวัติเชิงโมเลกุล (Theoretical investigation of Photo-induced Electron transfer in Flavin Mononucleotide Binding Proteins (FBP) From Molecular Dynamics Simulation Data)

โดย ณัฏฐาเนตร นันทบุตร และคณะ

# รายงานวิจัยฉบับสมบูรณ์

โครงการ การศึกษาเชิงทฤษฎีของการถ่ายโอนอิเล็กตรอนที่เหนี่ยวนำด้วยแสงในโปรตีน ฟลาวินโมโนนิวคลีโอไทด์ไบน์ดิงโปรตีน (เอฟบีพี) จากข้อมูลการจำลองพลวัติเชิงโมเลกุล (Theoretical investigation of Photo-induced Electron transfer in Flavin Mononucleotide Binding Proteins (FBP) From Molecular Dynamics Simulation Data)

> นางณัฏฐาเนตร นันทบุตร ภาควิชาเคมี คณะวิทยาศาสตร์ มหาวิทยาลัยมหาสารคาม

สหับสนุนโดยสำนักงานคณะกรรมการการอุดมศึกษา สำนักงานกองทุนสหับสนุนการวิจัย และมหาวิทยาลัยมหาสารคาม

(ความเห็นในรายงานนี้เป็นของผู้วิจัย สกอ. และ สกว. ไม่จำเป็นต้องเห็นด้วยเสมอไป)

# **CONTENTS**

	Page
Abstract in Thai	1
Abstract in English.	2
1. Introduction.	3
2. Objectives	5
3. Scopes of work	6
4. Literature review	7
5. Computational methods	14
6. Results and Discussion	22
7. Conclusion.	82
8. Suggestion for future work	82
9. References.	83
10. Appendices	92

## บทคัดย่อ

รหัสโครงการ: MRG๕๓๘๐๒๕๕

ชื่อโครงการ: การศึกษาเชิงทฤษฎีของการถ่ายโอนอิเล็กตรอนที่เหนี่ยวนำด้วยแสงในโปรตีน ฟลาวินโมโนนิวคลีโอไทด์ใบน์ดิงโปรตีน (เอฟบีพี) จากข้อมูลการจำลองพลวัติเชิงโมเลกุล

ชื่อนักวิจัย และสถาบัน : ณัฏฐาเนตร นันทบุตร ภาควิชาเคมี คณะวิทยาศาสตร์ มหาวิทยาลัยมหาสารคาม

อีเมล์: nadtanet@gmail.com, nadtanet.n@msu.ac.th

ระยะเวลาโครงการ: 2 ปี

# บทคัดย่อ:

การถ่ายโอนอิเล็กตรอนเป็นกระบวนการพื้นฐานที่สำคัญสามารถนำไปประยุกต์ใช้ไม่ว่าจะเป็นทาง ้ เคมี พิสิกส์ หรือชีววิทยา มีกระบวนการต่างๆมากมายในทางชีววิทยาและเคมีซึ่งเกี่ยวข้องการการถ่ายโอน อิเล็กตรอน เช่น การสังเคราะห์แสง การหายใจ หรือแม้กระทั่งการประยุกต์ใช้ในด้านไบโออิเล็กทรอนิกส์ ไบโอเซนเซอร์ ดังนั้นการศึกษาการถ่ายโอนอิเล็กตรอนในแบบจำลองจึงจำเป็นต่อความเข้าใจในกลไกการ ถ่ายโอนอิเล็กตรอน ฟลาวินโมโนนิวคลีโอไทด์ใบน์ดิงโปรตีน (โปรตีนเอฟบีพี) ประกอบด้วยโมเลกุลของฟ ลาวินโมโนนิวคลีโอไทด์ (เอฟเอ็มเอ็น) ซึ่งทำหน้าที่เป็นโคแฟคเตอร์ โดยกรดอะมิโนที่ล้อมรอบหมู่ไอโซแอล ลอกซาซีนของโมเลกุลเอฟเอ็มเอ็น ได้แก่ Trp32 Tyr35 และ Trp106 เมื่อโคแฟกเตอร์ดังกล่าวยึดจับกับ โปรตีนจะระงับการส่งสัญญาณฟลูออเรสเซนส์ การระงับนี้อาจมาจากการใช้แสงเหนี่ยวนำให้เกิดการถ่าย โอนของอิเล็กตรอนจากกรดอะมิโนดังกล่าวไปยัง หมู่ไอโซแอลลอกซาซีน ที่อยู่ในสภาวะเร้า (Iso\*) ใน ์ โครงการวิจัยนี้ได้ศึกษาผลของการเกิดโครงสร้างแบบไดเมอร์และการกลายพันธ์ในตำแหน่ง E13K E13R E13T และ E13Q ของโปรตีนเอฟบีพี ที่ได้จาก DesulfoVibrio Vulgaris (Miyazaki F) ซึ่งปัจจัยดังกล่าวมีผล ์ ต่อกระบวนการถ่ายโอนอิเล็กตรอนโดยใช้แสงเหนี่ยวนำจากกรดอะมิโน Trp32 และ Trp106 ไปยัง Iso\* ทั้งนี้ได้ประยุกต์ใช้ทฤษฎีการถ่ายโอนอิเล็กตรอนที่คิดคันโดย Kakitani และ Mataka หรือทฤษฎี KM ใน การศึกษาการถ่ายโอนอิเล็กตรอนและการสลายตัวอย่างรวดเร็วของฟลูออเรสเซนส์ในโปรตีนเอฟบีพี ้ ดังกล่าวเพื่อให้ได้ค่าไค-สแควร์ของความแตกต่างระหว่างค่าที่ได้จากการคำนวณและค่าการทดลองมีค่าน้อย ที่สุด อัตราการถ่ายโอนอิเล็กตรอนสามารถคำนวณได้โดยใช้โครงสร้างของโปรตีนที่ได้จากการจำลองพลวัติ เชิงโมเลกุลร่วมกับทฤษฎีการถ่ายโอนอิเล็กตรอนและค่าตัวแปรต่างๆ ที่ได้จากการทดลองทางด้านฟลูออเรส เซนส์

คำหลัก : การถ่ายโอนอิเล็กตรอนโดยใช้แสงเหนี่ยวนำ ฟลาวินโมโนนิวคลีโอไทด์ เอฟบีพี ทฤษฎี Kakitani และ Mataka การจำลองพลวัติเชิงโมเลกุล

#### **Abstract**

Project Code: MRG5380255

Project Title: Theoretical investigation of Photo-induced Electron transfer in Flavin Mononucleotide

Binding Proteins (FBP) From Molecular Dynamics Simulation Data

Investigator: Nadtanet Nunthaboot, Chemistry Department, Faculty of Science, Mahasarakham

University

E-mail Address: nadtanet@gmail.com, nadtanet.n@msu.ac.th

Project Period: 2 years

#### Abstract:

The electron transfer (ET) is of fundamental interest in the field of chemistry, biology and physics. Numerous essential processes in biology and chemistry are involving ET reactions such as photosynthesis, respiration and other important biological processes, including bioelectronics and biosensor. The study of ET in simple model has thus become a very useful to gain fundamental knowledge of ET mechanism. Flavin mononucleotide binding protein (FBP) contains flavin mononucleotide (FMN) as a cofactor. Aromatic amino acids as Trp32, Tyr35 and Trp106 exist near isoalloxazine ring (Iso) of FMN. Bright fluorescence of free FMN is remarkably quenched when it binds to the protein. The quenching is ascribed to photo-induced electron transfer (PET) from these amino acids to the excited Iso (Iso\*). In this project, the conformational changes of the single mutated FBPs (from Desulfovibrio vulgaris, strain Miyazaki F.) which are E13K, E13R, E13T, and E13Q upon the dimer formations were studied through the phenomena of PET from Trp32 and Trp106 to the Iso\*. The mechanism of ET was investigated by determining ET parameters contained in Kakitani and Mataga (KM) theory to obtain the minimum values of chi-square between the observed and calculated fluorescence decays of FBPs. The ET rates were obtained with atomic coordinates of the proteins determined by a method of molecular dynamics simulation (MDS) and an ET theory using our reported experimental fluorescence decays of these FBPs.

**Keywords :** Photoinduced electron transfer; flavin mononucleotide binding protein; FBP; Kakitani and Mataga theory; molecular dynamics simulation

#### 1. INTRODUCTION

#### 1.1 RATIONALE AND BACKGROUND

Electron transfer phenomena have been an important subjects in the fields of physics, chemistry and biology [1]. Photoinduced electron transfer (PET) plays an essential role in photosynthetic systems [2]. In the last decade a number of new flavin photoreceptors have been found. Among six families of the photoreceptors, phototropins [3], cryptochromes[4] and BLUF (blue-light sensing using flavin) contain flavins as the reaction center [5]. The PET from Tyr to the excited isoalloxazine (Iso\*) is considered as an initial step of the photo-regulation for photosynthesis in AppA.

Photo-induced electron transfer (ET) is basic and fundamental process in the field of photochemistry, energy conversion of light into electricity as solar energy, photo-synthesis and photo-receptors in plants and micro-organs. In these reaction systems the first step is always the ET reaction. Since Marcus [6] [7] [8] who has received Novel Prize in 1988, the mechanism of ET has been theoretically [9; 10; 11; 12] and experimentally [13; 14] investigated by several workers. The ET theories have been tried to verify with energy gap law, by changing solvent polarity and redox potential of the donor or acceptor. The distance-dependent ET rate, however, has never been investigated, since experimental systems are difficult in bulk solution.

In the last few decades, the mechanism of photoinduced electron transfer (PET) has been intensively studied in small molecules and proteins [15; 16; 17; 18]. However, the details of the mechanism have not been obtained, because any theoretical ET rates contain several unknown parameters, which cannot be determined by any experimental or theoretical methods.

Flavoproteins are ubiquitously distributed in various microorganisms [19] and pathogenic bacteria [20; 21] and in specific tissues of multicellular plants and animals, such as in milk, brain, kidney, liver and heart of mammals and in leafy vegetables. Flavoproteins play an essential role in many oxido-reduction reactions [21; 22] whilst in some systems flavins function as photoreceptors [23]. Their photochemistry and photophysics have been of considerable interest due to their important role in light-harvesting biological mechanisms. The one important characteristic that classifies flavoproteins is that they bind with one of the flavin molecules, flavin mononucleotide (FMN), flavin adenine dinucleotide (FAD) or riboflavin (RF, more commonly known as vitamin B2), as a cofactor [22]. In the case of FAD and FMN, they consisted of an isoalloxazine chromophore (Iso) connected to a ribityl adenine diphosphate or ribityl phosphate chain, respectively. Naturally, flavin has the three different redox states; that is the (i) oxidized form, (ii) a one electron reduced radical semiquinone, and (iii) a two-electron fully reduced hydroquinone [22]. Recently, because of this biochemical versatility, flavoproteins have become a popular model for both experimental studies, such as on the electron transfer process [24; 25; 26; 27], and also in theoretical works [28, 29] on their conformational dynamics.

Flavin mononucleotide binding protein (FBP) is a small flavoprotein (Mw 13 kDa with 122 amino acids) that contains a flavin mononucleotide as a cofactor [30]. The protein structure of the wild type FBP (WT) was initially determined by means of NMR spectroscopy in solution as a monomeric form [31] and X-ray diffraction method in crystal as a dimeric form [32]. It was believed that FBP is monomer in solution but forms a dimer in crystal. According to the NMR and X-ray structures, tryptophan 32 (Trp32) is closest to Iso and then tyrosine 35 (Tyr35) and Trp106 among the aromatic amino acids. Ultrafast fluorescence dynamics of WT FBP and E13T (Glu13 was replaced by Thr), E13Q (Glu13 replaced by Gln), W32Y (Trp32 replaced by Tyr), and W32A

(Trp32 replaced by Ala) FBP isoforms were measured by means of a fluorescence up-conversion method. These decays were simultaneously analyzed to obtain PET rate from individual donor and related physical quantities. In flavoproteins, the ET easily takes place from aromatic amino acids, such as tryptophan (Trp) and tyrosine (Tyr), to the excited state isoalloxazine (Iso\*), so flavoproteins are suitable for the investigation of the ET mechanism with their fluorescence dynamics [24; 27; 33; 34].

In the present work, the ET rates of four different single mutated FBPs (E13K, E13R, E13T, and E13Q) are investigated. Since it is recognized that the dynamic property of protein structure plays essential role on its function as enzyme reactions. Therefore, molecular dynamics simulations (MDSs) of the FBP are performed and the ET rates could be obtained with atomic coordinates of the simulated protein. Moreover, the electrostatic (ES) energy between the photoproducts and ionic groups inside the proteins that might play an important role on the ET rates in the flavoproteins is also elucidated.

#### 1.2 OBJECTIVES

- To study dynamical properties of the flavin mononucleotides binding protein (FBP) from
   *Desulfovibrio vulgaris* strain Miyazaki F.
- To calculate the ET rates of four different single mutated FBP dimers (E13K, E13R, E13T, E13Q).
- 3. To study the effects of dimer formation on the ET rates and related physical quantities in the mutated FBP dimers.
- 4. To study a physical quantity of ES energy of each residue (RES) in FBP dimer

## 1.3 SCOPES OF WORK

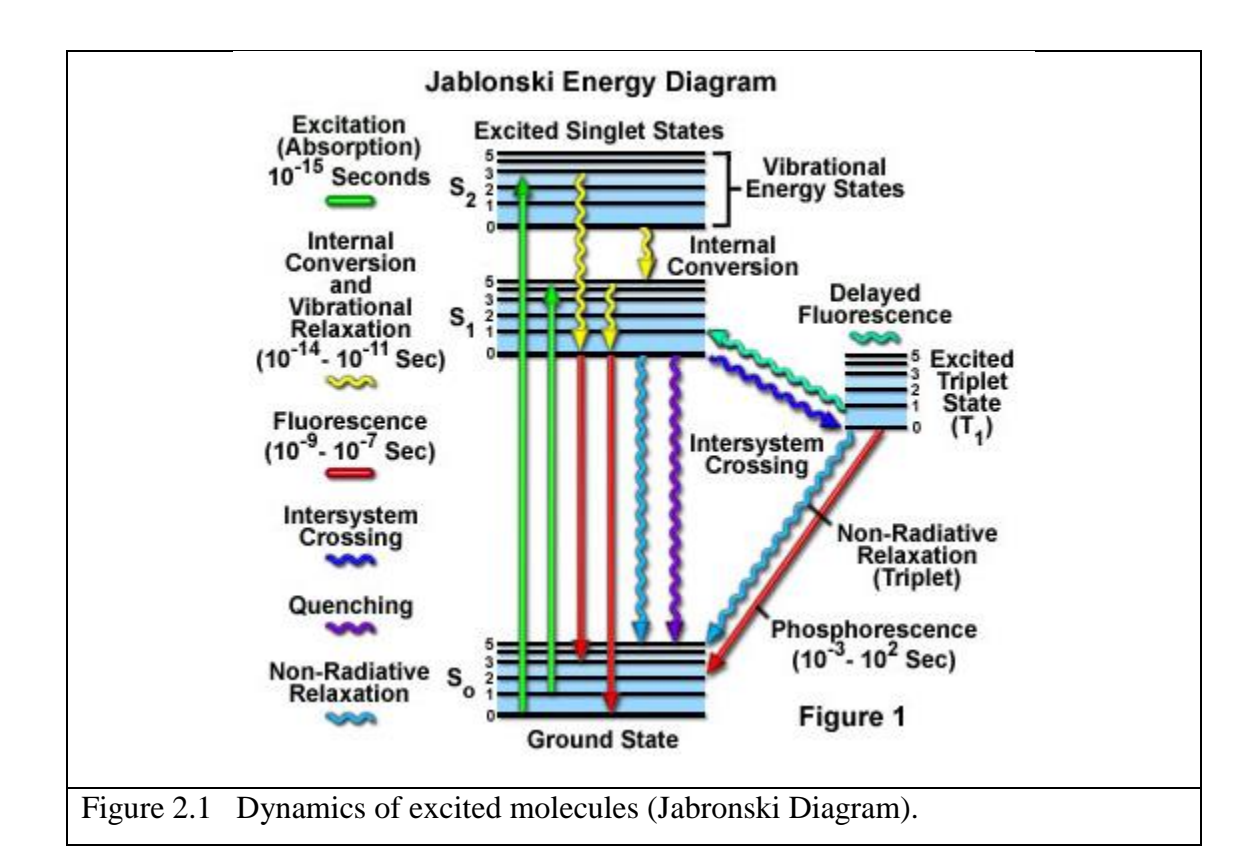
In this project, our developed method of analysis of ET mechanism in proteins is applied to FBPs as follows:

- 1) To perform MDSs of wild-type and four single mutated FBPs (E13K, E13R, E13T, E13Q)
- 2) Atomic coordinates of ET donors (Trp and/or Tyr) and acceptor (the excited Iso\*) are obtained by means of MDS, and then the donor-acceptor distances are to be determined.
- 3) ET rate is to be calculated with KM theory with a set of hypothetical ET parameters contained in KM theory, and the donor-acceptor distances.
- 4) Fluorescence decay of a protein is to be calculated taking average over MD time range.
- 5) These ET parameters are to be determined so as to obtain the minimum value of chi-square between the calculated and observed fluorescence decays.

#### 2. LITERATURE REVIEW

Molecules in the excited state generated by illumination with visible and ultraviolet light display various phenomena, which have been observed by fluorescence spectroscopy [35; 36]. Fluorescence is a light generated from various molecules in the excited state. Molecules in the excited state are much more interactive with other molecules than those in the ground state. The molecular interactions include large Stokes shift in polar solvents, proton transfer from the excited molecules with dissociable proton to a proton acceptor, Förster type resonance energy transfer (FRET), photoinduced charge transfer (CT) and electron transfer (ET).

The molecular interactions start at once in all excited molecules upon the pulsed excitation. The observation time domain depends on the pulsed width of light source and time-resolution of detector systems of fluorescence. Translational motions of molecules are in 1 - 10 ns (1 ns = 1 x  $10^{-9}$  s) time domain, rotational motions in 10 - 100 ps (1 ps = 1 x  $10^{-12}$  s) time domain, and vibrational motions in 10-100 fs (1 fs = 1 x  $10^{-15}$  s) time region. Electron in a molecule can move in  $10^{-15}$  s time domain. Fluorescence dynamics (time-dependent change in the fluorescence intensity, sometimes called fluorescence decay) closely relate with these molecular motions. If we excite molecules with very short pulsed laser (sub-picosecond pulse width), then we can see molecular dynamics in fs – ps time domain. Figure 2.1 shows dynamics of an isolated excited molecule.



Flavoproteins mainly function as electron transport, oxido-reduction reactions in cells, and sometimes photo-receptors in plant and bacteria. Flavoproteins contain flavin adenine dinucleotide (FAD), flavin mononucleotide (FMN), and riboflavin (FR) as reaction centers. These cofactors are called nutritionally as Vitamine  $B_2$ . Flavins contain isoalloxazine ring (Iso) as chromophore. Fluorescence from flavins was first observed by Weber in 1950 [37]. Green fluorescence of flavins is from Iso. Weber also found that fluorescence of flavins is quenched by various substances, including caffeine and aromatic amino acids. Later fluorescence quenching of flavin by tryptophan (Trp) and tyrosine (Tyr) were investigated by McCormick [38] under steady-state excitation and by Karen et al. [34] by means of transient absorption spectroscopy. Fluorescence intensity of a molecule is proportional to fluorescence quantum yield (QY) as Eq 2.1. Fluorescence lifetime is defined by Eq 2.2.

$$QY = \frac{k_f}{k_f + k_i + k_R} \tag{2.1}$$

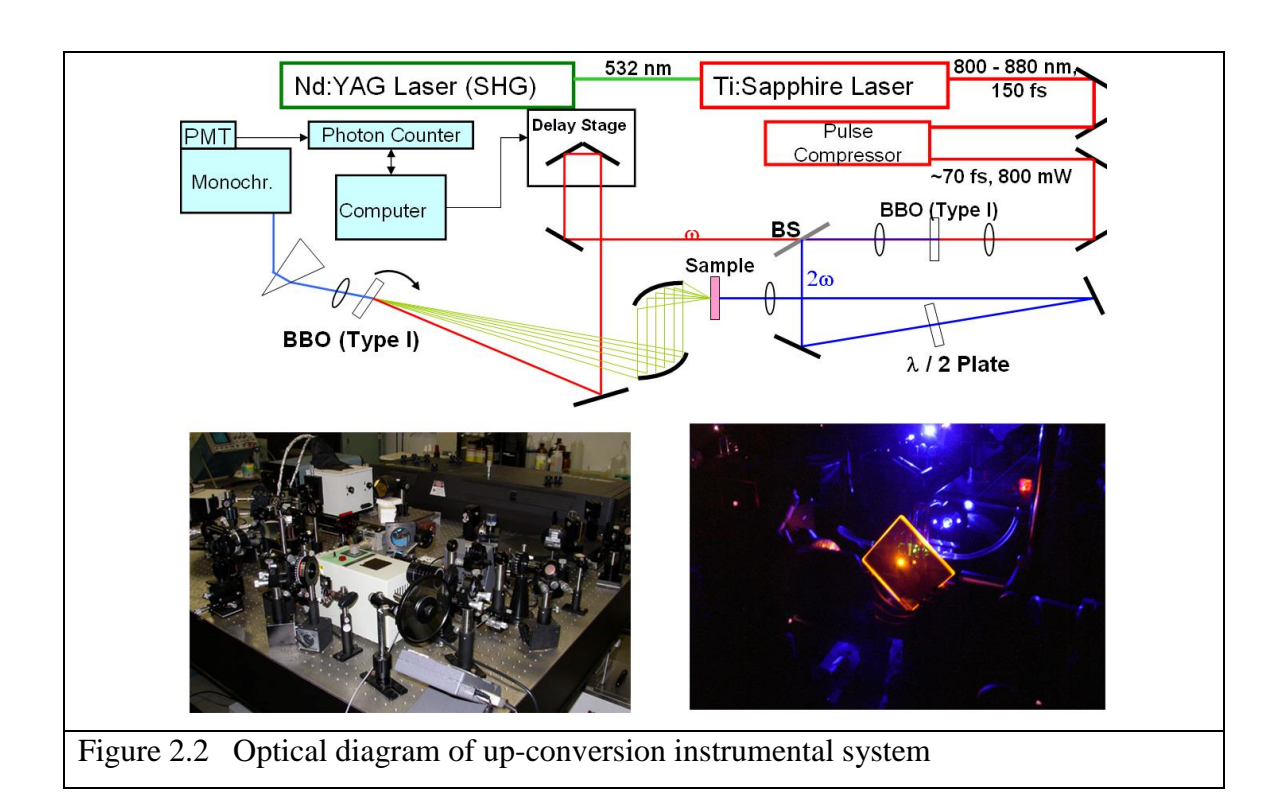
$$\tau = \frac{1}{k_f + k_i + k_R} \tag{2.2}$$

$$F(t) = \exp(-t/\tau) \tag{2.3}$$

$$F(t) = \sum_{i}^{n} \alpha_{i} \exp(-t/\tau_{i})$$
 (2.4)

 $k_f$ ,  $k_i$ , and  $k_R$  in Eqs 2.1 and 2.2 are radiative transition probability, internal conversion probability and reaction rate with other molecules in the ground state. When an excited molecule interacts with other molecules in the ground state rapidly, then  $k_R$  is greater, and QY becomes less (fluorescence is quenched and becomes weaker) and fluorescence lifetime shorter. In isolated molecules fluorescence intensity, F(t), upon pulsed excitation, decreases exponentially as Eq 2.3 with fluorescence lifetime,  $\tau$ . In more complex systems the intensity often decays non-exponentially as Eq 2.4. In Eq 2.4,  $\alpha_i$  and  $\tau_i$  are called to be pre-exponential factor and the lifetime of i-th fluorescence component, respectively. Fluorescence of Iso often markedly quenched when it binds to protein moiety [39; 40]. Namely, QY of flavin becomes markedly smaller and fluorescence lifetime remarkably shorter upon its binding to a protein. In protein systems fluorescence intensity normally decays non-exponentially. Origin of the non-exponential decay in protein systems has rarely been elucidated.

In many flavoproteins fluorescence lifetimes have been too short to measure by means of a picosecond-resolved fluorescence lifetime instruments. Ultrafast fluorescence dynamics of flavoproteins in the femtosecond time domain have been extensively worked with an upconversion technique by Mataga's group [24; 41; 42]. In these flavoproteins Trp and/or Tyr always exist near Iso. Figure 2.2 shows up-conversion instrumental system constructed by Mataga's group. It has been unclear why fluorescence lifetimes become very short when flavin is incorporated into protein moiety. Karen et al. suggested the remarkable quenching of flavin fluorescence to be due to ET from Trp and Tyr to the excited Iso (Iso\*), by means of picosecond-resolved transient absorption spectroscopy [43]. Recently, ET in glucose oxidase was verified by a femtosecond resolved transient absorption spectroscopy [25; 26].



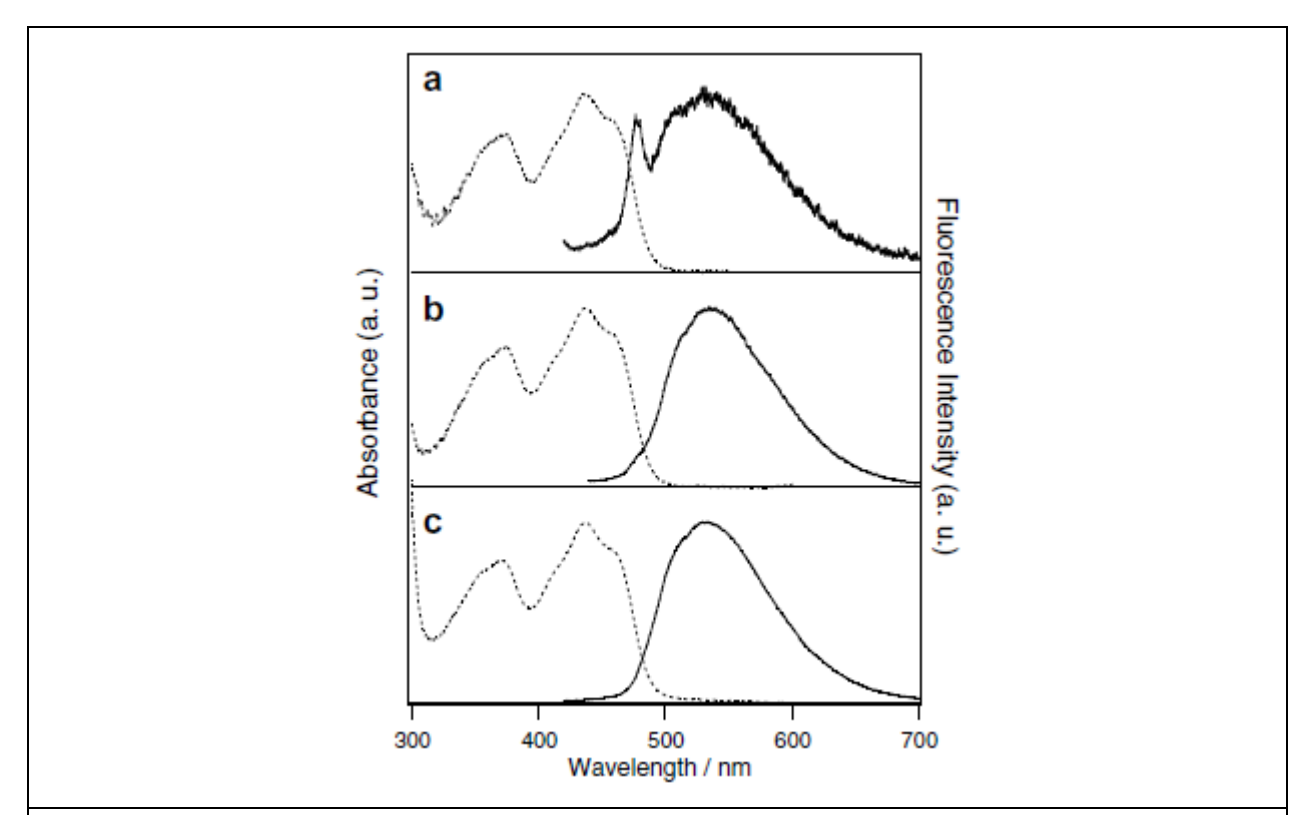


Figure 2.3 Normalized absorption and emission spectra of FBP and its mutants [27] (a) wild type FBP, (b) W32Y FBP, (c) W32A FBP. Emission spectra were measured upon excitation at 410 nm.

Figure 2.3 shows absorption and emission spectra of WT FBP, W32Y FBP (Trp32 is replaced by Tyr), and W32A FBP (Trp32 is replaced by Ala) [27; 44]. Both of absorption and emission spectra did not change much among the three FBPs. Fluorescence intensities and accordingly fluorescence lifetimes were, however, remarkably changed among them. Figure 2.4 shows fluorescence decays of FBPs. Very short lifetimes of FBPs compared to free FMN (lifetime is 4.7 ns) are ascribed to ET from Trp32, Tyr35 and Trp106 to Iso\*. Donor-acceptor distance-dependence of ET rate in flavoproteins has been analyzed with three kinds of ET theories stated above [28; 45].

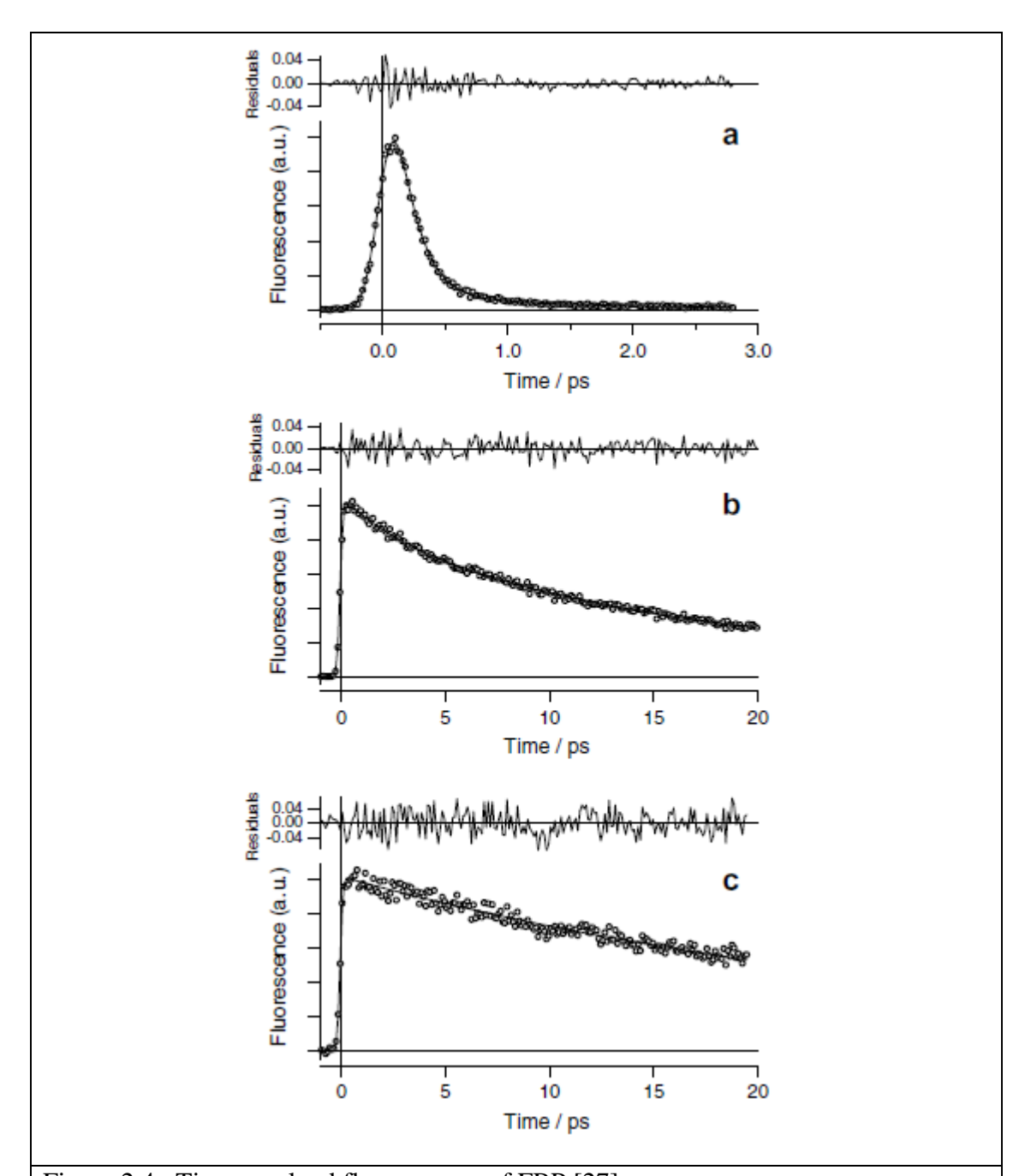


Figure 2.4 Time-resolved fluorescence of FBP [27]. Fluorescence decay curves were fitted using double- or single-exponential functions. (a) WT FBP;  $\tau_1 = 167$  fs ( $\alpha_1 = 0.96$ ) and  $\tau_2 = 1.5$  ps ( $\alpha_2 = 0.04$ ), (b) W32Y;  $\tau_1 = 3.4$  ps ( $\alpha_1 = 0.23$ ),  $\tau_2 = 18.2$  ps ( $\alpha_2 = 0.74$ ), and  $\tau_3 = 96$  ps ( $\alpha_3 = 0.03$ ), (c) W32A;  $\tau_1 = 0.03$ 

30.1 ps.

The studies of ET in flavoproteins, which is considered to be a model system for photoreceptors were reported [24; 41; 42]. The works demonstrated that averaged distance between
electron donor, tryptophan (Trp) or tyrosine (Tyr), and acceptor, isoalloxazine ring (Iso) of flavins,
is more important in ET of flavoproteins than edge to edge distance or inter-planar angles between
aromatic rings of the donor and acceptor[28]. Geometrical parameters in these flavoproteins were
obtained from the protein structure determined by X-ray diffraction method. Relation between the
observed ET rates in ten flavoprotein systems [41; 42] and the averaged distances has been tried
to elucidate with Marcus theory (M theory), Bixon and Jortner theory (BJ theory) [9] and Kakitani
and Mataga theory (KM theory) [11; 12]. KM theory could describe best the relation between the
observed ET rates and the averaged distances [45]. Role of water molecules on ET in flavoproteins
was investigated comparing ET rate of FMN binding protein from *Desulfovibrio vulgaris*, strain
Miyazaki F (FBP), in solution and in crystal [44].

Investigation on ET in flavoproteins stated above is based on the static protein structures obtained by X-ray diffraction method. Protein structure is, however, inherently dynamic. It is required to analyze the observed ET rates in flavoproteins based upon the dynamic structure, in order to obtain more precise microscopic feature of the ET processes.

#### 3. COMPUTATIONAL METHODS

#### 3.1 MDS calculations

The calculations were performed using the AMBER 10 suite of software programs [46]. The amber FF03 force field [47] and the parameters developed by Schneider and Suhnel [48] were used for the proteins and FMN, respectively. All missing hydrogen atoms of the WT FBP dimer were added using the LEap module. The FBP dimers were dissolved into 10,386 TIP3P water molecules in cubic cells with 9 x 9 x 9 nm dimensions. Two Cl- counter ions were added to neutralize the charge of each system.

The added water molecules were first minimized using 1,000 steps of steepest descent, while the protein and FMN coordinates were kept fixed. The complete systems were then optimized using 2,000 steps for each steepest descent and conjugated gradient minimizations. Consequently, the whole system was heated from 10 K to 298 K over 50 ps and was further equilibrated under periodic boundary conditions at 298 K. The systems were set up under the isobaric-isothermal ensemble (*NPT*) with a constant pressure and temperature of 1 atm and 298 K, respectively. Electrostatic interaction was corrected for by the Particle Mesh Ewald method [49], and all bonds involving hydrogen atoms were constrained using the SHAKE algorithm [50]. A cutoff distance of 1 nm was employed for a non-bonded pair interaction. MDS calculations were performed with the time steps of 2 fs, and the coordinates of the 10,000 MDS snapshots were collected every 2 ps. The simulations were performed over 30 ns, and after equilibrium judged by the root of the mean square deviations, the data from the last 20 ns were used for the analysis.

#### 3.2 ET rate

The ET rate described by the KM model [11; 51] is expressed by Eq. (3.1).

$$k_{M}^{jk} = \frac{v_{0}}{1 + \exp\{\beta \left(R_{jk}^{M} - R_{0}\right)\}} \sqrt{\frac{k_{B}T}{4\pi\lambda_{jk}^{M}}} \exp\left[-\frac{\left\{\Delta G_{M}^{0} - e^{2} / \varepsilon_{0}^{k} R_{jk}^{M} + \lambda_{jk}^{M} + E_{Net}^{Mk}(j)\right\}^{2}}{4\lambda_{jk}^{M} k_{B}T}\right]$$
(3.1)

Here  $k_M^{jk}$  is the ET rate from a donor j (Trp32 or Trp106) in subunit k of the FBP isoform M (M=WT, E13K, E13R, E13T and E13Q) to Iso\*.  $v_0$  is an adiabatic frequency;  $\beta$  is the ET process coefficient.  $R_{jk}^{M}$  and  $R_0$  are the donor j–Iso distance in subunit k of FBP dimer M and the critical distance for the ET process, respectively.  $R_{jk}^{M}$  is expressed with a center-to-center distance (Rc) [52; 53; 54; 55]. The ET process is adiabatic when  $R_{jk}^{M} < R_0$ , and non-adiabatic when  $R_{jk}^{M} > R_0$ . The term,  $-e^2/\varepsilon_0^k R_{jk}^{M}$ , in Eq. (S1), is the electrostatic energy between the Iso anion and a donor cation (ESDA), where  $\varepsilon_0^k$  is the static dielectric constant near the Iso and donors in subunit k. The constants  $k_B$ , e and T are the Boltzmann constant, electron charge and temperature expressed in K unit, respectively.  $E_{Net}^{Mk}(j)$  is a net electrostatic energy (NetES) of the donor j in subunit k of the FBP isoform M, which is described below.

 $\lambda_{jk}^{M}$  is the solvent reorganization energy [6] of the ET donor j in subunit k of the FBP isoform M, and it is expressed as Eq. (3.2).

$$\lambda_{jk}^{M} = e^{2} \left( \frac{1}{2a_{lso}} + \frac{1}{2a_{Trp}} - \frac{1}{R_{jk}^{M}} \right) \left( \frac{1}{\varepsilon_{\infty}} - \frac{1}{\varepsilon_{0}^{k}} \right)$$
(3.2)

Here  $a_{Iso}$  and  $a_{Trp}$  are the radii of Iso and Trp, with these reactants being assumed to be spherical, and  $\varepsilon_{\infty}$  is the optical dielectric constant assumed to be 2.0. The radii of Iso ( $a_{Iso}$ ) and Trp ( $a_{Trp}$ ) were previously determined to be 0.224 and 0.196, respectively [52; 53; 55].

The standard free energy gap between the photo-products and reactants was expressed with the ionization potential of Trp,  $E_{IP}^{Trp}$ , as in Eq. (3.3).

$$\Delta G_M^0 = E_{IP}^{T_{TP}} - G_M^0 \tag{3.3}$$

Here  $G_M^0$  is the standard Gibbs energy related to the electron affinity of the Iso\* in the FBP dimer M. The values of  $G_M^0$  were assume to be equal between Sub A and Sub B. The value of  $E_{IP}^{Trp}$  is 7.2 eV [6].

## 3.3 ET rates and related physical quantities.

The original Marcus theory [6; 7] of the ET rate has been modified in various ways [2,3, 27-32]. In the present analysis, the KM rate[16] was used because it is applicable for non-adiabatic ET processes in addition to adiabatic processes, and has been found to provide satisfactory results for both static [56; 57] and dynamic ET analyses[54]. FBP contains two Trps (Trp32 and Trp106) and one Tyr (Tyr35) in each subunit. The logarithmic ET rate (ln Rate) may be decomposed into three terms as in Eq. (3.4).

$$\ln \text{Rate} = \ln \text{EC} + \ln \text{SQ} - \text{GTLAM}$$
 (3.4)

Here,

$$\ln \text{Rate} = \ln k_M^{jk} \tag{3.5}$$

$$\ln EC = \ln \frac{V_0}{1 + \exp\{\beta (R_{ik}^M - R_0)\}}$$
 (3.6)

$$\ln SQ = \ln \sqrt{\frac{k_B T}{4\pi \lambda_{jk}^M}}$$
 (3.7)

$$GTLAM = -\frac{\left\{GT\right\}^2}{4\lambda_{jk}^M k_B T}$$
(3.8)

The total free energy gap (GT) in Eq. (3.8) is expressed as Eq. (3.9).

$$GT = SFEG + ESDA + SROE + NetES$$
 (3.9)

Here, SFEG =  $\Delta G_M^0$ , ESDA =  $-e^2 / \varepsilon_0^k R_{jk}^M$ , SROE =  $\lambda_{jk}^M$ , and NetES =  $E_{Net}^{Mk}(j)$  (see below Eq. (S1) for the notations in the SM). Likewise, the quantity GP is defined by Eq. (3.10), which eliminates the NetES term from GT.

$$GP = SFEG + ESDA + SROE \tag{3.10}$$

# 3.4 ES energy between photo-products and ionic groups inside proteins

The WT FBP contains eight Glus, three Asps, four Lyss and nine Args residues per monomer. The ES energy between the Iso anion or donor cation j and all other ionic groups in subunit k (Sub A or Sub B) of the FBP dimer M was expressed by Eq. (3.11).

$$E_{k}^{M}(j) = \sum_{i=1}^{l} \frac{C_{j}C_{Glu}}{\varepsilon_{0}^{M}R_{jk}^{M}(Glu-i)} + \sum_{i=1}^{6} \frac{C_{j}C_{Asp}}{\varepsilon_{0}^{M}R_{jk}^{M}(Asp-i)}$$

$$+\sum_{i=1}^{m} \frac{C_{j}C_{Lys}}{\varepsilon_{0}^{M}R_{ik}^{M}(Lys-i)} + \sum_{i=1}^{n} \frac{C_{j}C_{Arg}}{\varepsilon_{0}^{M}R_{ik}^{M}(Arg-i)} + \sum_{i=1}^{4} \frac{C_{j}C_{P}}{\varepsilon_{0}^{M}R_{ik}^{M}(P-i)}$$
(3.11)

Here  $l = 8 \times 2$ ,  $m = 4 \times 2$  and  $n = 9 \times 2$  for the WT;  $l = 7 \times 2$ ,  $m = 5 \times 2$  and  $n = 9 \times 2$  for E13K; l $= 7 \times 2$ ,  $m = 4 \times 2$  and  $n = 10 \times 2$  for E13R; and  $l \times 2 = 7$ ,  $m = 4 \times 2$  and  $n = 9 \times 2$  for E13T and E13Q for the dimers.  $\varepsilon_0^M$  is the static dielectric constant inside the entire FBP dimer M.  $C_j$  is the charge of the aromatic ionic species j, and it is -e for j = 0 (Iso anion), +e for j = 1 and 2 (j = 1 for Trp32+, j=2 for Trp106+).  $C_{Glu}$  (= - e),  $C_{Asp}$  (= - e),  $C_{Lys}$  (= + e),  $C_{Arg}$  (= + e) and  $C_P$  (= - e) are the charges of the Glu, Asp, Lys and Arg residues and the phosphate anions, respectively. We assumed that these groups were all in an ionic state in solution at pH 7.0 since the pKa values of these amino acids in water are 4.3 in Glu, 3.9 in Asp, 10.5 in Lys and 12.5 in Arg. In proteins these values of the pKa may be modified, but only within the range of  $\pm$  0.3. Although histidine (His) has a pKa of 6.0 in water, all the measurements were performed in a 0.1 M phosphate buffer at pH 7.0, where nearly all of the His residues should be deprotonated and neutral. Distances between the aromatic ionic species j and the ith Glu (i = 1-16 or 14) in the M isoform are denoted as  $R_{ik}^{M}(Glu-i)$ , those between k and the ith Asp (i=1-6) in the M isoform are denoted as  $R_{ik}^{M}(Asp-i)$  and so on. The net electrostatic energy (NetES) between the photo-products and ionic groups,  $E_{Net}^{Mk}(j)$  (j = 1 and 2) was expressed as in Eq. (3.12).

$$E_{Net}^{Mk}(j) = E_k^M(0) + E_k^M(j)$$
(3.12)

# 3.5 Fluorescence decays

The experimental fluorescence decay functions of the WT; E13T and E13Q; and E13K and E13R FBP isoforms have been reported previously [58] and are given by Eq. (3.13).

$$F_{obs}^{M} = \sum_{i=1}^{2073} \alpha_{i}^{M} \exp(-t/\tau_{i}^{M})$$
 (3.13)

The *i*th lifetime components ( $\tau_i^M$ ) in ps unit with the pre-exponential factor ( $\alpha_i^M$ ) of the isoform M are given in Table S1. The calculated decay function of the M isoform with the ET rate given by Eq. (S1) is expressed as a mean of the decays of Sub A and Sub B by Eq. (3.14).

$$F_{calc}^{M}(t) = \frac{1}{2} \left( \exp \left[ -\left\{ \sum_{j=1}^{2} k_{M}^{j1}(t') \right\} t \right] \right)_{AV} + \left\langle \exp \left[ -\left\{ \sum_{j=1}^{2} k_{M}^{j2}(t') \right\} t \right] \right\rangle_{AV} \right)$$
(3.14)

The fluorescence decays of the dimer M were calculated up to 2 ps with 0.004 ps time intervals. Note that  $\langle ... \rangle_{AV}$  denotes the averaging procedure of the exponential function in Eq. (3.14), and was performed over t' up to 20 ns with 2 ps time intervals. In Eq. (3.14) we assumed that the decay functions at every instant of time (t') during the MDS time range can always be expressed by an exponential function.

#### 3.6 Determination of unknown ET parameters

The unknown parameters in the KM model are  $v_0$ ,  $\beta$ ,  $R_0$ ,  $G_M^0$  (M = WT, E13K, E13R, E13T, E13Q),  $\varepsilon_0^M$ ,  $\varepsilon_0^A$  (static dielectric constant near Iso and the donors in Sub A) and  $\varepsilon_0^B$  (the static dielectric constant near Iso and the donors in Sub B). The chi-square of the FBP isoform M between the observed [ $F_{obs}^M(t)$ ] and calculated [ $F_{calc}^M(t)$ ] fluorescence intensities is defined by Eq. (3.15).

$$\chi_M^2 = \frac{1}{N} \sum_{i=1}^N \frac{\left\{ F_{calc}^M(t_i) - F_{obs}^M(t_i) \right\}^2}{F_{calc}^j(t_i)}$$
(3.15)

Here, N denotes the number of time intervals in the fluorescence decay, and was 500 for all evaluations. The deviation between the observed and calculated fluorescence intensities at  $t = t_i$  is expressed by Eq. (3.16).

$$Dev_{M}(t_{i}) = \frac{\left\{F_{calc}^{M}(t_{i}) - F_{obs}^{M}(t_{i})\right\}}{\sqrt{F_{calc}^{M}(t_{i})}}$$
(3.16)

All of the unknown ET parameters were determined to obtain the minimum value of the total chisquare given by Eq. (3.17), by a non-linear least square's method according to the Marquardt algorithm.

$$\chi_T^2 = \chi_{WT}^2 + \chi_{E13K}^2 + \chi_{E13R}^2 + \chi_{E13T}^2 + \chi_{E13O}^2$$
(3.17)

The ET parameters for the FBP monomer were also obtained with the present model, where the unknown parameters are  $V_0$ ,  $\beta$ ,  $R_0$ ,  $G_M^0$  (M = WT, E13K, E13R, E13T, E13Q),  $\varepsilon_0^M$  and  $\varepsilon_0^{DA}$  (static dielectric constant near Iso and the donors in the monomer).

#### 3.7 Residue ES energy

A physical quantity of REST is defined as ES energy of a residue number n in subunit s interacting with atoms in subunit r (r and s are Sub A or Sub B) was obtained by Eq (3.18) with a snapshot.

$$REST(s, r, n) = \sum_{m=1}^{N} \sum_{k=1}^{n(j)} \sum_{l=1}^{m(l)} \frac{CD(snk)CD(rml)}{\varepsilon_0 R(s, n, k, r, m, l)}$$
(3.18)

Here N denotes total number of the residues (123, 122 amino acids and FMN), n(j) number of atoms in the residue n of subunit s, and m(l) number of atoms in residue m of subunit r. The value of REST is time-dependent. A distance R(s,n,k,r,m,l) between an atom k of residue m in subunit s and atom s of residue s in subunit s and atom s of residue s in subunit s and atom s of residue s in subunit s and atom s of residue s in subunit s and atom s of residue s in subunit s and atom s of residue s in subunit s and atom s of residue s in subunit s and atom s of residue s in subunit s and atom s of residue s in subunit s and atom s in subunit s in subunit s and atom s in subunit s in

$$R(s,n,k,r,m,l) = \sqrt{\left\{X_s(s,n,k) - X_r(r,m,l)\right\}^2 + \left\{Y_s(s,n,k) - Y_r(r,m,l)\right\}^2 + \left\{Z_s(s,n,k) - Z_r(r,m,l)\right\}^2}$$
(3.19)

Here  $X_s(s,n,k)$  denotes X-coordinate of atom k of residue n in subunit s, and  $X_r(r,m,l)$ , X-coordinate of atom l of residue m in subunit r, and so on for other coordinates. CD(snk) denotes charge density of atom k of residue n in subunit s, and CD(rml) charge density of atom l of residue m in subunit s, which were obtained from the AMBER 10 [46]. The value of a static dielectric constant inside the protein ( $\varepsilon_0$  equal to 9.2) was taken from the previous work [59]. Schematic representation of REST is illustrated in Figure. 3.1.

RES was obtained as mean value of REST over all snapshots as Eq. (3.20).

$$RES(s,r,n) = \frac{1}{M} \sum_{i=1}^{M} \sum_{m=1}^{N} \sum_{k=1}^{n(j)} \sum_{l=1}^{m(l)} \frac{CD(snk)CD(rml)}{\varepsilon_0 R(s,r,n,j,m,l)}$$
(3.20)

Numbers of snapshots, M, were 5000 with 4 ps intervals for 20 ns of MDS time.

#### 4. RESULTS AND DISCUSSION

# 4.1 PET study of four different single mutated FBP dimers

## 4.1.1 Theoretical fluorescence dynamics of mutated FBP dimers

Figure 4.1 shows the MDS snapshots of the four mutated FBP dimers, where FMN, Trp32 and amino acids at position 13 are indicated with one letter notations for the amino acids in addition to the peptide backbone [59]. The mean values of Rc over 10,000 snapshots are listed in Table 4.1 in the SM. The Rc values of Trp32 were 1.19 nm and 1.22 nm in Sub A and in Sub B of E13K; 1.20 nm in both Sub A and Sub B of E13R; 0.89 nm in both Sub A and Sub B of E13T; 1.11 nm in Sub A and 1.13 nm in Sub B of E13Q; and 0.70 and 0.99 nm in Sub A and Sub B of WT. In the crystal structure, the Rc values were always shorter than those from solution.

The reported experimental fluorescence lifetimes of the wild-type and four mutated FBP dimers are listed in Table 4.2 [60]. The experimental and theoretical fluorescence decays are shown in Figure 4.22. The deviations between the two decays (see Eq. (3.16) in the section 3.) are illustrated in the upper panels of the decays. The agreement between the experimental and calculated decays in all FBP dimers was much better than those with the FBP monomers [61]. The best-fit ET parameters together with the chi-squared values are also listed in Table 4.3.

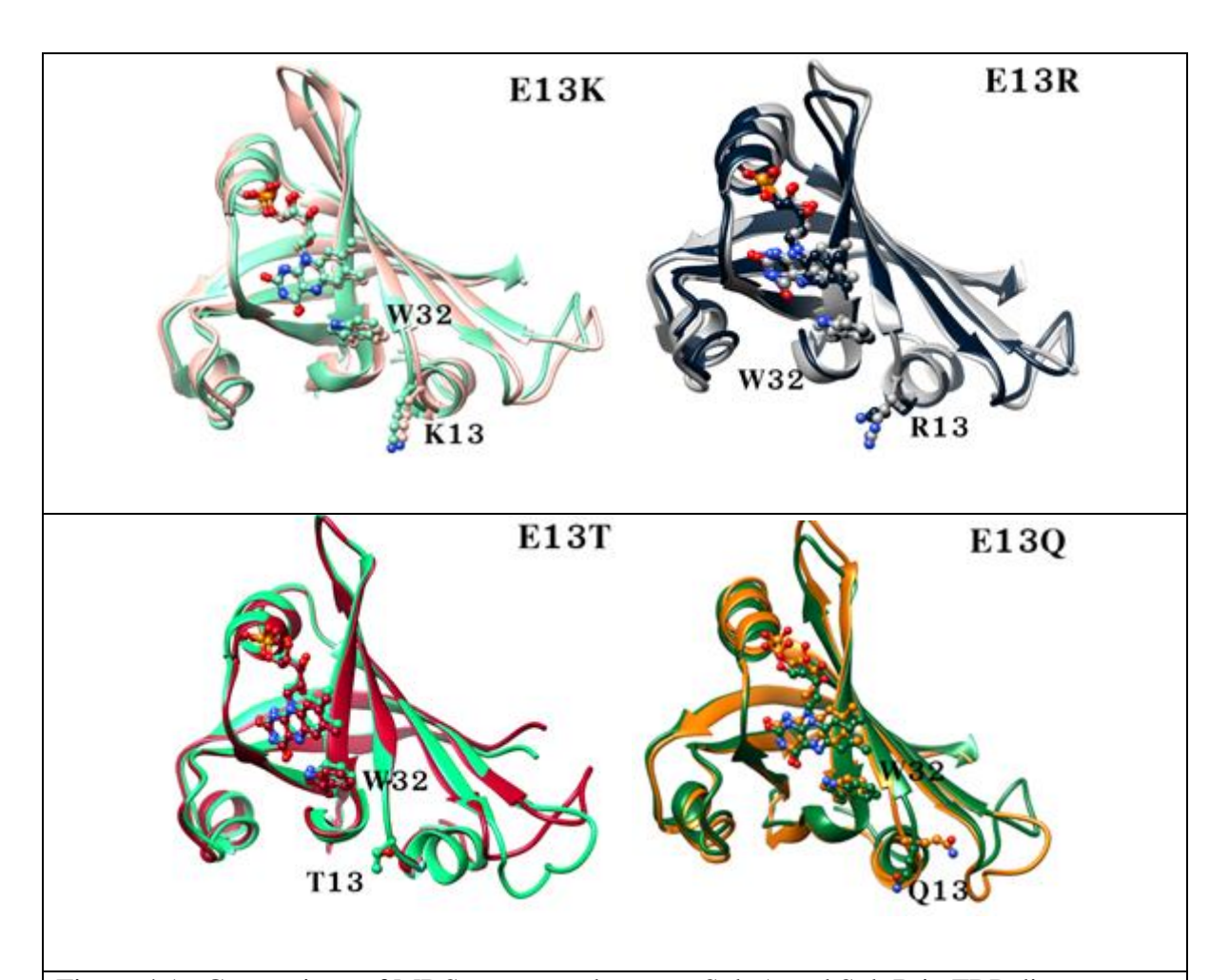


Figure 4.1 Comparison of MDS structures between Sub A and Sub B in FBP dimers.

Structures of peptide back bones, FMNs, Trp32s and amino acids at 13 locations of five FBP dimers are superimposed between Sub A and Sub B. The amino acids are indicated with one letter notations, W (Trp), K (Lys), R (Arg), T (Thr) and Q (Gln).

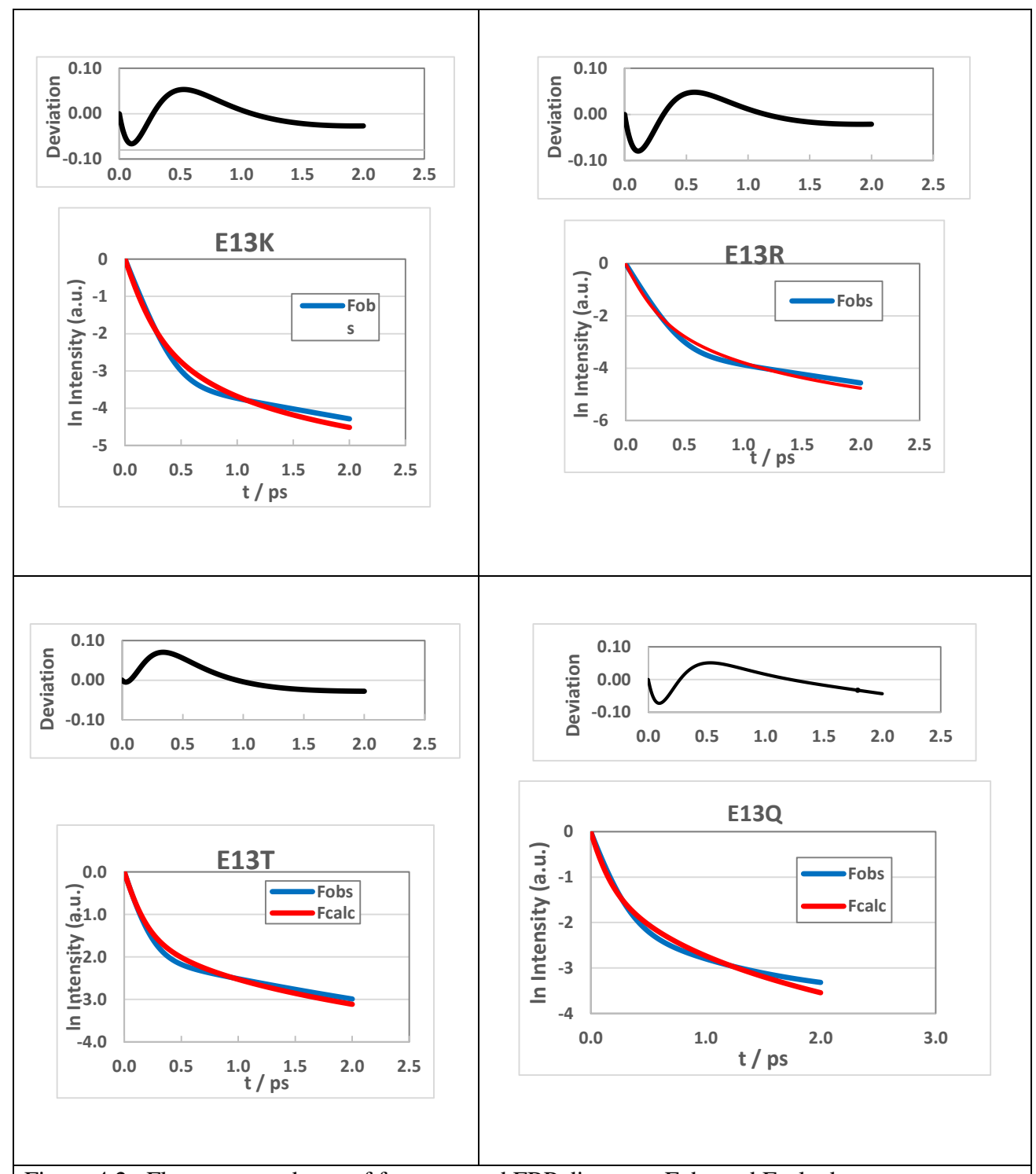


Figure 4.2 Fluorescence decay of four mutated FBP dimmers. Fobs and Fcalc denote experimental fluorescence decay given by Eq. (3.13)] and calculated decay given by Eq. (3.14).

Table 4.1 Geometry of ET donors, acceptor and amino acid at 13 locations in FBP dimers.

Method	FBP	Subunit		R	213			Rc			Re			Angle	
			Trp32	Tyr35	Trp106	Iso	Trp32	Tyr35	Trp106	Trp32	Tyr35	Trp106	Trp32	Tyr35	Trp106
MDS	WT	A	0.70	0.77	1.35	1.25	0.71	0.90	0.94	0.28	0.31	0.26	-53	76	71
		В	0.99	0.88	1.47	1.51	0.68	1.03	1.03	0.28	0.40	0.29	-58	95	71
Crystal		A	0.45	0.65	1.37	1.24	0.85	1.00	1.18	0.39	0.46	0.61	-85	-81	84
		В	0.45	0.65	1.37	1.18	0.81	0.91	1.09	0.38	0.46	0.61	-86	-88	-85
MDS	E13K	A	1.19	1.10	1.67	1.74	0.71	0.98	0.97	0.27	0.39	0.27	-53	-70	-46
		В	1.22	1.16	1.68	1.74	0.68	0.94	0.97	0.27	0.33	0.27	-52	-81	-44
Crystal		A	1.07	1.28	1.86	1.73	0.74	0.86	0.98	0.39	0.47	0.60	-79	79	84
		В	1.06	1.37	1.98	1.75	0.84	0.97	1.17	0.39	0.46	0.61	84	-80	82
MDS	E13R	A	1.20	1.18	1.69	1.74	0.73	0.85	0.95	0.26	0.29	0.28	91	-67	50
		В	1.20	1.04	1.56	1.69	0.73	0.98	1.01	0.28	0.37	0.27	-96	-63	41
Crystal		A	0.97	1.00	1.70	1.61	0.75	0.84	0.98	0.39	0.46	0.60	-80	80	86
		В	0.75	0.80	1.46	1.50	0.84	0.97	1.17	0.39	0.46	0.61	86	-82	82
MDS	E13T	A	0.89	1.03	1.58	1.45	0.70	0.97	0.97	0.28	0.37	0.28	-46	-86	78

В	0.89	1.01	1.58	1.43	0.70	0.97	0.97	0.27	0.37	0.27	-51	116	77
A	0.90	1.19	1.88	1.46	0.68	0.79	0.99	0.39	0.45	0.60	-49	-75	85
В	0.90	1.19	1.87	1.49	0.72	0.84	1.03	0.39	0.45	0.61	-85	-85	84
A	1.11	1.17	1.71	1.65	0.70	0.88	0.97	0.27	0.28	0.30	29	54	79
В	1.13	1.43	1.97	1.62	0.70	0.92	0.97	0.27	0.32	0.27	22	78	80
A	0.87	1.13	1.70	1.49	0.71	0.82	1.02	0.39	0.45	0.60	-51	-85	81
В	0.51	0.70	1.37	1.16	0.70	0.82	1.00	0.39	0.46	0.60	-87	83	85
	A B A B	<ul> <li>A 0.90</li> <li>B 0.90</li> <li>A 1.11</li> <li>B 1.13</li> <li>A 0.87</li> </ul>	A 0.90 1.19 B 0.90 1.19 A 1.11 1.17 B 1.13 1.43 A 0.87 1.13	A 0.90 1.19 1.88 B 0.90 1.19 1.87 A 1.11 1.17 1.71 B 1.13 1.43 1.97 A 0.87 1.13 1.70	A       0.90       1.19       1.88       1.46         B       0.90       1.19       1.87       1.49         A       1.11       1.17       1.71       1.65         B       1.13       1.43       1.97       1.62         A       0.87       1.13       1.70       1.49	A       0.90       1.19       1.88       1.46       0.68         B       0.90       1.19       1.87       1.49       0.72         A       1.11       1.17       1.71       1.65       0.70         B       1.13       1.43       1.97       1.62       0.70         A       0.87       1.13       1.70       1.49       0.71	A       0.90       1.19       1.88       1.46       0.68       0.79         B       0.90       1.19       1.87       1.49       0.72       0.84         A       1.11       1.17       1.71       1.65       0.70       0.88         B       1.13       1.43       1.97       1.62       0.70       0.92         A       0.87       1.13       1.70       1.49       0.71       0.82	A       0.90       1.19       1.88       1.46       0.68       0.79       0.99         B       0.90       1.19       1.87       1.49       0.72       0.84       1.03         A       1.11       1.17       1.71       1.65       0.70       0.88       0.97         B       1.13       1.43       1.97       1.62       0.70       0.92       0.97         A       0.87       1.13       1.70       1.49       0.71       0.82       1.02	A       0.90       1.19       1.88       1.46       0.68       0.79       0.99       0.39         B       0.90       1.19       1.87       1.49       0.72       0.84       1.03       0.39         A       1.11       1.17       1.71       1.65       0.70       0.88       0.97       0.27         B       1.13       1.43       1.97       1.62       0.70       0.92       0.97       0.27         A       0.87       1.13       1.70       1.49       0.71       0.82       1.02       0.39	A       0.90       1.19       1.88       1.46       0.68       0.79       0.99       0.39       0.45         B       0.90       1.19       1.87       1.49       0.72       0.84       1.03       0.39       0.45         A       1.11       1.17       1.71       1.65       0.70       0.88       0.97       0.27       0.28         B       1.13       1.43       1.97       1.62       0.70       0.92       0.97       0.27       0.32         A       0.87       1.13       1.70       1.49       0.71       0.82       1.02       0.39       0.45	A       0.90       1.19       1.88       1.46       0.68       0.79       0.99       0.39       0.45       0.60         B       0.90       1.19       1.87       1.49       0.72       0.84       1.03       0.39       0.45       0.61         A       1.11       1.17       1.71       1.65       0.70       0.88       0.97       0.27       0.28       0.30         B       1.13       1.43       1.97       1.62       0.70       0.92       0.97       0.27       0.32       0.27         A       0.87       1.13       1.70       1.49       0.71       0.82       1.02       0.39       0.45       0.60	A       0.90       1.19       1.88       1.46       0.68       0.79       0.99       0.39       0.45       0.60       -49         B       0.90       1.19       1.87       1.49       0.72       0.84       1.03       0.39       0.45       0.61       -85         A       1.11       1.17       1.71       1.65       0.70       0.88       0.97       0.27       0.28       0.30       29         B       1.13       1.43       1.97       1.62       0.70       0.92       0.97       0.27       0.32       0.27       22         A       0.87       1.13       1.70       1.49       0.71       0.82       1.02       0.39       0.45       0.60       -51	A       0.90       1.19       1.88       1.46       0.68       0.79       0.99       0.39       0.45       0.60       -49       -75         B       0.90       1.19       1.87       1.49       0.72       0.84       1.03       0.39       0.45       0.61       -85       -85         A       1.11       1.17       1.71       1.65       0.70       0.88       0.97       0.27       0.28       0.30       29       54         B       1.13       1.43       1.97       1.62       0.70       0.92       0.97       0.27       0.32       0.27       22       78         A       0.87       1.13       1.70       1.49       0.71       0.82       1.02       0.39       0.45       0.60       -51       -85

Table 4.2 Experimental fluorescence lifetimes in five FBP dimers.

FBP	$ au_1$	$\alpha_{_{1}}$	$ au_2$	$\alpha_2$	$ au_3$	$\alpha_{_3}$	$ au_{AV}^{b}$
	(ps <sup>-1</sup> )		(ps <sup>-1</sup> )		(ps <sup>-1</sup> )		(ps <sup>-1</sup> )
WT	0.167	(0.96)	1.5	(0.04)			0.22
E13K	0.128	(0.96)	1.87	(0.04)			0.198
E13R	0.132	(0.96)	1.49	(0.04)			0.186
E13T	0.107	(0.86)	1.5	(0.12)	30	(0.02)	0.872
E13Q	0.134	(0.85)	0.746	(0.12)	30	(0.03)	1.10

 $<sup>\</sup>overline{\phantom{a}^{a} \tau_{Av} = \sum_{i=1}^{2or3} \tau_{i} \alpha_{i}}$ 

Table 4.3 Best-fit ET parameter.

FBP	$G_{M}^{0}$ a	SFEG <sup>b</sup>	$\mathcal{E}_0^{M \ \mathrm{c}}$		$\chi_M^2$ d
(M)	(eV)	(eV)			
E13K	8.32	-1.12	3.03	-	1.02 x 10-3
E13R	8.25	-1.05	3.26	-	1.02 x 10-3
E13T	8.62	-1.42	2.20	-	1.12 x 10-3
E13Q	8.31	-1.11	2.45	-	1.15 x 10-3
WTf	7.67	-0.47	9.15	-	6.13 x10-5
$\nu_0^{\ \ e}$	$\beta^{\mathrm{e}}$	$R_0^{e}$	$\mathcal{E}_0^{A\mathrm{f}}$	$\mathcal{E}_0^{B\mathrm{h}}$	$\chi_T^{2i}$
(ps <sup>-1</sup> )	(nm <sup>-1</sup> )	(nm)			
239	13.1	0.977	2.74	2.69	8.75 x 10-4

<sup>&</sup>lt;sup>a</sup> Standard free energy of Iso\* ( $G_M^0$ ) in Eq. (3.3). <sup>b</sup> Standard free energy gap ( $\Delta G_M^0$ ) obtained from  $G_M^0$  by Eq (3.3).

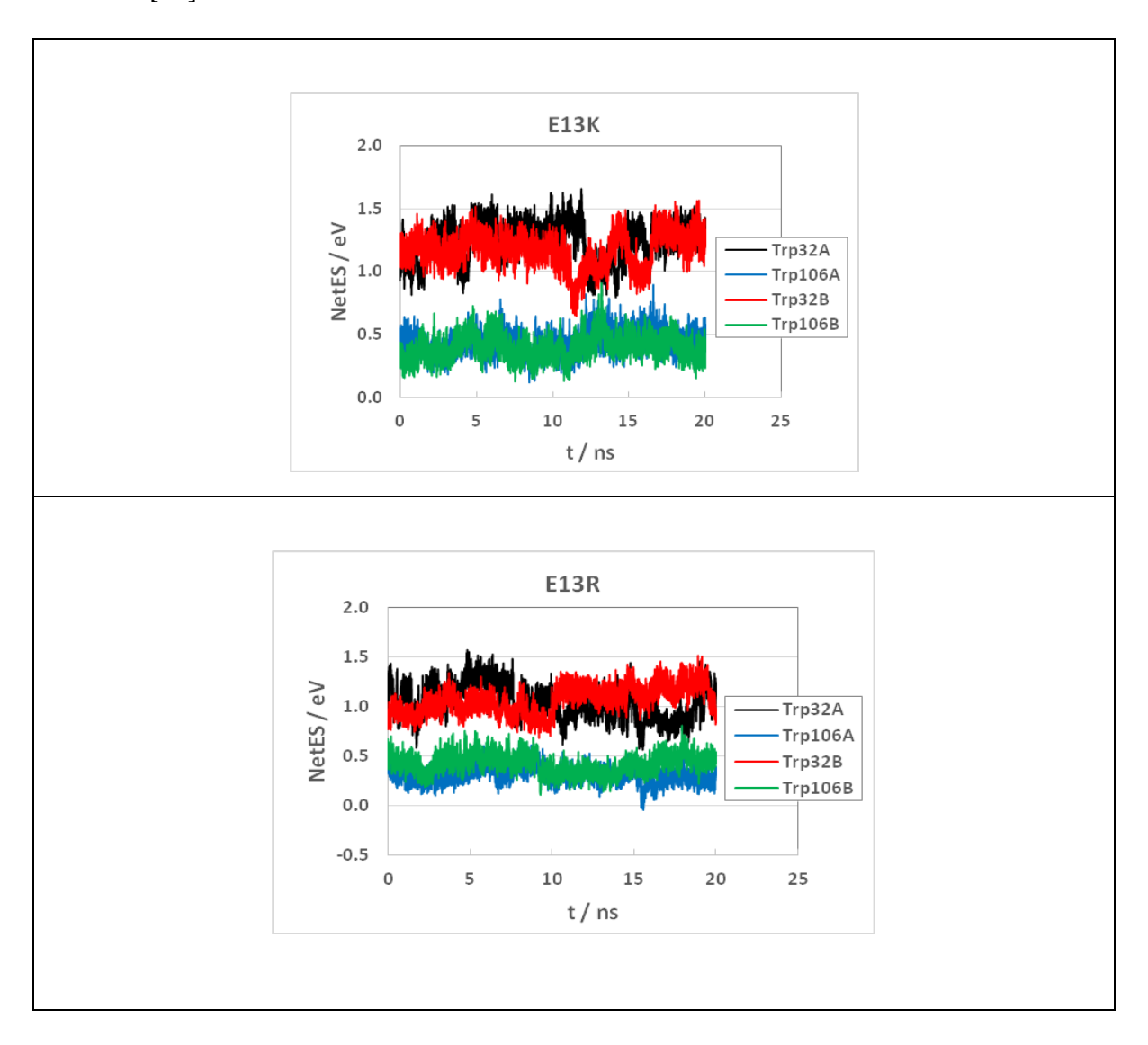
<sup>&</sup>lt;sup>c</sup> Static dielectric constant inside the dimer, M, in Eq. (3.11). <sup>d</sup> Chi-square of the dimer M, given by Eq. (3.15).

<sup>&</sup>lt;sup>e</sup> ET parameters appeared in  $k_M^{jk}$  in Eq. (3.1). <sup>f</sup> Static dielectric constant near Iso and donors in Sub A.

<sup>&</sup>lt;sup>h</sup> Static dielectric constant near Iso and donors in Sub B. <sup>i</sup> Total chi-square given by Eq. (3.17).

# 4.1.2 Dynamics and distributions of NetES

The time-evolutions of NetES are shown in Figure 4.3. In E13K, the NetES fluctuated within 0.7 - 1.5 eV in Trp32 and 0.2 - 0.6 eV in Trp106. In E13R, the NetES varied in the ranges of 0.6 - 1.5 eV in Trp32 and 0 - 0.7 eV in Trp106. In E13T, the values varied in the ranges of 0.9 - 1.9 eV in Trp32 and 0.3 - 1.2 eV in Trp106. In E13Q, the values varied in the ranges of 0.6 - 1.7 eV in Trp32 and 0.3 - 1.7 eV. The values of NetES in the WT fluctuated around 0.05 - 0.4 eV with time [62].



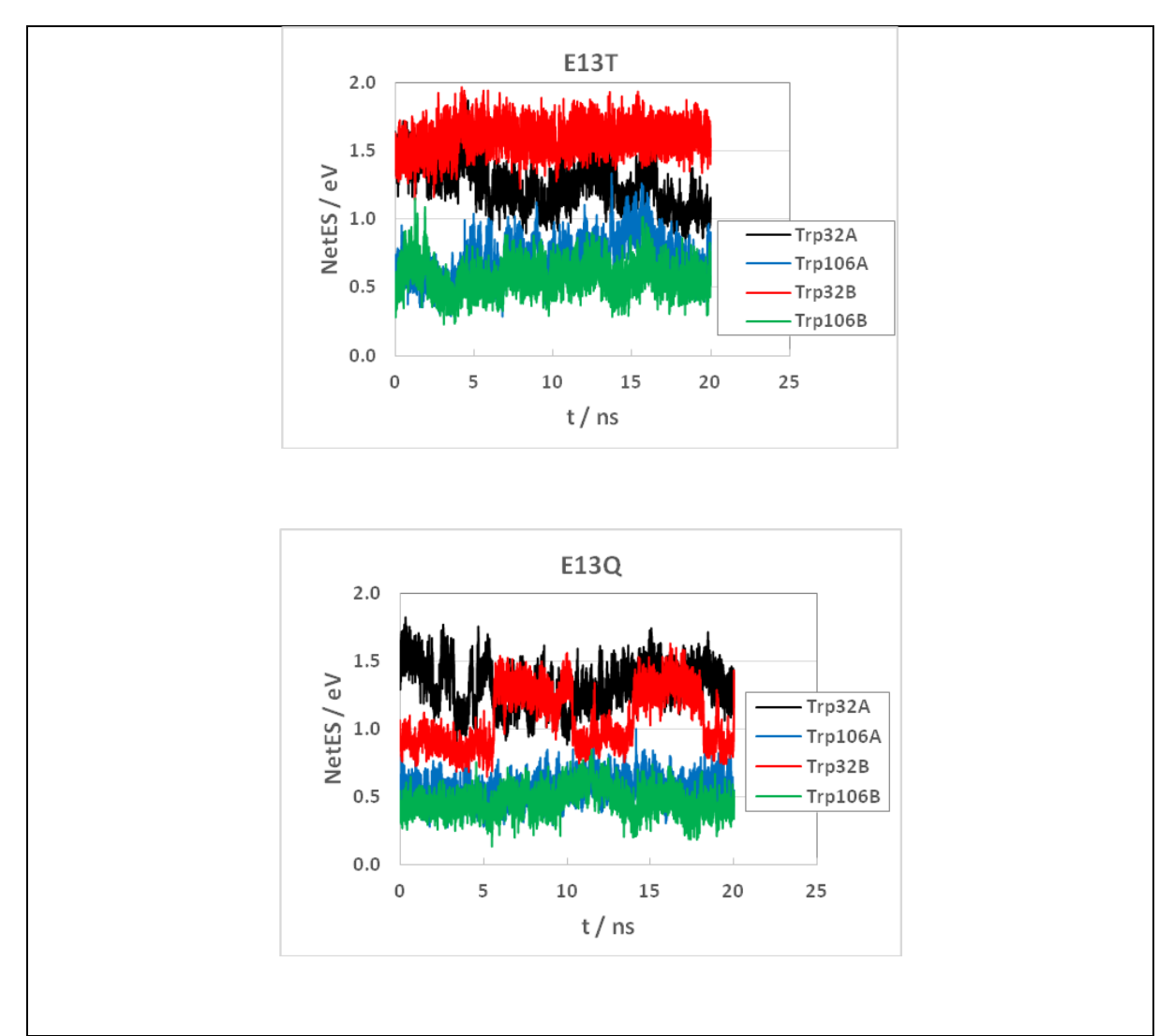
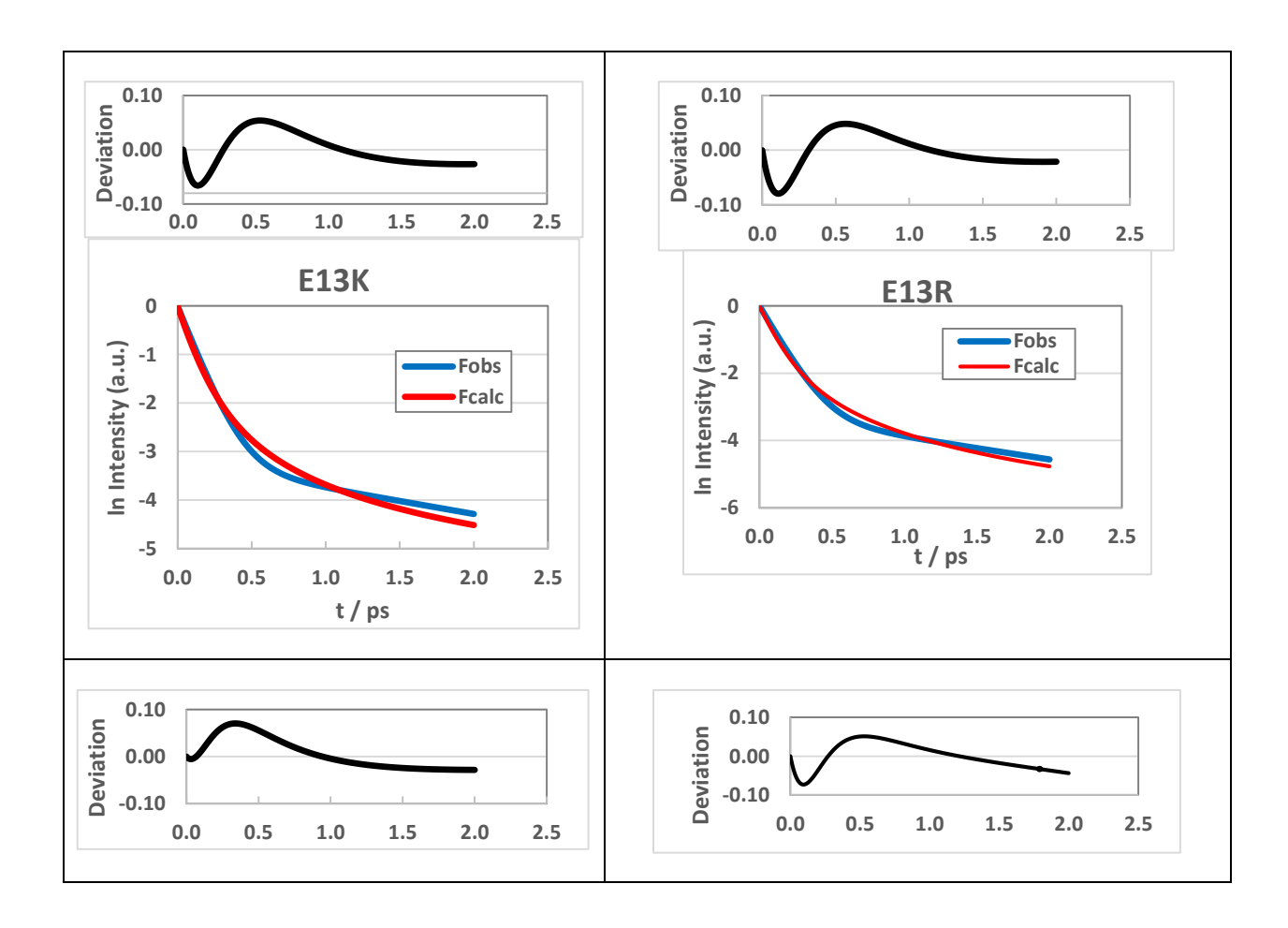


Figure 4.3 Dynamics of NetES in FBP dimers. NetES is given by Eq. (3.12). Trp32A, Trp32B, Trp106A and Trp106B in inserts denote Trp32 in Sub A and Sub B as well as Trp106 in Sub A and Sub B, respectively.

The distributions of the NetES are shown in Figure 4.4. In E13K, the distribution of Trp32KA (Trp32 in Sub A of E13K dimer) displayed double maxima with a minor peak at *ca.* 1.0 eV. In both Trp32KB (Trp32 in Sub B of E13K) and Trp106KB (Trp106 in Sub B of E13K) the distributions were not symmetric along with Rc. The distribution of Trp32RA (Trp32 in Sub A of E13R) also displayed broad and double maxima at *ca.* 1.0 and 1.3 eV, though it was not as clear

as Trp32KA. The distribution of Trp32RB (Trp32 in Sub B of E13R) was also broad with a single peak. The distributions of Trp106RA (Trp106 in Sub A of E13R) and Trp106RB (Trp106 in Sub B of E13R) displayed relatively sharp peaks at around 0.3 and 0.5 eV. The distributions in E13T displayed double maxima at *ca*.1.2 and 1.4 eV in Trp32TA (Trp32 in Sub A of E13T) and a single peak at *ca*. 1.7 eV in Trp32TB (Trp32 in Sub B of E13T). The distributions in Trp32QB (Trp32 in Sub B of E13Q) displayed clear double peaks at around 0.9 and 1.3 eV, while Trp32QA (Trp32 in Sub A of E13Q) showed a single peak. In the WT, the distributions display almost symmetrical single peaks, including Trp106WTB (Trp106 in Sub B of WT) where the Rc values displayed a discontinuous change at around 15 ns of MDS time[62].



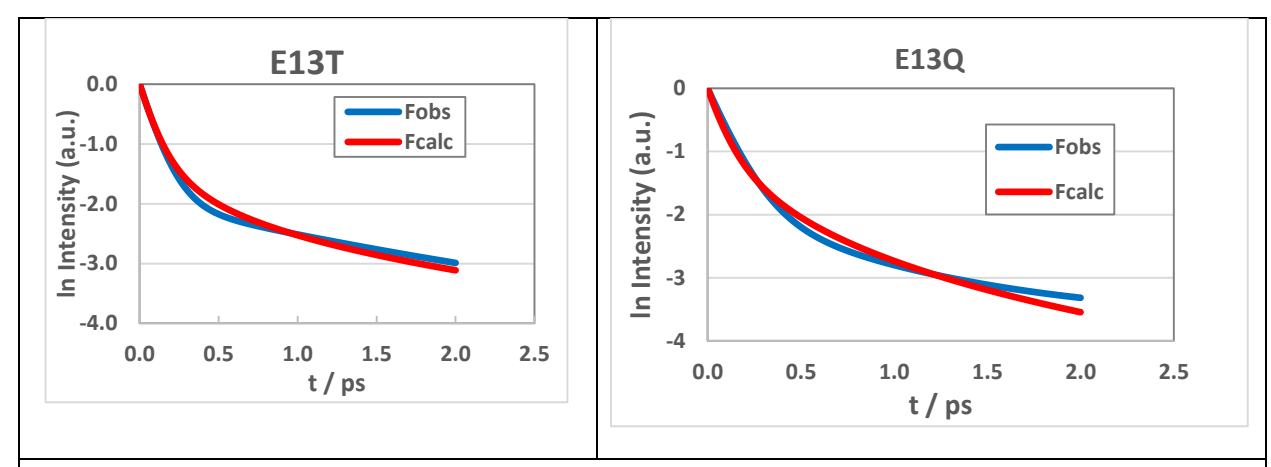


Figure 4.4 Fluorescence decay of the four mutated FBP dimers

Fobs in inserts denotes the experimental fluorescence decay given by Eq. (3.13). Fcalc the calculated decay given by Eq. (3.14).

The mean values of NetES are listed in Table 4.4. The values in E13K were 1.24 and 1.17 eV in Trp32KA and Trp32KB as well as 0.43 and 0.39 eV in Trp106KA and Trp106KB, respectively. The values in E13R were 1.05 and 1.07 eV in Trp32RA and Trp32RB as well as 0.31 and 0.42 eV in Trp106RA and Trp106RB. The values in E13T were 1.26 and 1.59 eV in Trp32TA and Trp32TB as well as 0.70 and 0.57 eV in Trp106TA and Trp106TB. The values in E13Q were 1.32 and 1.08 eV in Trp32QA and Trp32QB as well as 0.55 and 0.46 eV in Trp106QA and Trp106QB. The average values of Trp32WTA (Trp32 in Sub A of WT) and Trp32WTB (Trp32 in Sub B of WT) were 0.22 eV, and that of Trp106WTA (Trp106 in Sub A of WT) and Trp106WTB was 0.16 eV in the WT with a negative charge of Glu13. In E13K and E13R with a positive charge at amino acid-13, the average value among Trp32KA, Trp32KB, Trp32RA and Trp32RB was 1.13 eV, and that of Trp106KB, Trp106RA and Trp106RB was 0.39 eV. In E13T and E13Q with neutral charge at amino acid-13, the average value among the four Trp32 residues was 1.31 eV and the average value among the four Trp106 residues was 0.57 eV. In both Trp32 and Trp106,

the average values of NetES were the least in the WT and the greatest in E13T and E13Q with the neutral charge while the second was in E13K and E13R with the positive charge. In the WT dimer, the values were 0.2 eV in Trp32A, 0.23 eV in Trp32B, 0.14 eV in Trp106A and 0.18 eV in Trp106B.

Table 4.4 ET rate and related physical quantity<sup>a</sup>.

FBP	Donor	Subunit	ET	SROE <sup>c</sup>	ESDA <sup>d</sup>	NetESe	GP <sup>f</sup>
			Rate <sup>b</sup>	(eV)	(eV)	(eV)	(eV)
			(ps <sup>-1</sup> )				
E13K	Trp32	A	9.17	0.65	-0.74	1.24	-1.21
		В	8.58	0.61	-0.79	1.17	-1.29
		Monomer <sup>g</sup>	14.0	0.468	-0.830	0.268	-
							0.528
	Trp106	A	0.30	0.72	-0.55	0.43	-0.94
		В	0.12	0.69	-0.55	0.39	-0.98
		Monomer <sup>g</sup>	2.86 x	0.518	-0.621	-0.472	-
			10-4				0.269
E13R	Trp32	A	8.31	0.66	-0.72	1.05	-1.11
		В	9.21	0.63	-0.73	1.07	-1.15
		Monomerg	11.5	0.457	-0.875	0.306	-
							0.113

	Trp106	A	0.16	0.72	-0.56	0.31	-0.88
	111100	A	0.10	0.72	-0.30	0.31	-0.00
		В	0.37	0.70	-0.53	0.42	-0.88
		Monomer <sup>g</sup>	2.27 x	0.518	-0.623	-0.347	0.200
			10-3				
E13T	Trp32	A	5.48	0.65	-0.75	1.26	-1.51
		В	11.0	0.62	-0.77	1.59	-1.56
		Monomerg	9.77	0.474	-0.803	0.822	-
							0.749
	Trp106	A	0.48	0.72	-0.55	0.70	-1.24
		В	0.03	0.70	-0.55	0.57	-1.27
		Monomer <sup>g</sup>	5.07 x	0.515	-0.636	-0.949	-
			10 <sup>-7</sup>				0.541
E13Q	Trp32	A	8.61	0.65	-0.75	1.32	-1.21
		В	6.60	0.62	-0.77	1.08	-1.26
		Monomer <sup>g</sup>	7.05	0.481	-0.777	0.873	-
							0.776

Tr	p106 A	1.17	0.72	-0.55	0.55	-0.93
	В	0.32	0.69	-0.55	0.46	-0.96
	Monomer	9.70 x	0.519	-0.619	-0.846	-
		10-8				0.580

a ET rates and related physical quantities were obtained with the best-fit ET parameters. The mean values are listed over 10,000 snapshots with 2 ps intervals.

b ET rate given by Eq. (3.1).

c Solvent reorganization energy given by Eq. (3.2).

d ES energy between photo-products, ESDA =  $-e^2 / \varepsilon_0^k R_{jk}^M$  in Eq. (3.1).

e Net ES energy given by Eq. (3.12).

f GP is defined by Eq. (3.14) in text.

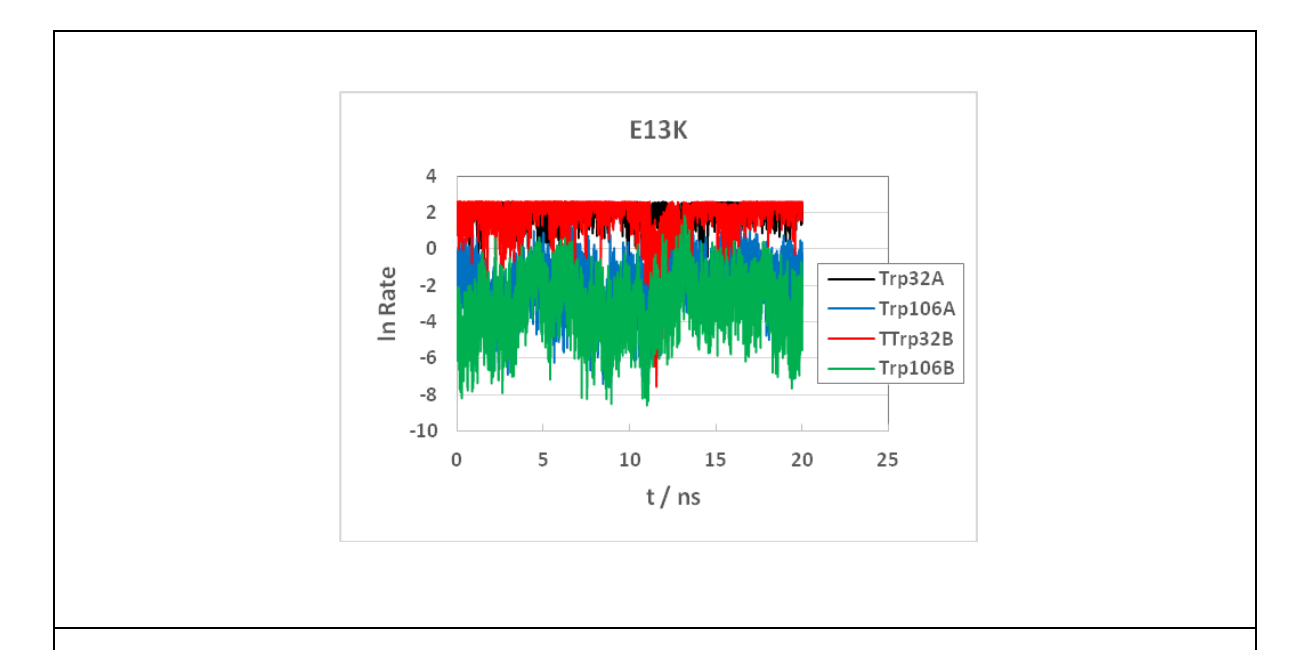
g Data for Monomer were obtained with the same method as for the dimers.

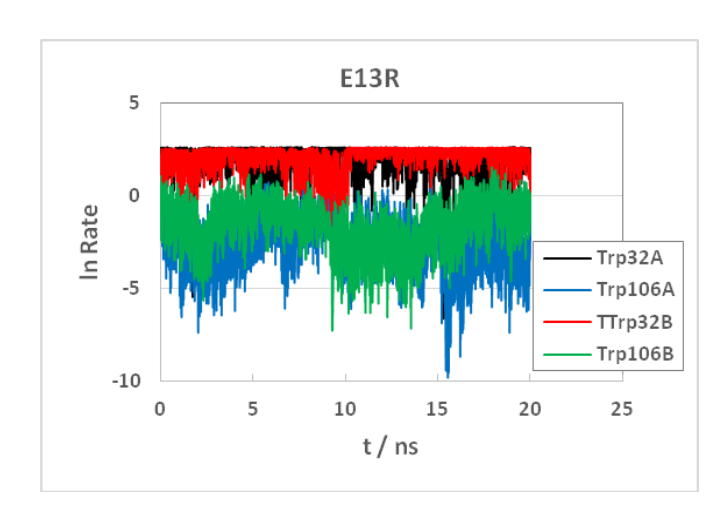
#### 4.1.3 Mean values of SROE and ESDA over MDS times

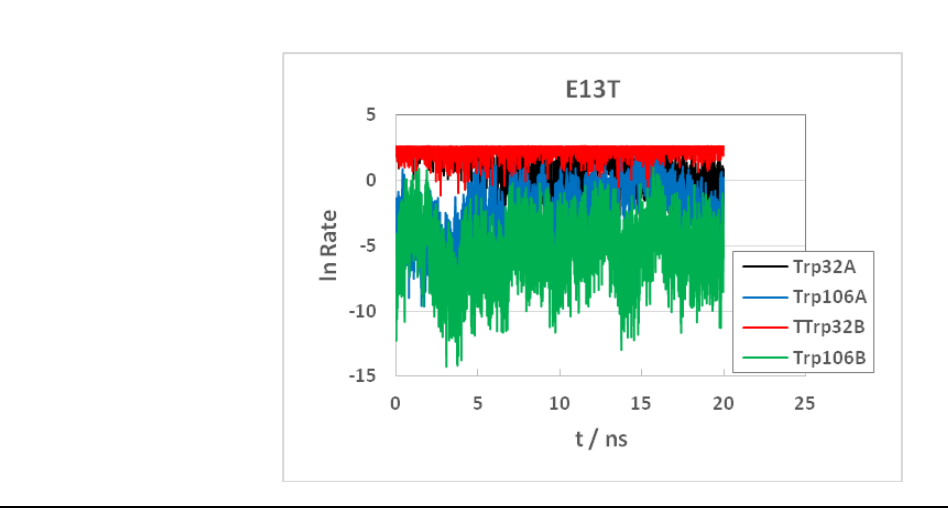
The mean values of SROE and ESDA are also listed in Table 4.4. These values did not vary much among the FBP dimers and subunits. The values of SROE were always lower in Trp32 compared to Trp106 because of the shorter donor-acceptor distances in Trp32. The ESDA also depended on the Rc as SROE. The variations in ESDA were not as remarkable as those in NetES. The values of ESDA were always lower in Trp32 than those in Trp106 because of the shorter Rc in Trp32 than that in Trp106, as in SROE.

#### **4.1.4 ET rates**

Time-evolutions of the ln Rate are shown in Figure 4.5 in the SM. In every mutated FBP dimer, the values of the ln Rate in Trp106 greatly fluctuated with time, but not so much in Trp32. Figure 4.6 shows the distributions of the ln Rate. The ln Rate values at the peak distributions of Trp32 were always greater than those of Trp106 in the mutated FBP dimers, where the Rc of Trp32 was always shorter than that of Trp106. All rates display an upper-limit because of the GTLAM terms, which always are negative and reduce the rates. The mean values of the ET rates over all snapshots are listed in Table 4.4. In E13K, the ET rates of Trp32KA and Trp32KB were 9.17 and 8.58 ps<sup>-1</sup>, while they were 0.30 and 0.12 ps<sup>-1</sup> in Trp106KA and Trp106KB. In E13R, the ET rates of Trp32RA and Trp32RB were 8.31 and 9.21 ps<sup>-1</sup>, while they were 0.16 and 0.37 ps<sup>-1</sup> in Trp106AR and Trp106RB. In E13T, the ET rates of Trp32TA and Trp32TB were 5.48 and 11.0 ps<sup>-1</sup>, while they were 0.48 and 0.03 ps<sup>-1</sup> in Trp106TA and Trp106TB. In E13Q, the ET rates of Trp32QA and Trp32QB were 8.61 and 6.60 ps<sup>-1</sup>, while they were 1.17 and 0.32 ps<sup>-1</sup> in Trp106QA and Trp106QB. For the WT FBP dimer, the ET rates and related physical quantities are shown in Table 4.4 for comparison.







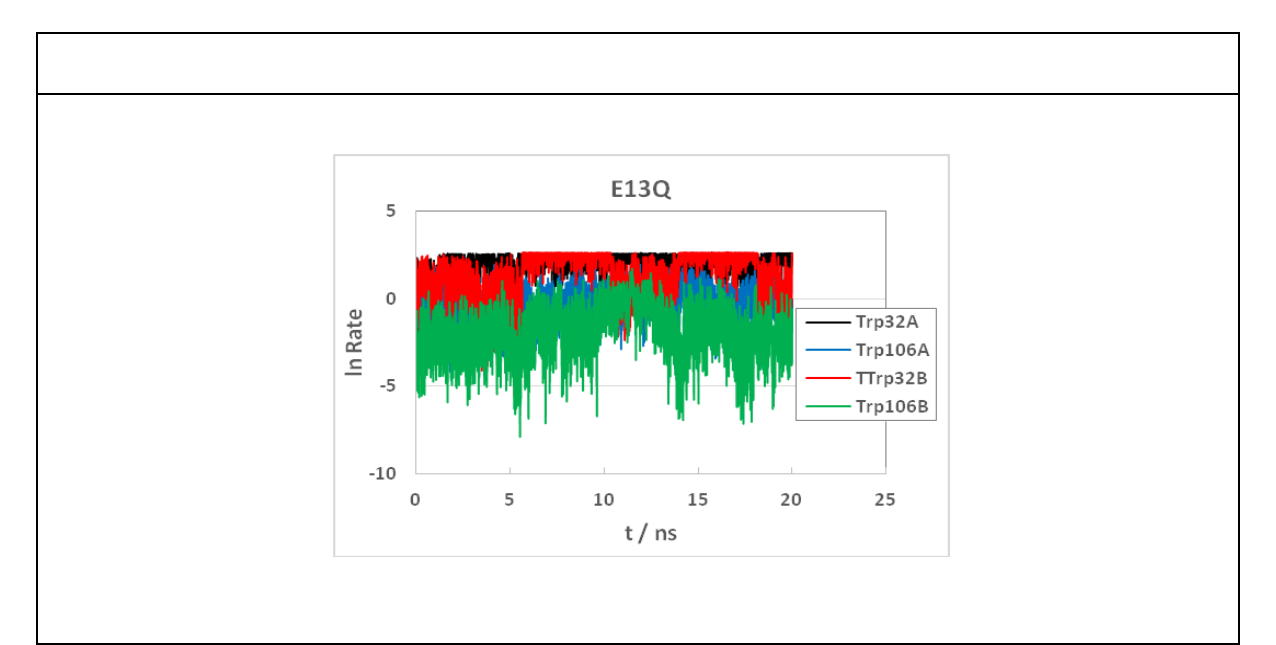
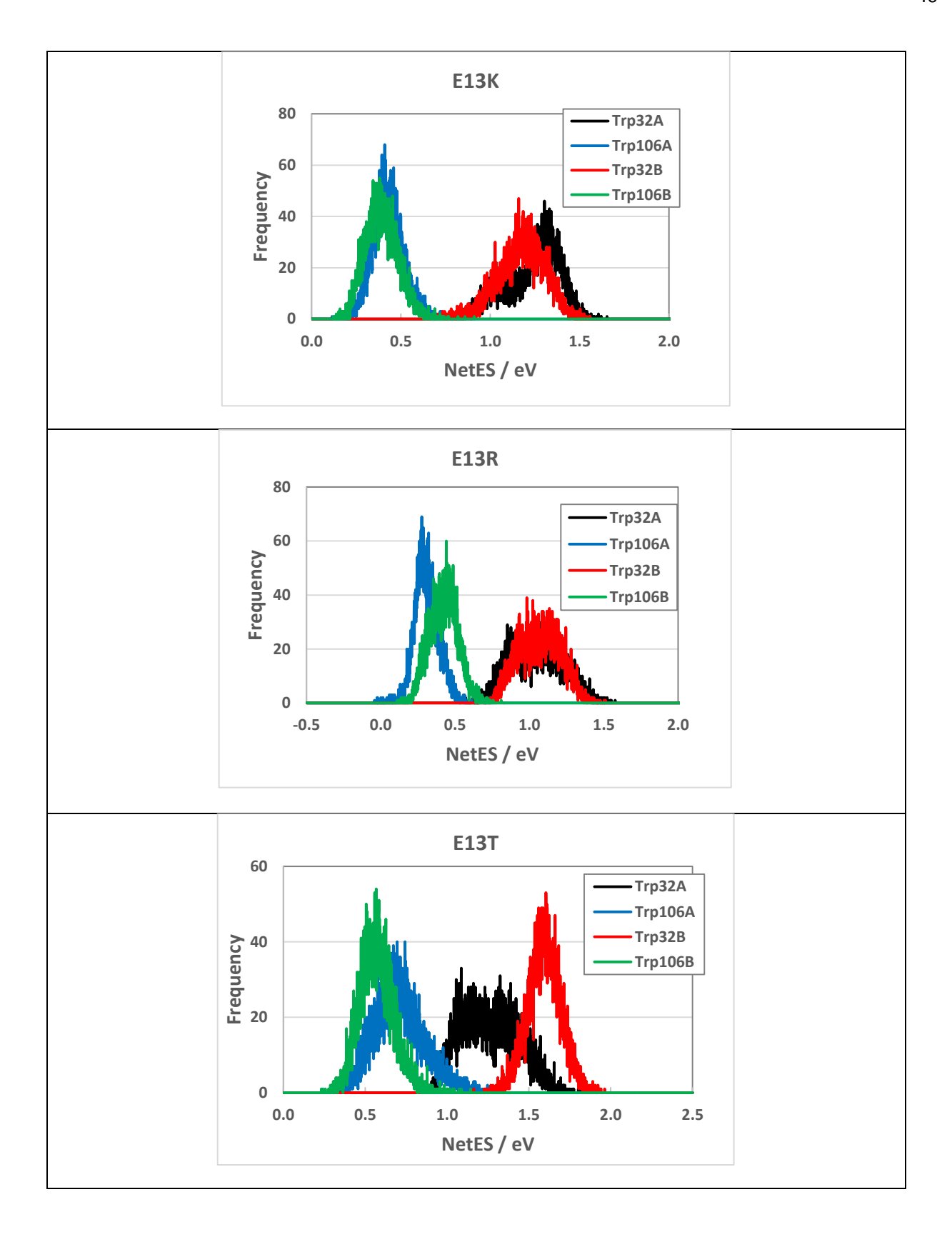


Figure 4.5 Dynamics of logarithmic ET rate. Logarithmic ET rates (ln Rate) were obtained by Eq. (3.1) in SM with ET parameters listed in Table 4.3. Trp32A and Trp32B denote Trp32 in Sub A and Sub B, respectively.



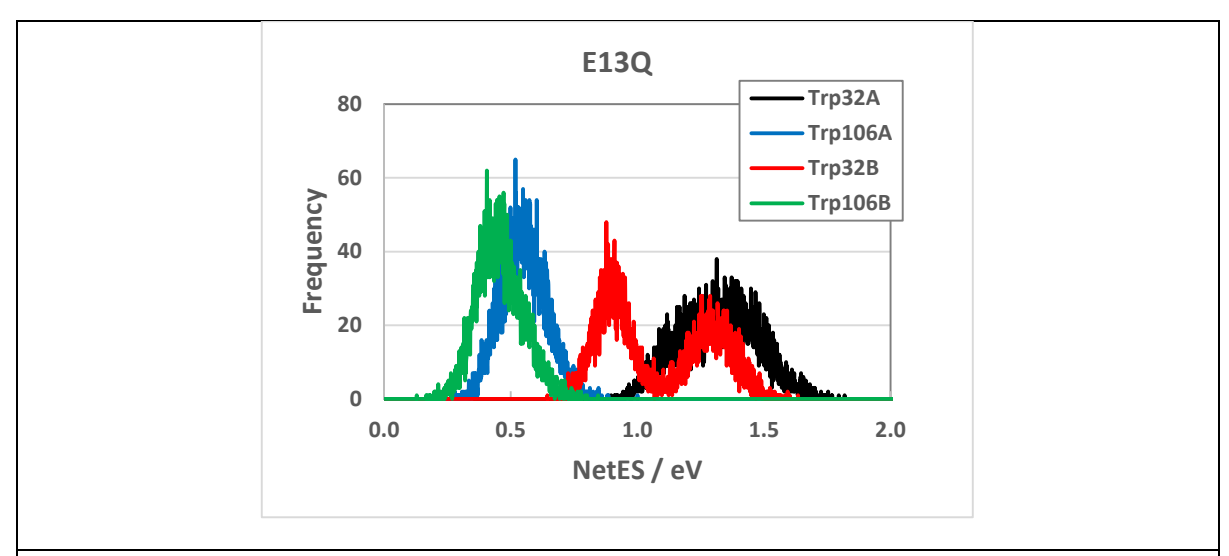


Figure 4.6 Distribution of NetES in the FBP dimers

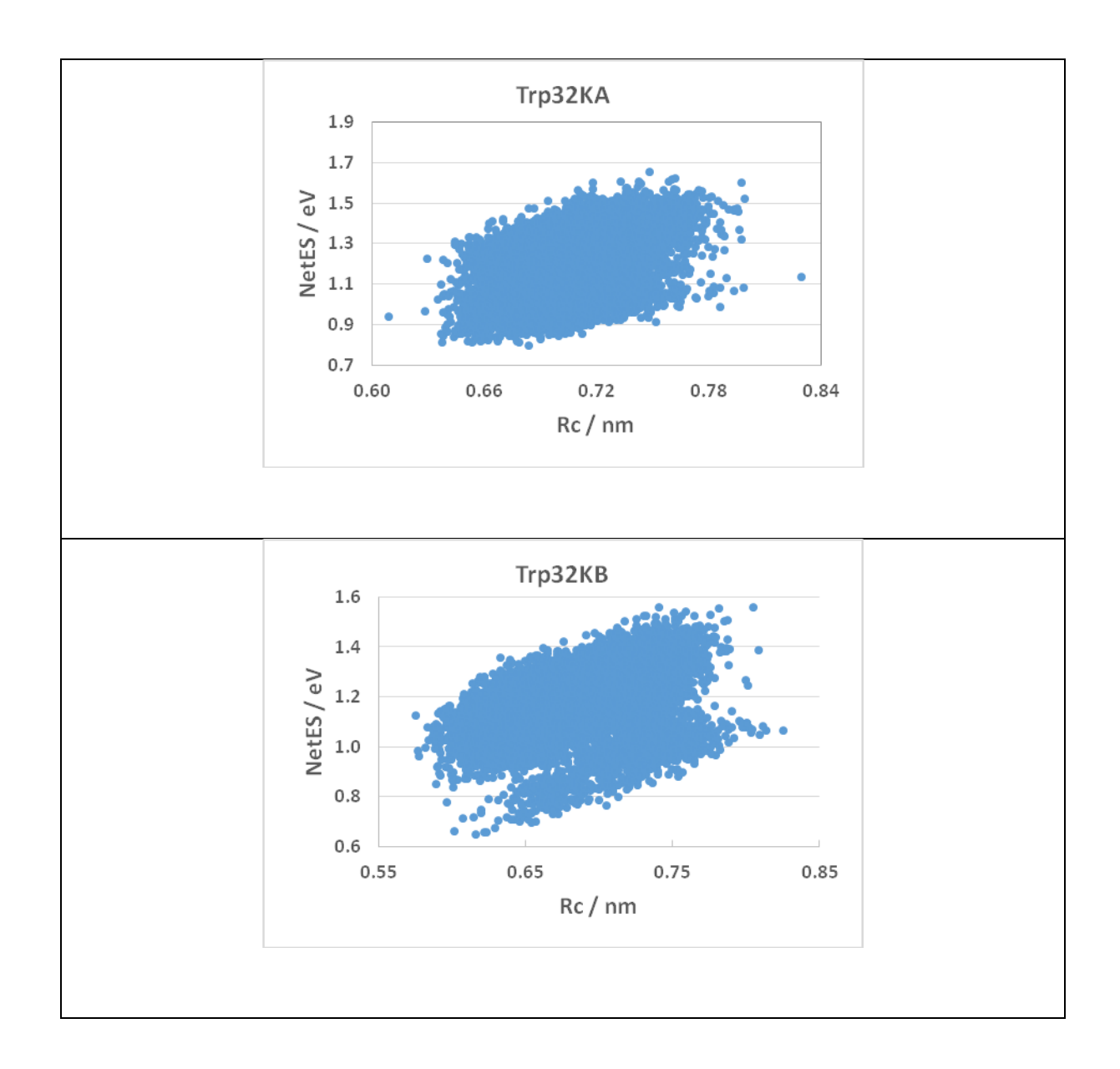
The NetES is given by Eq. (3.12). Trp32A, Trp32B, Trp106A and Trp106B in inserts denote Trp32 in Sub A and Sub B, and Trp106 in Sub A and Sub B, respectively.

## 4.1.5 Dependence of NetES on Rc

Figure 4.7 shows the relationship of NetES *vs* Rc for some donors, which were not uniform. The relations in Trp32KA and Trp32KB seemed to display two groups of NetES at higher and lower parts, as shown in the top and second panels. The distinction of the NetES into two groups was more pronounced in Trp32KB than in Trp32KA.

The correlation was not clear between the NetES *vs* Rc relation (Figure 4.7) and the distribution of the NetES with time (Figure 4.4). The distributions of Trp32KA, Trp32RA, Trp32TA and Trp32QB displayed double maxima (Figure 4.4). However, the NetES *vs* Rc relationship did not show much heterogeneity with Trp32KA, Trp32RA and Trp32TA. The distribution of NetES in Trp32KA displayed clear double maxima, but the heterogeneity in the NetES *vs* Rc relation was not as pronounced as in the second panel of Figure 4.7. Further the distribution in Trp32QB did not show any double maxima, but the NetES and Rc relation displayed

two distinct groups as in the bottom panel of Figure 4.7, though its distribution was broad. In Trp32QB the distribution of NetES displayed clear double maxima, and the NetES *vs* Rc relation also displayed two distinct groups.



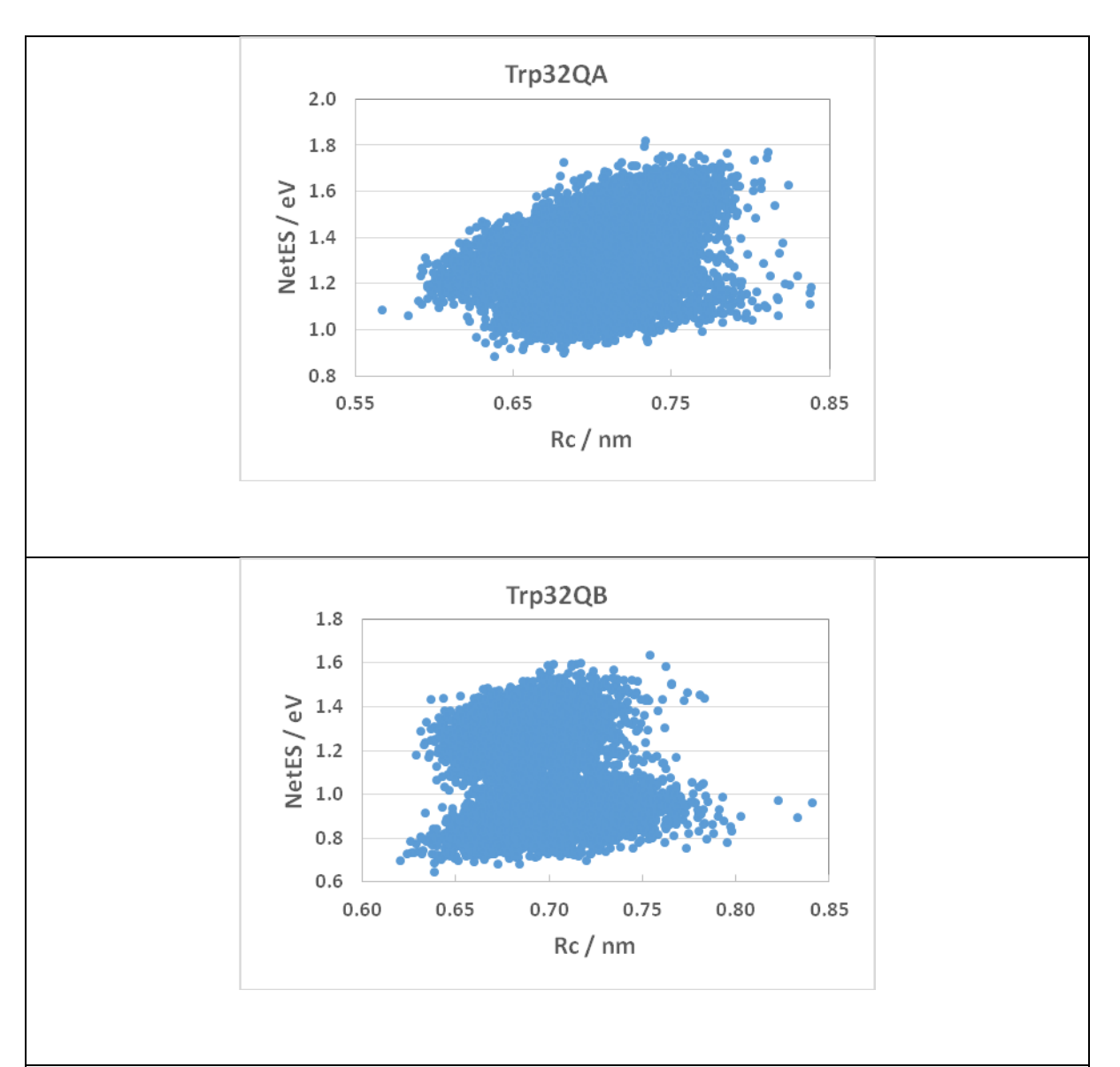
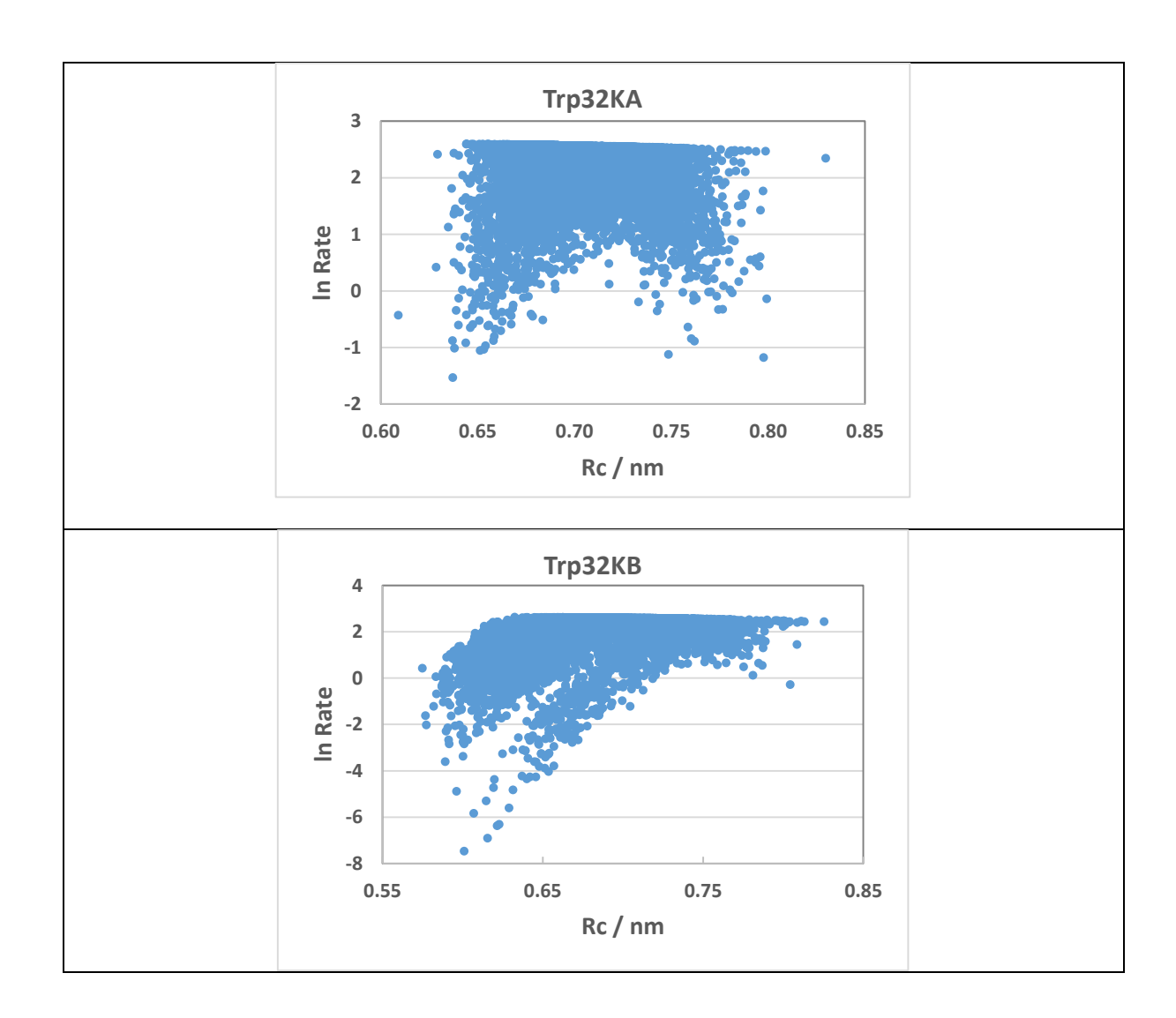


Figure 4.7 NetES *vs* Rc relation in Trp32KA, Trp32KB, Trp32QA and Trp32QB. NetES is given by Eq. (3.12). Trp32KA and Trp32KB denote Trp32 in Sub A and Sub B of E13 FBP dimer, respectively. Likewise, Trp32QA and Trp32QB denote Trp32 in Sub A and Sub B of E13Q, respectively.

# 4.1.6 Dependence of ln Rate on Rc

The linear relation of the ln Rate with Rc is called the Dutton rule, which was experimentally demonstrated in photosynthetic proteins. Figure 4.8 shows the relationships of the ln Rate and Rc in FBP dimers in some donors. In any donors in this figure, the relationships of ln Rate and Rc were not linear nor simply parabolic [63]. In these donors, the mean values of NetES were quite great, and further, the NetES *vs* Rc relation displayed at least two distinct groups. The ln Rate in these donors exhibited much more complicated functions of Rc, which are ascribed to heterogeneity in the NetES *vs* Rc relations, as shown in Figure 4.7.



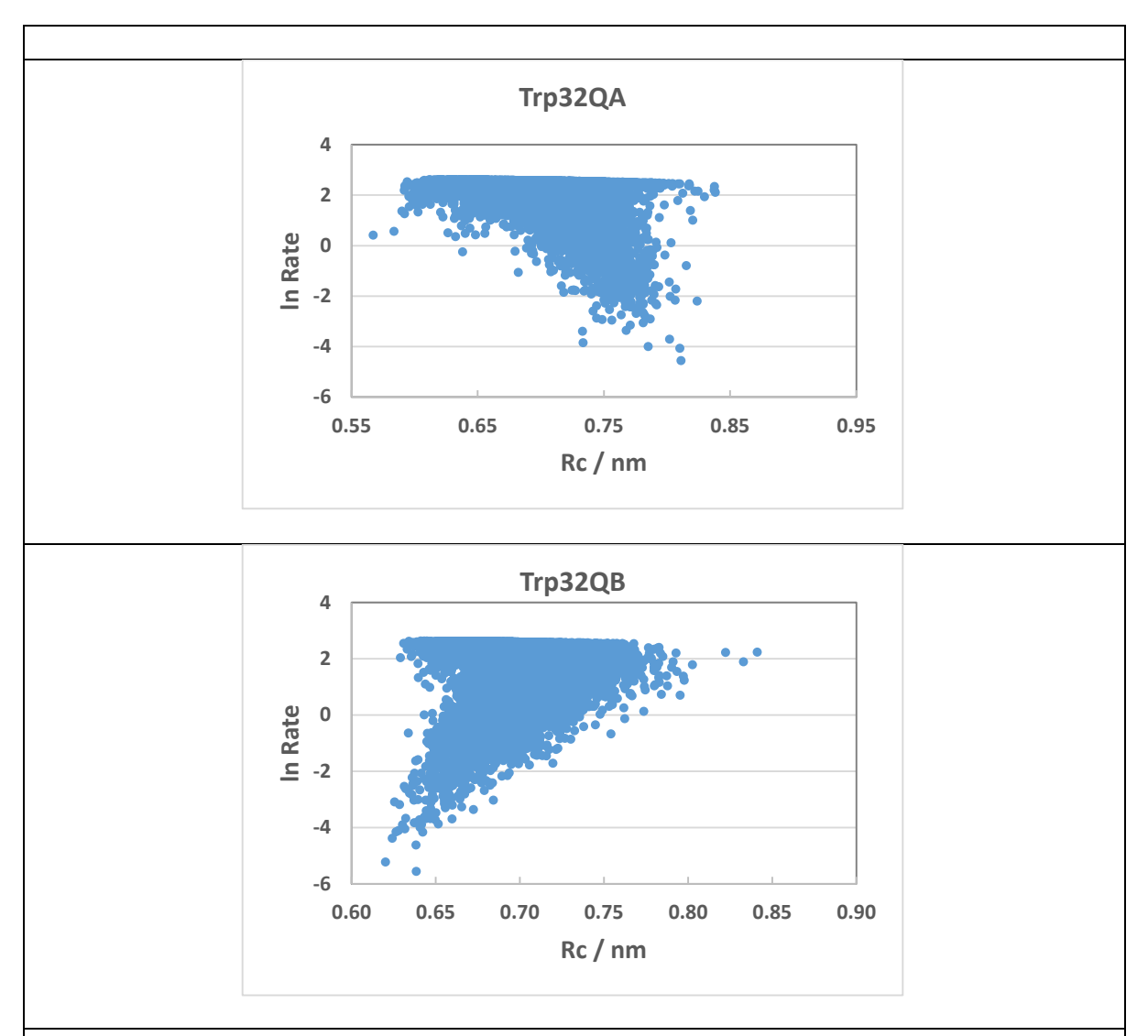


Figure 4.8. Relationships between ln Rate and Rc in Trp32KA, Trp32KB, Trp32QA and Trp32QB. The values of ln Rate were obtained by Eq. (1) in text with ET parameters listed in Table 4.3 in SM. Trp32KA, Trp32KB, Trp32QA and Trp32QB denote Trp32 in Sub A and Sub of E13K, and Trp32 in Sub A and Sub B of E13Q, respectively.

### 4.1.7 Relative magnitude of GP and NetES

The mean values of the GP as defined by Eq. (3.10) are listed in Table 4.4. When the NetES was not negligible compared to the GP, the ET rates were strongly dependent on NetES. The relations of the ln Rate *vs* Rc in FBP dimers were very much influenced by the NetES *vs* Rc relations. The mean values of GP in Trp32A were -1.21 in E13K, -1.11 in E13R, -1.51 in E13T and -1.21 eV in E13Q. The values of GP in Trp32B were -1.29 in E13K, -1.15 in E13R, -1.56 in E13T and -1.26 eV in E13Q. The values did not differ much between Trp32A and Trp32B in all the dimers. The values of GP in Trp106A were -0.94 in E13K, -0.88 in E13R, -1.24 in E13T and -0.93 eV in E13Q. The values of GP in Trp106B were -0.98 in E13K, -0.88 in E13R, -1.27 in E13T and -0.96 eV in E13Q. In the WT, the absolute values of the GP are higher than those of NetES in all donors [24]. However, the absolute values of the GP were comparable or lower than those of NetES in any donors in E13K, E13R, E13T and E13Q.

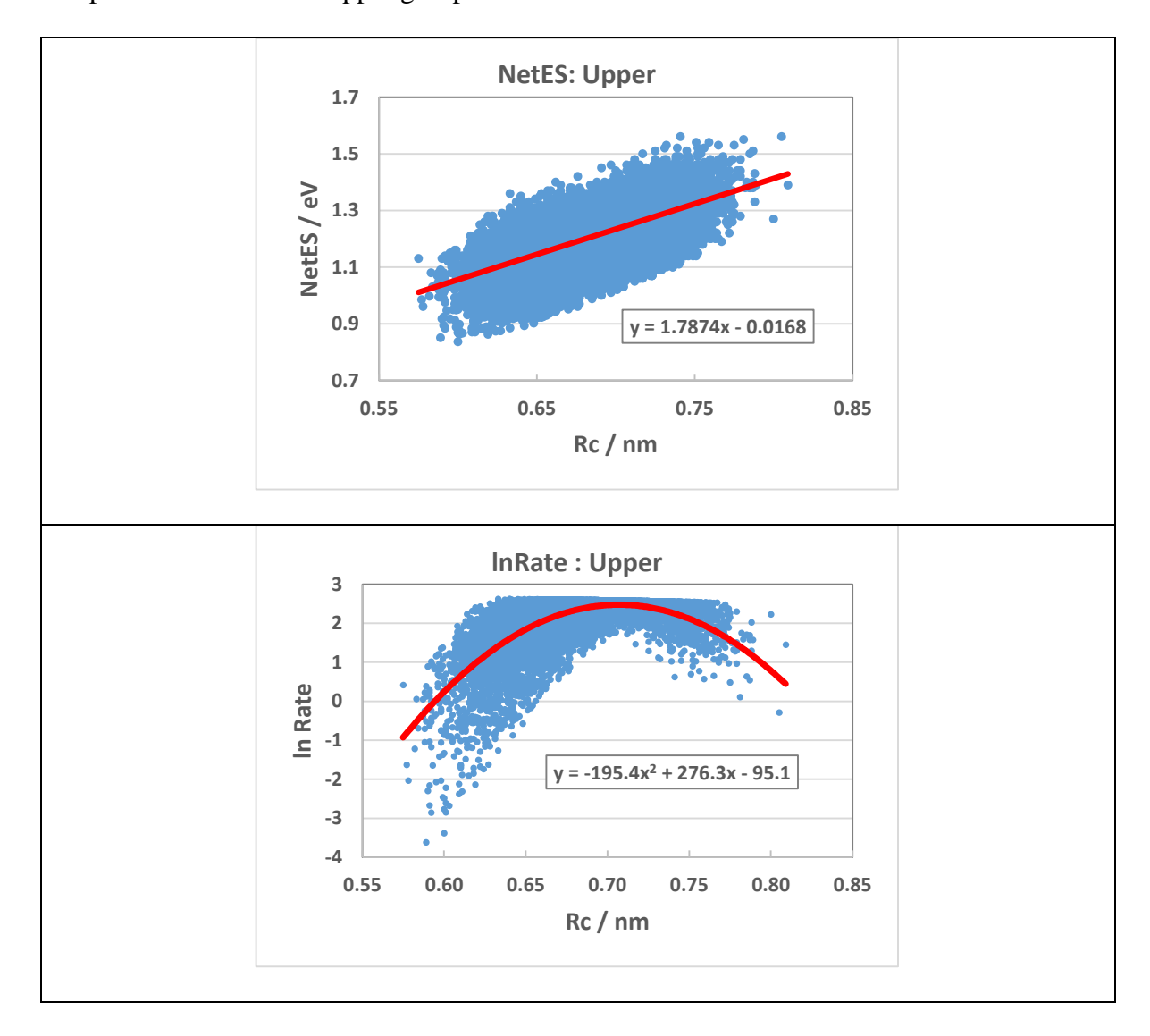
### 4.1.8 Comparison of NetES and ET rates between dimer and monomer

The ET rates and related quantities for the FBP monomer are listed in Table 4.4 for comparison. The data in Table 1 for the monomers were revised from the reported values [61; 63] where the  $G_M^0$  is given by Eq. (3.3) in the SM and was common in all FBP monomers, and different among the dimers in the present work [62]. Using different values of  $G_M^0$  for each dimer, the fittings between the experimental and calculated decays were much improved. The values of NetES remarkably increased in the dimers compared to those in the monomers. This should be ascribed to the formation of the dimer, and thus the NetES of a donor in Sub A was influenced by the ionic groups in Sub B, and *vice versa*. In the monomers, the absolute values of NetES were always smaller than GP (Table 4.4), while those in the dimers were not negligible compared to the GP. The ET rates of Trp106 in the dimers increased more than 1000 times compared to those of the corresponding monomers, while the rates of Trp32 in any dimers did not differ much from those in the monomers.

#### 4.1.9 Separation of NetES and In Rate into two groups

Figure 4.9 shows two groups of NetES vs Rc and ln Rate vs Rc relations in Trp32KB. The NetES and Rc relation was separated with a straight line determined by the coordinates (Rc = 0.596 nm, NetES = 0.776 eV) and (Rc = 0.801 nm, NetES = 1.25 eV). The upper group denotes an ensemble of the NetES data above this straight line and lower group below the straight line. The top panel of Figure 4.9 shows the relationship of NetES and Rc in the upper group. The values of NetES displayed a tendency to increase with Rc, though the data scattered a lot. The approximate linear function was  $y = 1.787 \times -0.017$  (y, NetES; x, Rc). The second panel shows the ln Rate vs Rc relation in the upper group. The values of the ln Rate displayed an approximate

parabolic function,  $y = -195.4 \text{ } x^2 + 276.3 \text{ } x - 95.1$ . The third panel shows the relationship of NetES vs Rc in the lower group. The values of NetES increased with Rc, for which the approximate function was y = 2.131 x - 0.580. The slope of the NetES vs Rc functions was 2.13 in the lower group while 1.79 in the upper group. The relationship of ln Rate vs Rc in the lower group displayed a parabolic function,  $y = -284.4 \text{ } x^2 + 442.4 \text{ } x - 169.8$ , in which the data were less scattered when compared to those in the upper group.



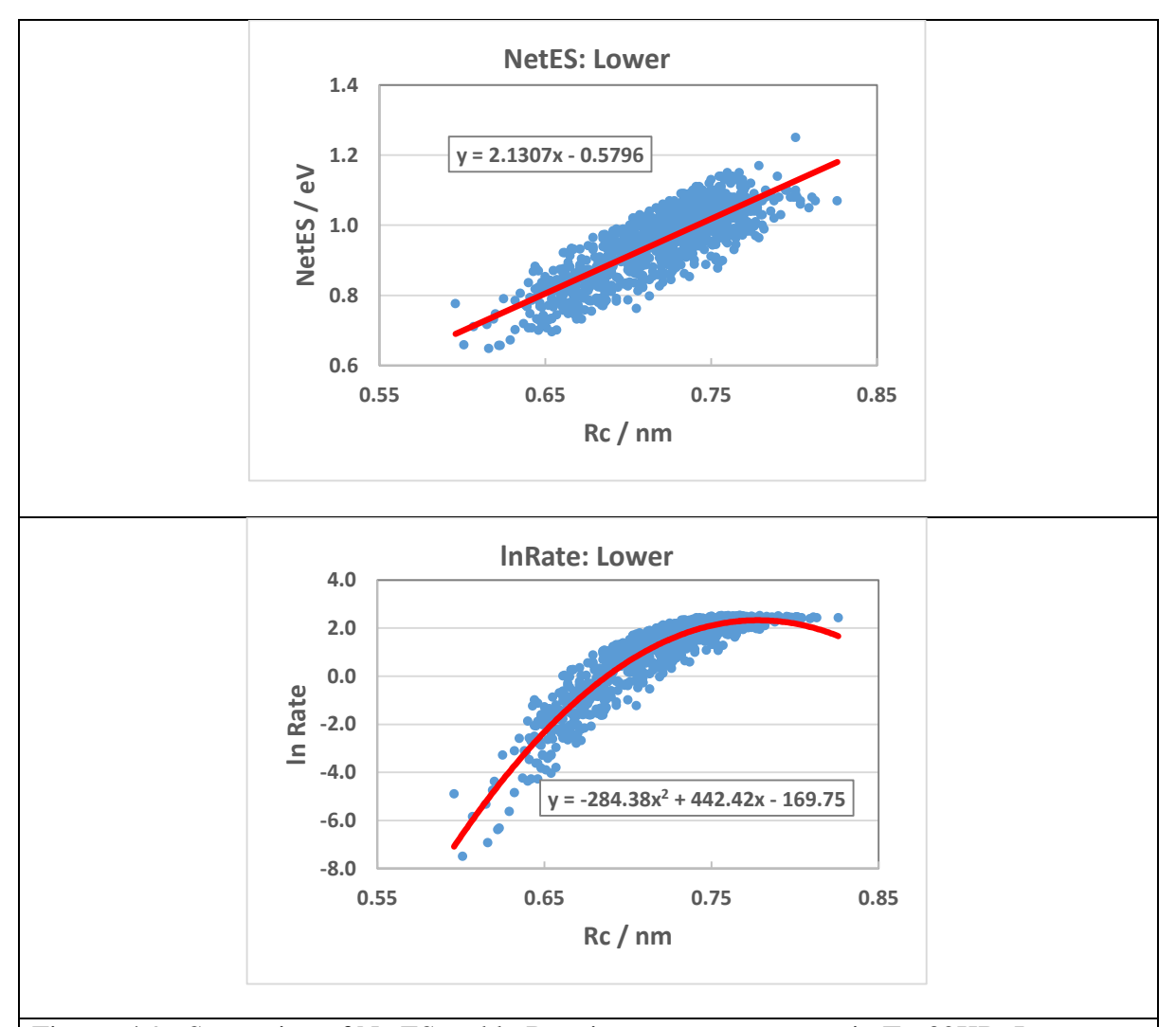
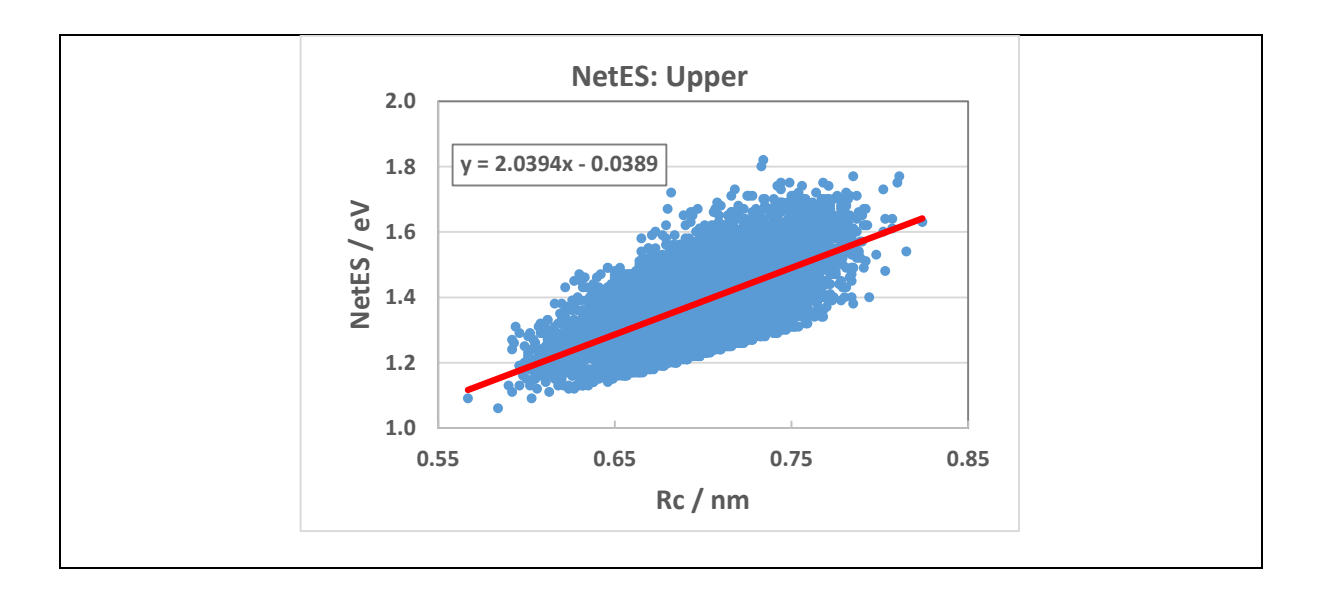


Figure 4.9 Separation of NetES and ln Rate into two components in Trp32KB. Inserts show approximate functions of NetES or ln Rate (y) with Rc (x). The data of NetES in Figure 4.7 is divided with a straight line determined by Rc = 0.569 nm and NetES = 0.776 eV, and Rc = 0.801 nm and NetES = 1.25 eV. Upper and Lower denote upper and lower groups of the NetES above and below the straight line.

Figure 4.10 shows the relations of NetES vs Rc and ln Rate vs Rc in Trp32QA. The top panel shows the dependence of NetES on Rc. The values of NetES linearly increased with Rc, for which the approximate function was y = 2.040 x - 0.039. The second panel shows the ln Rate and Rc relation in the upper group. The values of the ln Rate changed with an approximate parabolic function,  $y = -191 \text{ x}^2 + 248 \text{ x} - 77.9$ . The third panel shows the NetES vs Rc relation in the lower group, for which the values of NetES increased with a linear function of Rc, y = 0.838 x + 0.534. The slope of the linear function was 0.84 in the lower group, while it was 2.04 in the upper group. The bottom panel shows the ln Rate vs Rc relation in the lower group. The approximate function was  $-81.9 \text{ x}^2 + 121 \text{ x} - 42.2$ .



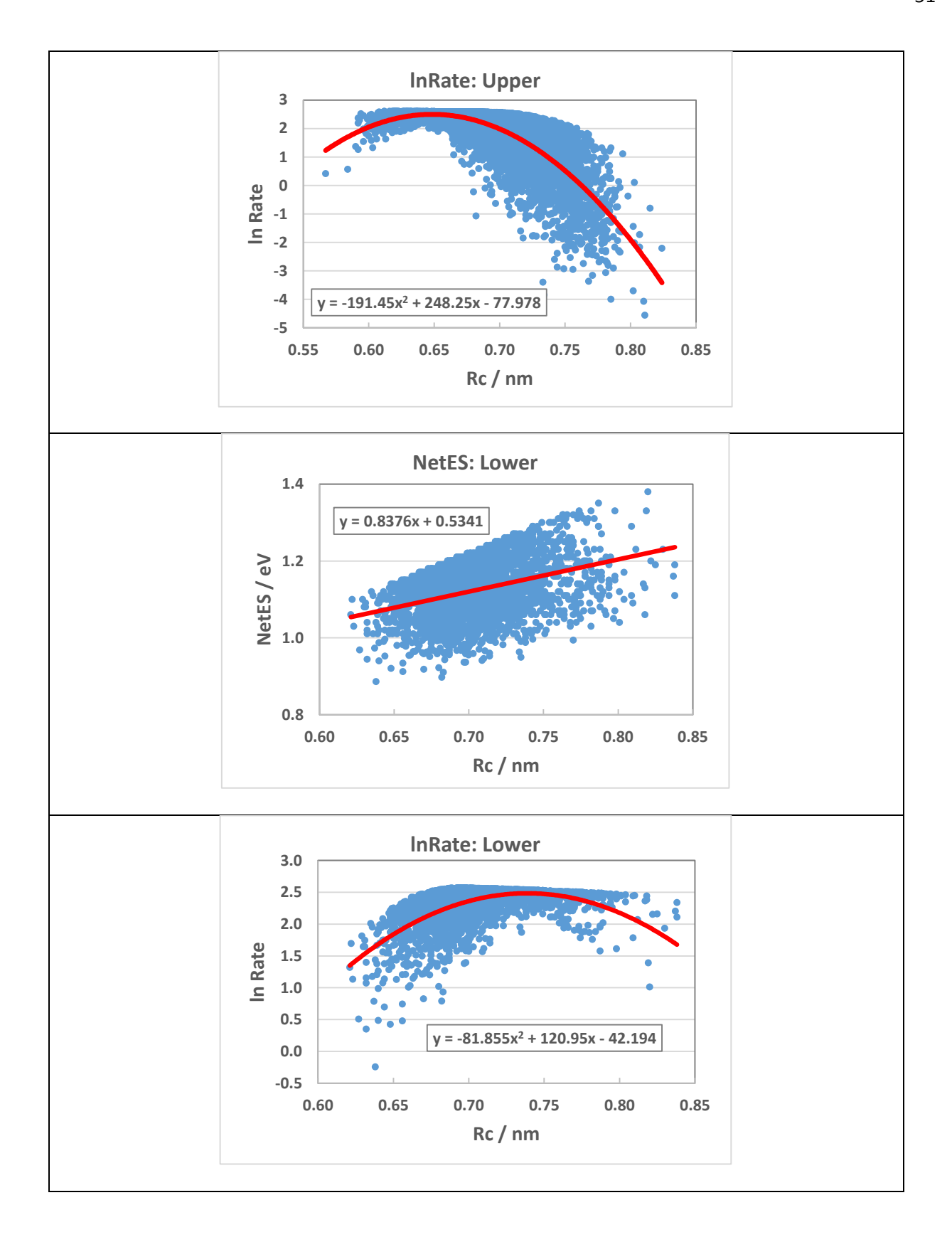
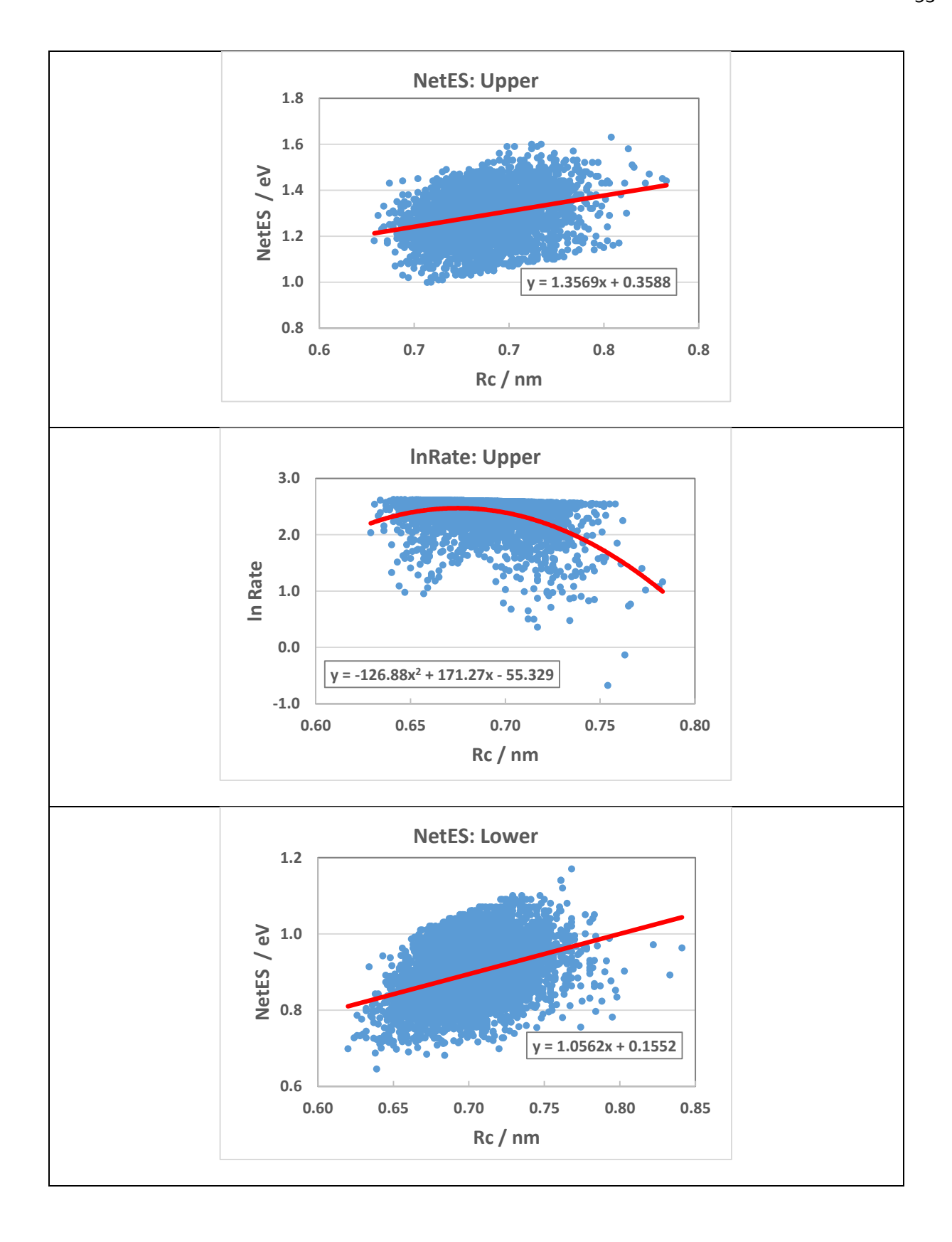


Figure 4.10 Separation of NetES and ln Rate into two components in Trp32QA. Inserts show approximate functions of NetES or ln Rate (y) with Rc (x). The NetES data in Figure 4.7 is divided with a straight line determined by Rc = 0.622 nm and NetES = 1.10 eV, and Rc = 0.798 nm and NetES = 1.33 eV. Upper and Lower denote the data above and below the line.

Figure 4.11 shows the relations in Trp32QB. The NetES vs Rc relation in the upper group shown in the top panel approximately increased with a linear function of Rc, y = 1.36 x + 0.36, though the linearity was much poorer than the other donors. The ln Rate vs Rc relation is shown in the second panel. The ln Rate values were more scattered with the Rc. The values of the ln Rate were approximated with a parabolic function of Rc,  $y = -127 x^2 + 171 x - 55.3$ . The NetES and Rc relation in the lower group is shown in the third panel. The values of NetES were more scattered with Rc, as in the upper group. The approximate function of NetES with Rc was y = 1.06 x + 0.16. The bottom panel shows the ln Rate and Rc in the lower group. The approximate function of the ln Rate with Rc was  $y = -233 x^2 + 358 x - 136$ .

The complex profiles of the ln Rate *vs* Rc relationship became much clearer when the NetESs were separated into two groups. This suggests that the proteins hold at least two conformations, which were especially clear in Sub B of E13K and in both Sub A and Sub B of E13Q. The heterogeneity in Sub B of E13K and in the Sub A and Sub B of E13Q are considered to be brought about by conformational changes in the entire proteins, because NetES is related to all charged groups inside the dimer proteins.



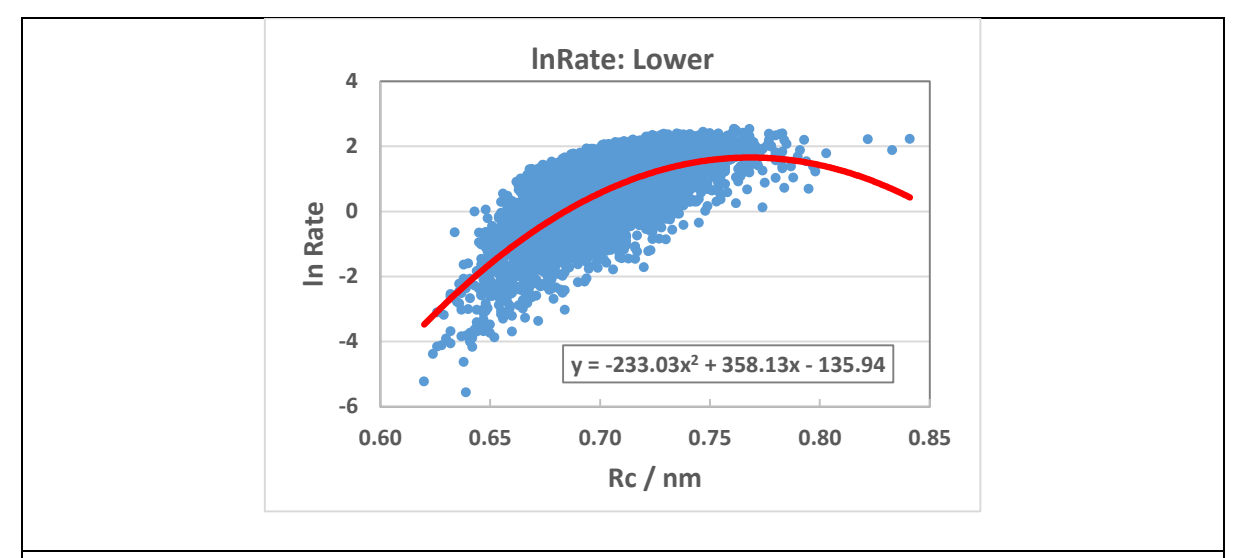


Figure 4.11. Separation of NetES and In Rate into two groups in Trp32QB. Inserts show approximate functions of NetES or In Rate (y) with Rc (x). The NetES data in Figure 4.7 is divided by a straight line determined with Rc = 0.647 nm and NetES = 1.02 eV, and Rc = 0.768 nm and NetES = 1.17 nm. Upper and Lower denote the data above and below the line.

The donor-acceptor distance is one of the most important index determining ET rates not only in flavoproteins, but also in ET phenomena in general. The ET mechanism from aromatic amino acids to Iso\* in flavoproteins has been categorized into four groups with sub-groups of adiabatic and non-adiabatic processes, through the relationship of the ln Rate and Rc. The criteria of the classification were the relative magnitudes of NetES against GP. When the absolute value of the GP is greater than that of NetES, the ln Rate displays a clear parabolic or linear function of Rc. When the NetES is dominant compared to the GP, the ln Rate *vs* Rc does not display any clear function. It was believed that NetES does not display any relations with Rc. The present work, however, has demonstrated that sometimes the NetES displays a weak relation with Rc.

The dependencies of the ET rates, NetES, SROE and ESDA on Rc were examined for the donors of Trp32 and Trp106 in both subunits in the four mutated FBP dimers. Explicit relations between the ET rate and Rc were given for SROE and ESDA in Marcus and KM rates, but not for NetES. In FBP dimers other than the WT, the absolute values of NetES were quite large and comparable to or even greater than those of the GP, as shown in Table 4.4. In the WT, the most remarkable difference between the dimer and monomer was SFEG, while the values of NetES were not so much different between the WT dimer and monomer in Trp32 as in the mutated FBP dimers. The greater values of NetES were ascribed to the formation of a dimer, in which the NetES of a donor in Sub A is influenced by Sub B, and *vice versa* as in the D-amino acid oxidase dimer [64] and pyranose 2-oxidase tetramer [65]. In some cases, the ln Rate *vs* Rc relations were determined by the NetES and Rc relations as in Trp32KB, Trp32QA and Trp32QB. In these donors, the values of NetES could be divided into two groups, and accordingly the ln Rate and Rc relation displayed two kinds of profile.

It is believed that the NetES is a useful index for the detection of conformational changes in the entire protein. The two groups in the NetES of Trp32KB, Trp32QA and Trp32QB could be due to two different conformations of the entire subunits. Similar behaviors for the NetES vs Rc relation were also found in other donors, though they were not so clear as in Trp32KB, Trp32QA and Trp32QB. The conformational change revealed that Trp106B of the WT FBP dimer may be local because it is brought about by a discontinuous change in the Rc. The relationship between the heterogeneous distribution of the NetES and heterogeneity in the NetES vs Rc relation is of interest, though it is not clear at the moment.

Recently, Ivanov's group has reported theoretical work on the ET rate in small molecules, and they emphasized the importance of a solvent reorganization from high-frequency vibrational

modes and dynamical solvent effect on the ET rate [66], based on Zusman's ET theory [67]. In flavoproteins the medium surrounding the ET donors and accepter is not uniform, as in a bulk solution. The terms of SROE plus NetES in the present systems are considered to correspond to the solvent reorganization energy in the ET processes in a bulk solution. Accordingly, the dynamic solvent effect is already taken into account through the time-dependent changes of Rc and the NetES. In flavoproteins, the ET takes place from Trp or Tyr in the ground state to Iso\*, so the population of the vibrational modes should be mostly in the lowest vibrational-energy level at room temperature. It is conceivable that the ET takes place from the donors in the ground states to higher vibration states of Iso\*. The effects of the higher vibrational modes on the ET rate have been already reported by Bixon and Jortner (BJ theory). In our earlier work, the non-exponential fluorescence decay of the WT was analyzed with the Marcus and Huch (MH) theory, BJ theory and KM theory, and the values of  $\chi^2$  between the experimental and calculated decays were compared among these theories. The values of  $\chi^2$  were 1.83 x  $10^{-4}$  with the MH theory, 4.31 x 10<sup>-4</sup> with the BJ theory and 1.47 x 10<sup>-4</sup> with the KM theory. The vibrational relaxation from the higher states to the fluorescent state in Iso\* in flavoproteins should be much faster than the solvent relaxation time of the amino acids near to the donors and acceptor, which is because the amino acids are covalently linked by peptide bonds, and further free water molecules do not exist near Iso in FBP dimers, as in other flavoenzymes.

Currently, satisfactory results on the ET phenomena in flavoproteins have been obtained with the present method with relation to the following points: 1) the structure of each subunit is not equivalent: the flavoproteins consist of two subunits in a complex dimer of D-amino acid oxidase with benzoate or four subunits in pyranose 2-oxidase, which have been verified by the experimental fluorescence dynamics. 2) A temperature induced transition of the protein structure

in D-amino acid oxidase, as experimentally found in earlier work was satisfactorily elucidated with ET parameters [34]. 3) The static dielectric constants near ET donors and acceptor obtained by the present method have been elucidated with the presence of water molecules near Iso obtained by MDS as discussed in previous work. 4) The Dutton rule has been demonstrated in the ET processes with relatively slow rates in FBP and D-amino acid oxidase dimer.

# 4.2 residue electrostatic energy in flavin mononucleotide binding protein dimer

## 4.2.1 Dynamics and distributions of REST of some ionic residues

A snapshot of the protein structure of wild type FBP dimer is shown in Figure 4.12. The structures display quite different between Sub A and Sub B. Figure 4.13 shows the dynamics and distributions of REST of Glu13 obtained by Eq (3.18). The distances of Glu13 from Iso are 1.25 nm in Sub A and 1.51 nm in Sub B. Figure 4.13A shows four components of the REST, RESTAA, RESTAB, REST BA and REST BB, where the REST AA denotes REST of Glu13 in Sub A interacting with all atoms in Sub A except for those of Glu13 in Sub A, REST AB one in Sub A interacting with all atoms in Sub B, REST BA, the REST of Glu13 in Sub B interacting with all atoms in Sub A, and REST BB, one in Sub B interacting with all atoms in Sub B except for those of Glu13 in Sub B.

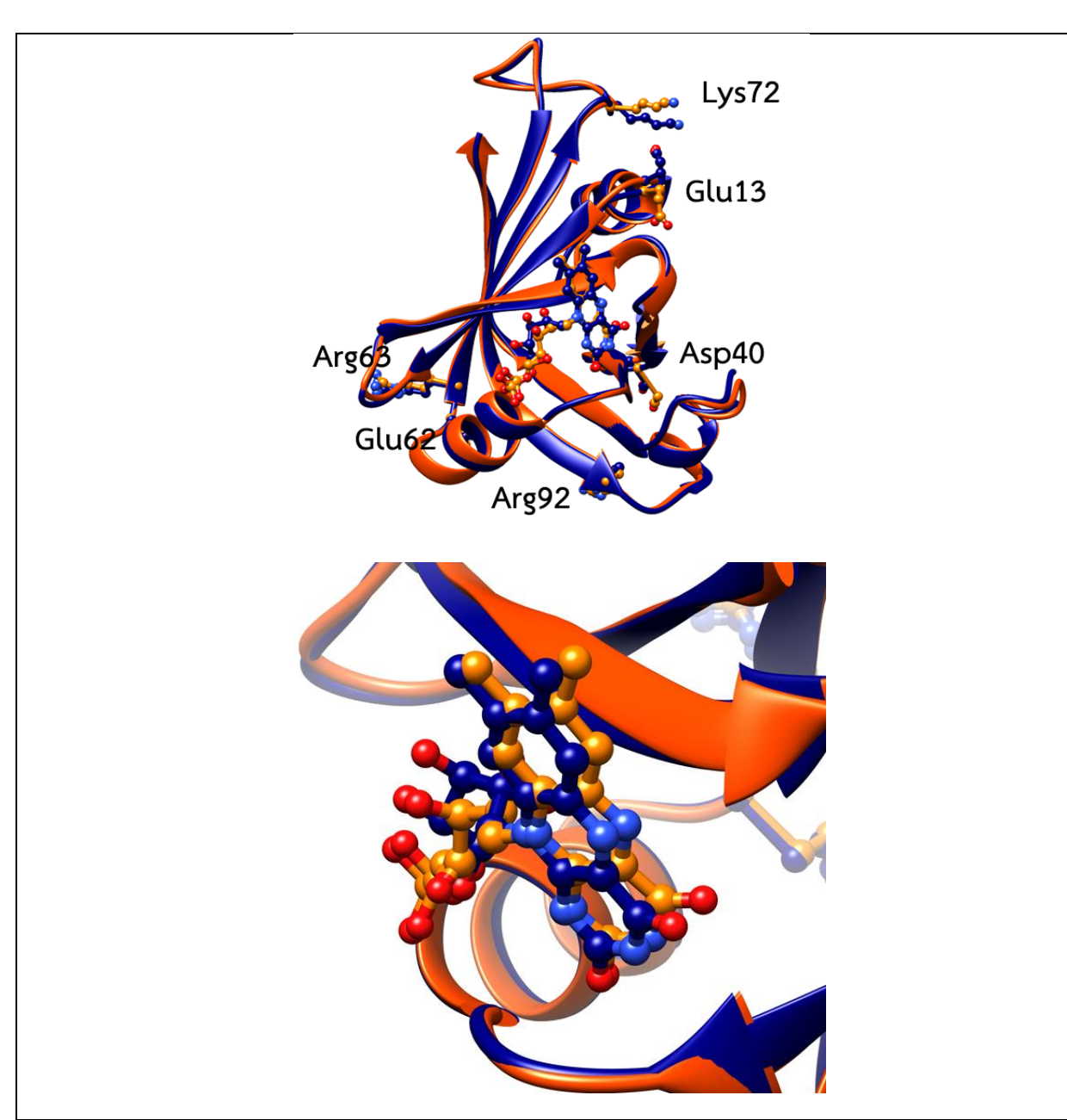
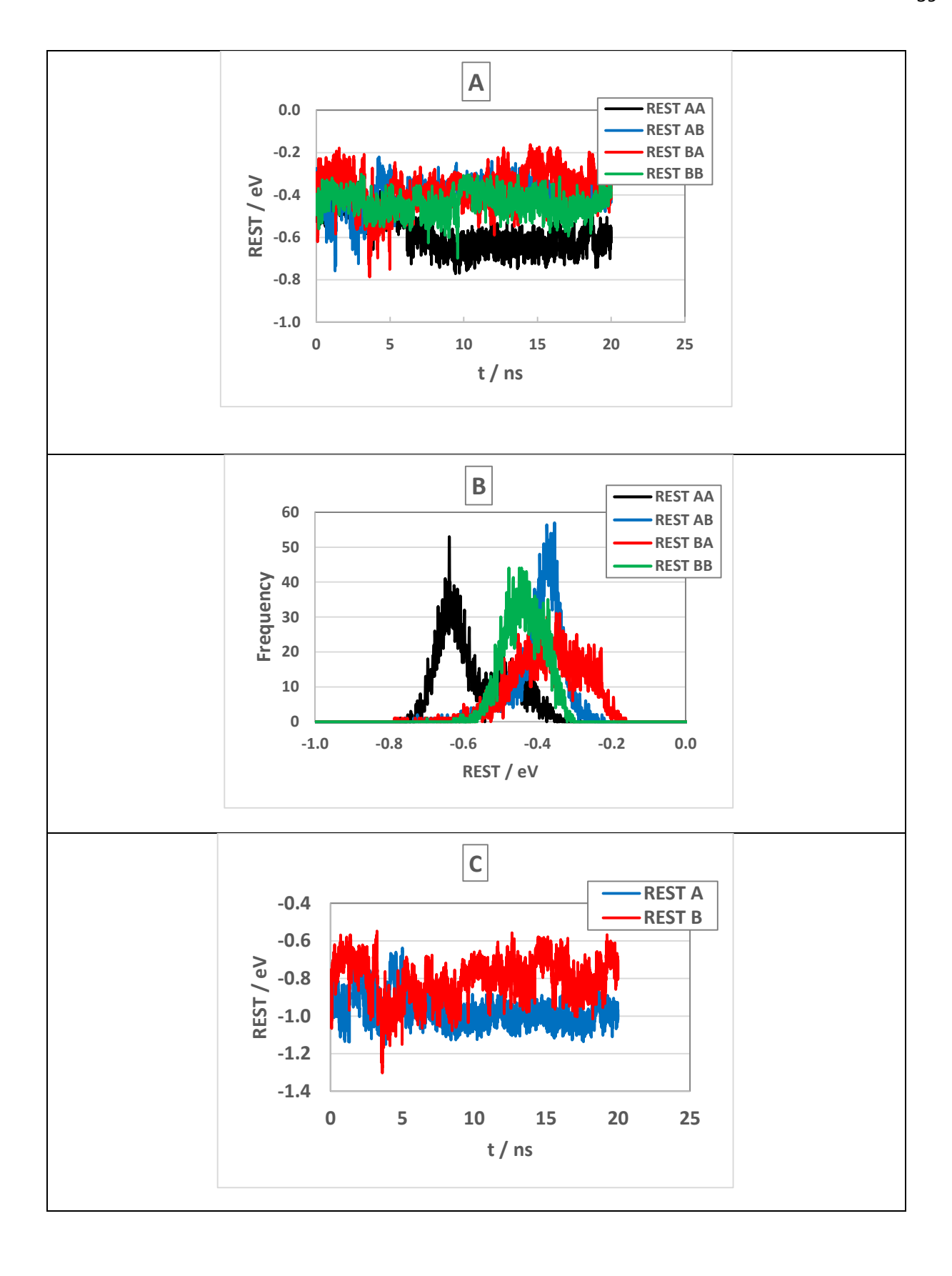


Figure 4.12 Structural comparison of the MD structures between the two subunits

Upper panel shows the whole structures, where Sub A is illustrated in blue and Sub B in orange.

The residues of FMN, Glu13, Asp40, Glu62, Arg 63 and Arg 92 are shown with ball model.

Bottom panel shows the structures near isoalloxazine ring.



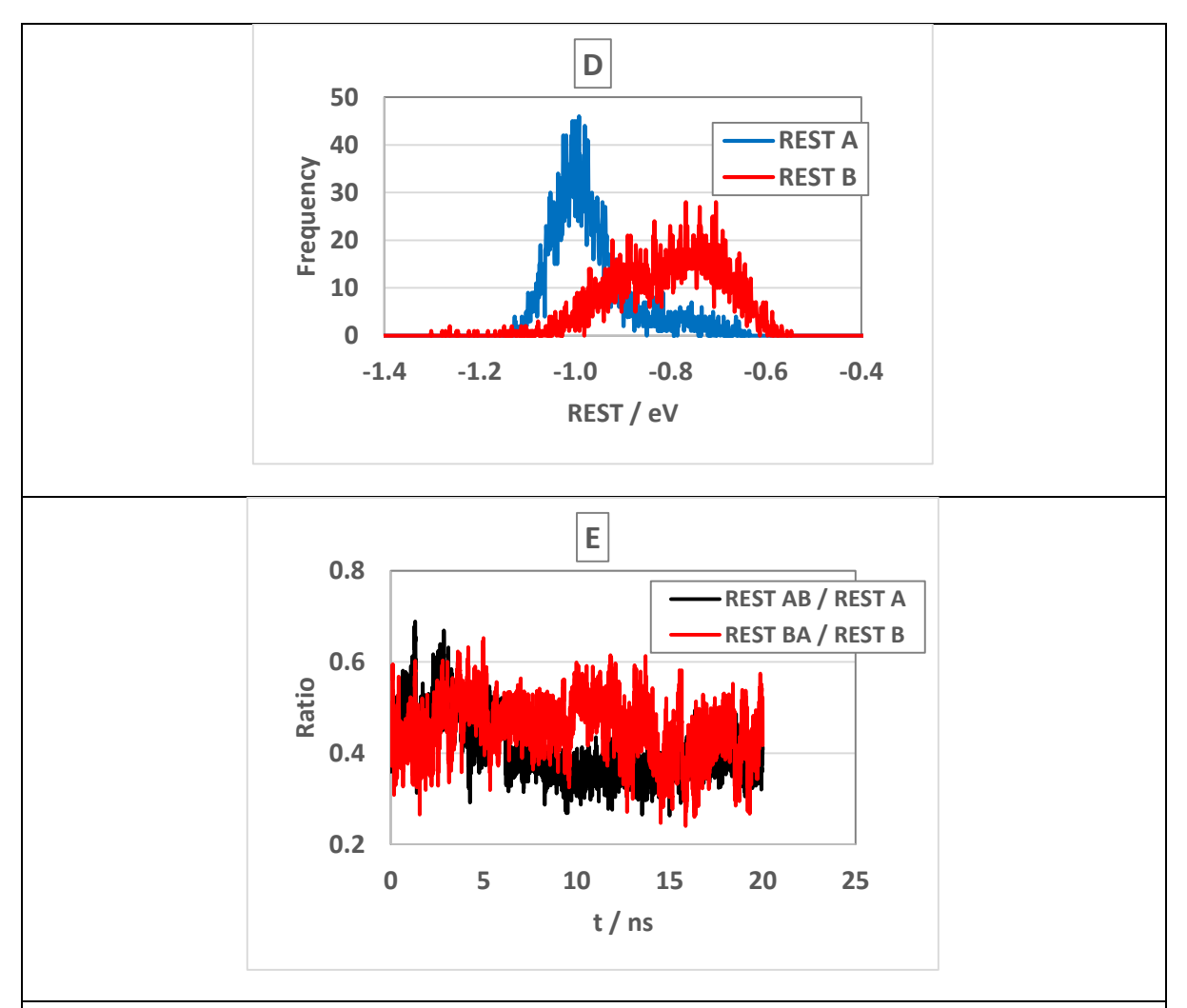


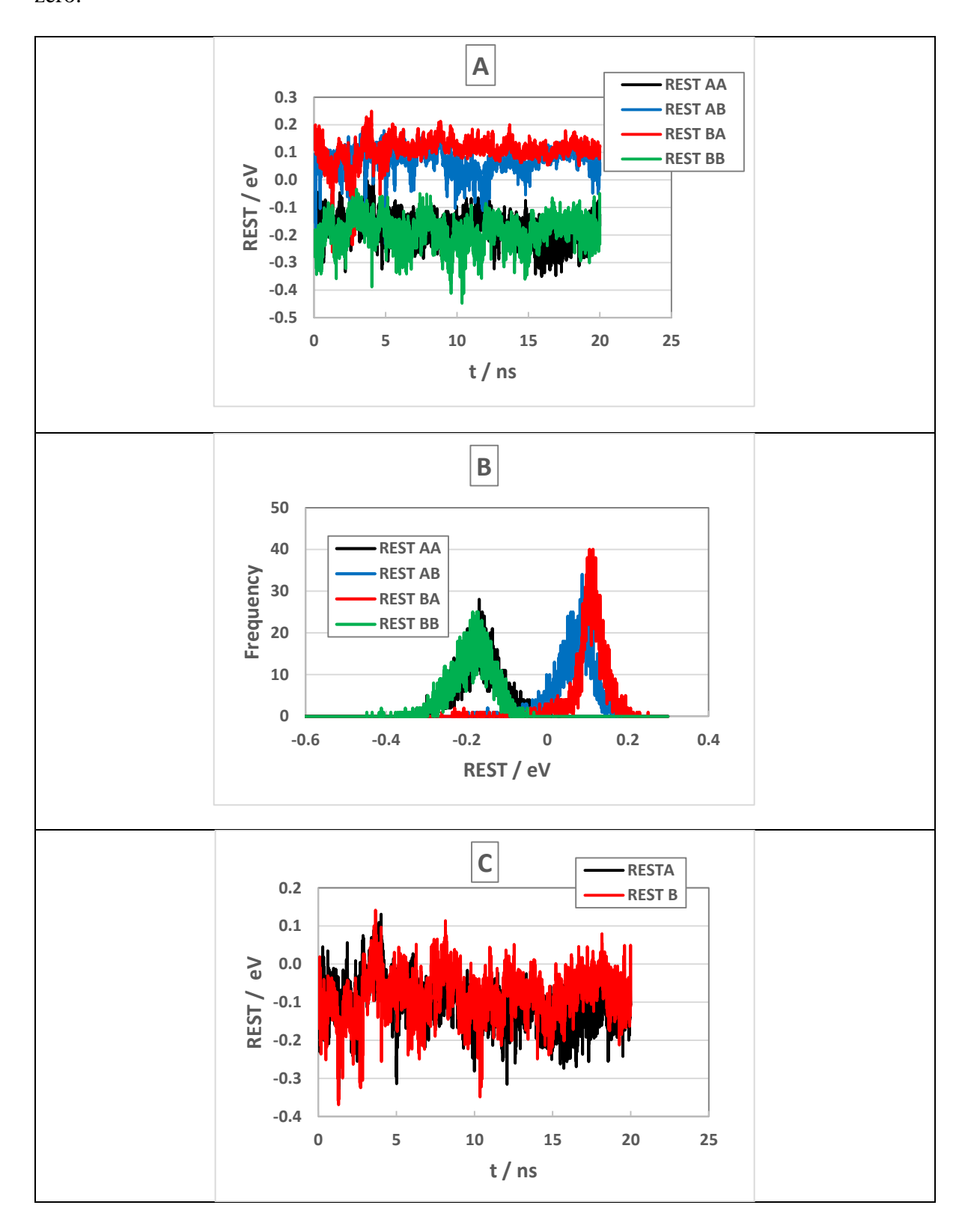
Figure 4.13 Dynamics and distribution of REST of Glu13

The values of REST were obtained with Eq (3.18). The four components of REST of Glu13 shown by REST AA, REST AB REST BA and REST BB in inserts denote REST of Glu13 within Sub A, and that between a residue in Sub A and those in Sub B, that between a residue in Sub B and those in Sub A and within Sub B. Panel A shows dynamics of the four components of the REST. Panel B shows their distributions. Panel C shows dynamics REST A (REST AA + REST AB) and REST B (REST BA + REST BB). Panel D shows the distributions of REST A and REST B. Panel E shows ratios of REST AB / REST A and REST BA / REST B.

The values of REST greatly fluctuated with MDS time in all components. Figure 4.13B shows the distributions of these components. The distribution REST AA displayed a main peak at around -0.65 eV, which was greatest in magnitude among the four components, and additional minor peak at around -0.45 eV. The distributions of REST AB and BB displayed sharp single peaks, while that of REST BA broad band with a shoulder at around -0.25 eV. Figure 4.13C shows time-evolutions of REST A (REST AA + REST AB) and REST B (REST BA + REST BB). The values of REST A were mostly lower than those of REST B. Figure 4.13D shows the distributions of REST A and REST B. The peak distribution of REST A was at around -1.0 eV, while that of REST B was -0.75 eV. The distribution of REST A displayed a minor peak at around -0.8 eV, which is ascribed to double-maxima distribution of REST AA. Figure 4.13E shows time-evolutions of fractions of REST AB / REST A, and REST BA / REST B, which represent contributions of REST in one subunit from the other. The contributions of REST from the other subunit were quite high by around 50 % of REST A or REST B.

Figure 4.14 shows the dynamics and distributions of REST in Lys72 with positive charge. Figure 4.14A shows time-evolutions of REST AA, REST AB, REST BA and REST BB. The values of REST AB and REST BA displayed mostly positive while those of REST AA and REST BB were always negative. The absolute values of REST AA and REST BB were about half of those in Glu13. Figure 4.14B shows the distributions of the four components. The peak distributions of REST AA and REST BB were at around -0.2 eV while those of REST AB and REST BA ca. 0.1 eV. Time-evolutions of total values of REST A and REST B are shown in Figure 4.14C. They fluctuated around -0.1 eV. Figure 4.14D shows the distributions of REST A and REST B, of which values at peak distributions were both similar, -0.1 eV. Figure 4.14E shows time-evolutions of the ratios, REST AB / REST A and REST B. The values were very

high by *ca.* 8000 at some MDS times, where the values of REST A or REST B became close to zero.



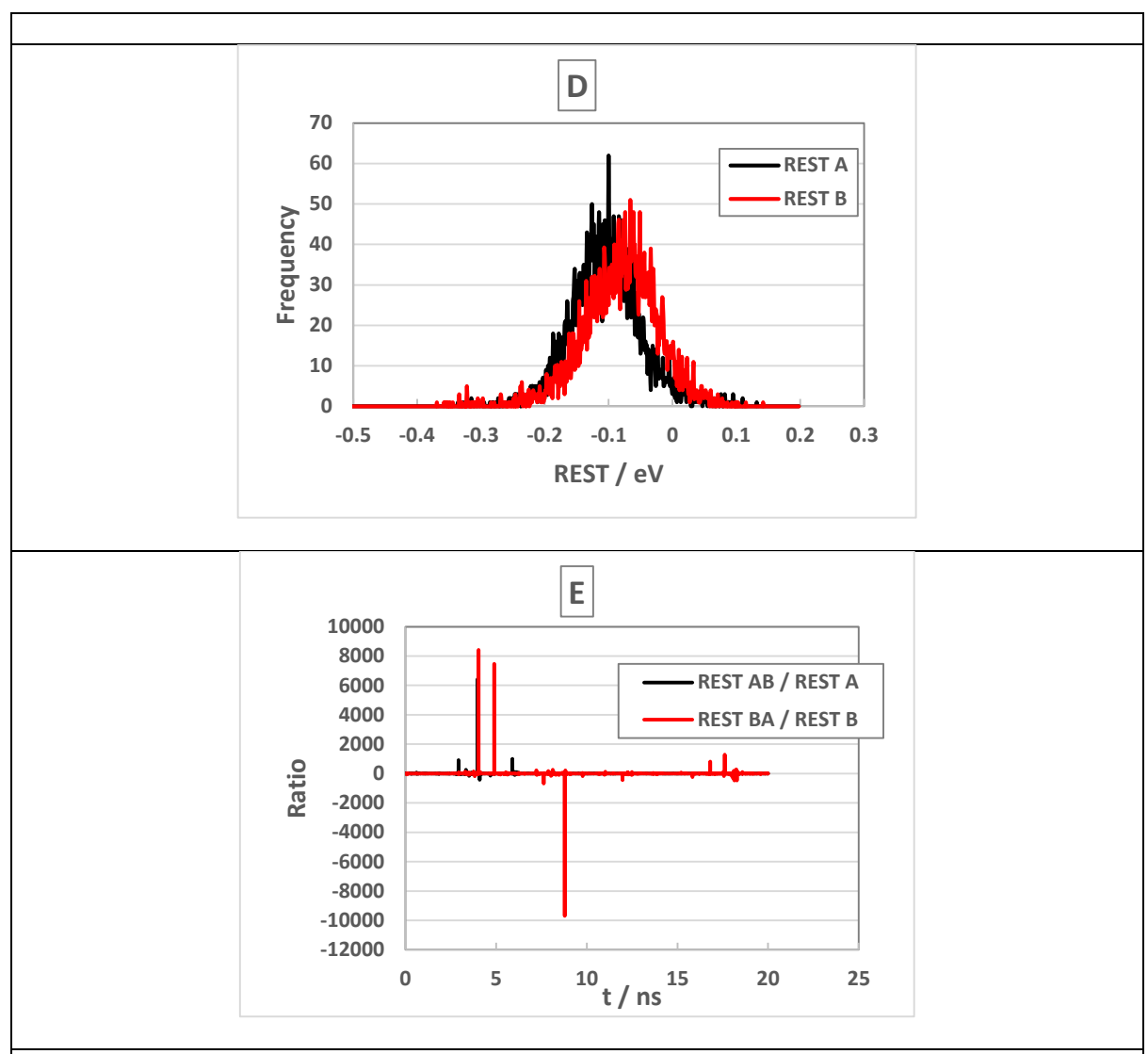
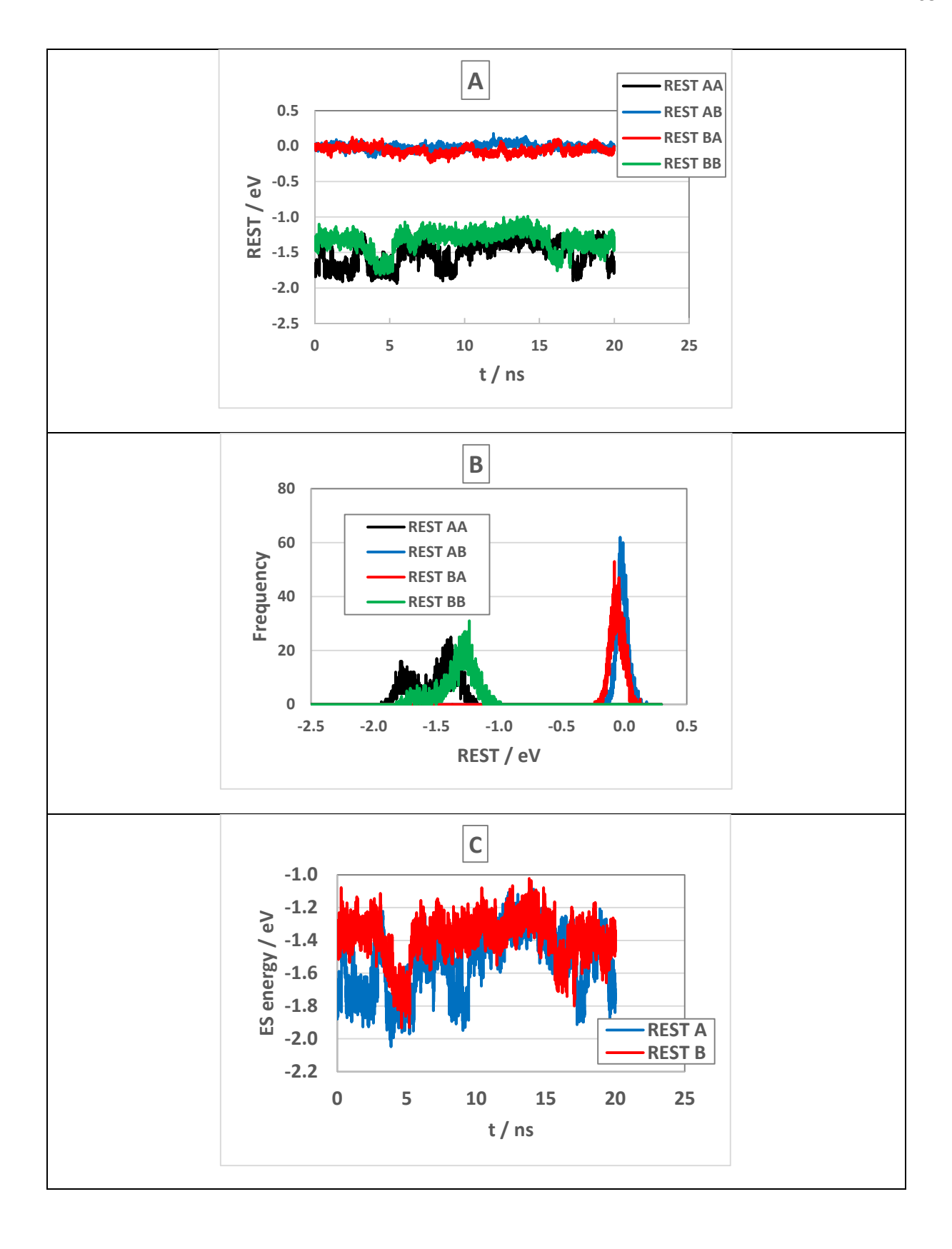


Figure 4.14 Dynamics and distribution of REST of Lys72

The meanings of notations are described in the caption of Figure 4.13

The dynamics and distributions of REST in FMN are shown in Figure 4.15, which contains two negative charges at phosphate oxygens. The values of REST AB and REST BA were nearly zero, while REST AA and REST BB displayed large negative values extending -1 to -2 eV as shown in Figure 4.15A and 4.15B. The values of REST A and REST B fluctuated around -1 to -2 eV which were similar with those in Figure 4.15A, because the values of REST AB and REST BA were negligibly small. Figure 4.15D shows the distributions of REST A and REST B. The both displayed double maxima, major at -1.4 eV and minor -1.8 eV in REST A, and major at -1.3 eV and small peak at -1.7 eV in REST B. Figure 4.15E shows time-evolutions of the ratios, REST AB / REST BA / REST B, which varied within ± 0.1 eV.

Glu62 and Arg63 are at close proximity with opposite charges. Figure 4.16 shows REST A and REST B of these amino acids. Both of REST A and REST B in Glu62 varied with slightly negative values, while those of Arg63 did around -1 eV. REST B of Arg63 displayed double maxima at -1.1 and -0.9 eV, while REST A shoulder at around -1.1 eV.



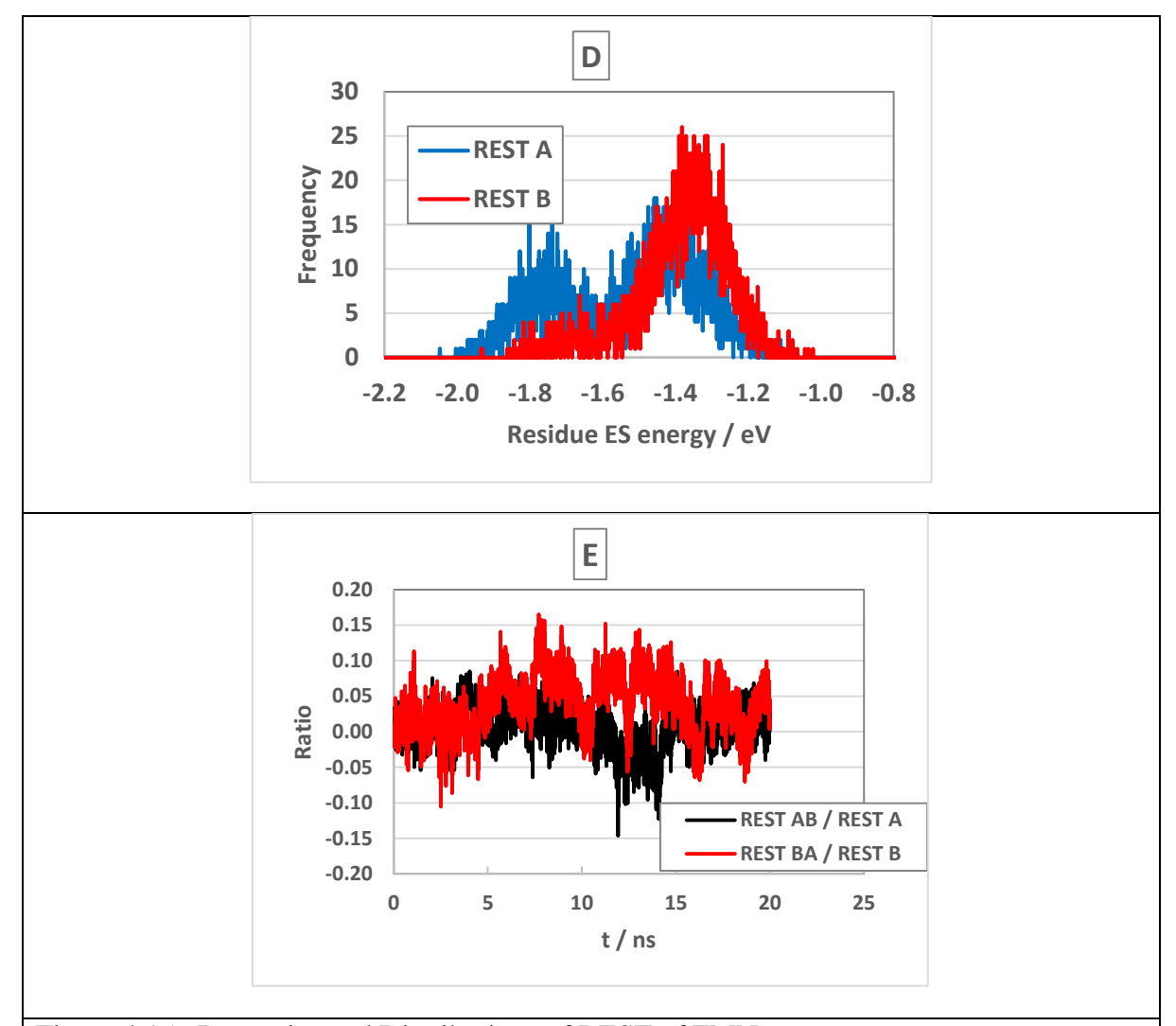


Figure 4.15 Dynamics and Distributions of REST of FMN

Meanings of the notations are described in the caption of Figure 4.13.

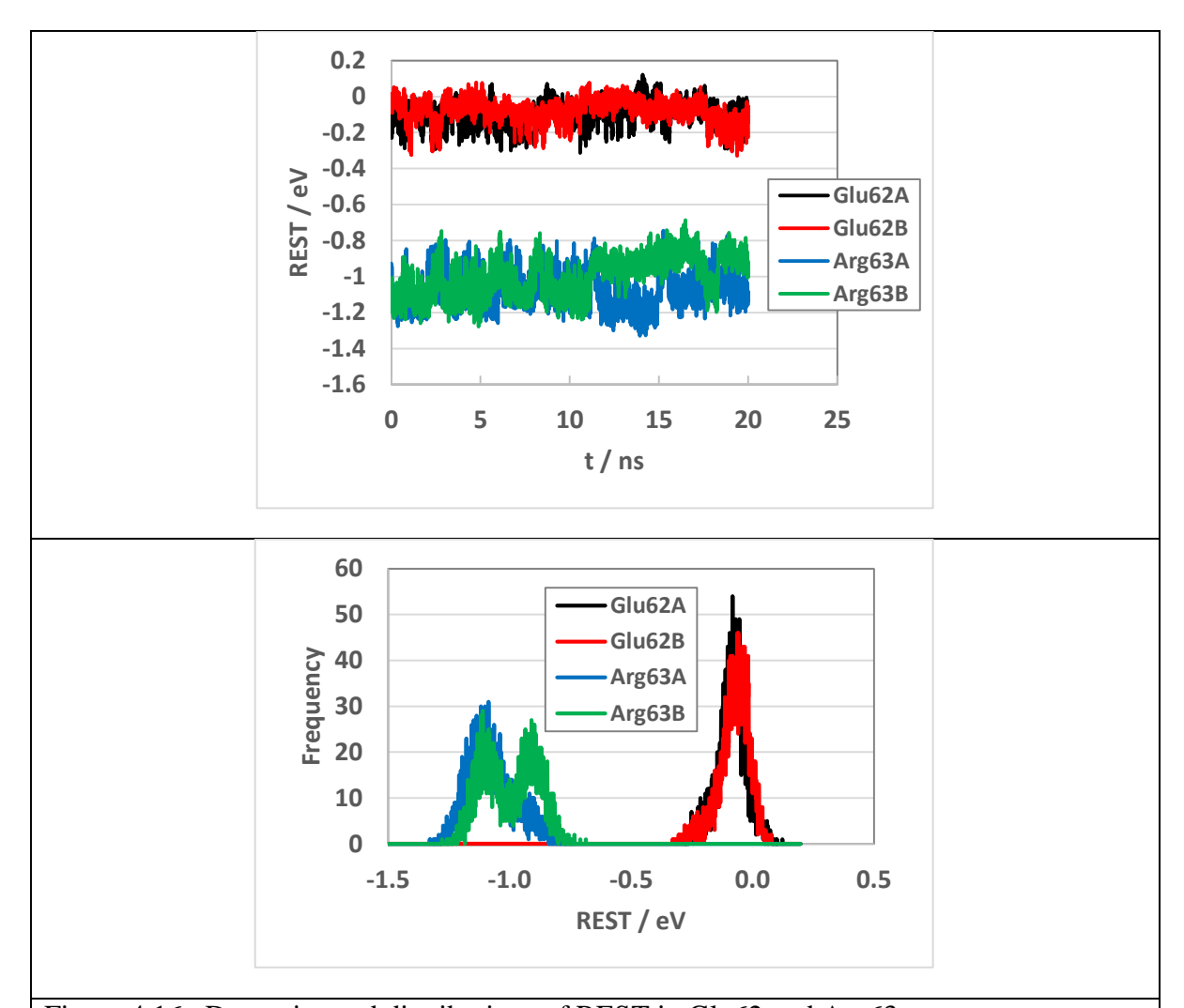
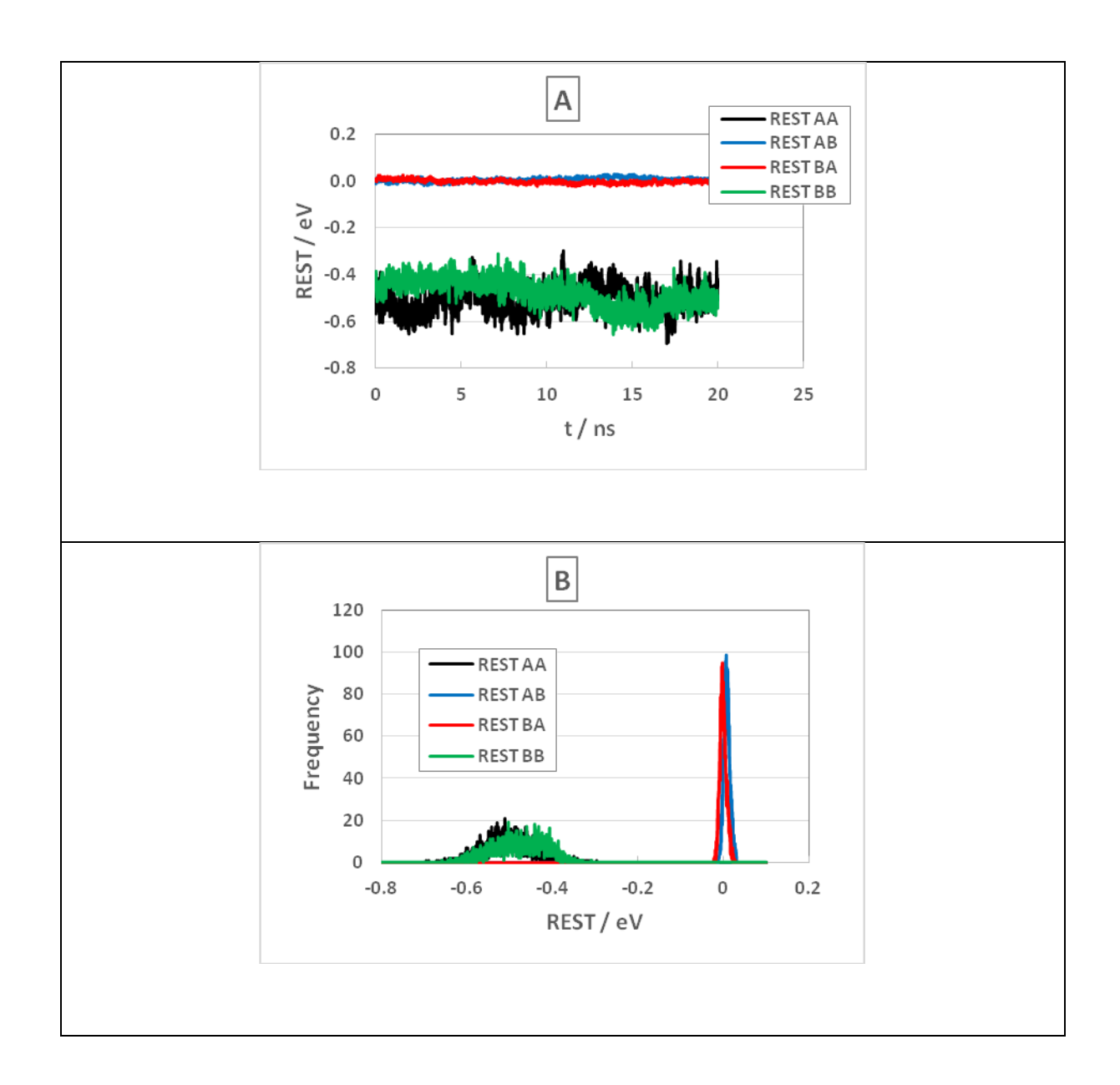


Figure 4.16 Dynamics and distributions of REST in Glu62 and Arg63

Glu62A and Glu62B denote RESTs of Glu62 in Sub A and in Sub, respectively, and Arg63A and Arg63B, RESTs of Arg63 in Sub A and Sub B. Upper panel shows dynamics, and lower panel distributions of these REST values.

The dynamics and distributions in Asp40 and Arg92 are also shown in Figures 4.17 and 4.18. The distribution of REST A in Asp40 with negative charge displayed at around -0.5 eV with single peak, while that in REST B displayed double maxima at around -0.4 eV and -0.5 eV. The peak values of REST AB and REST BA were close to zero at around 0.01 eV. The distribution of REST B displayed a double maxima at -0.5 and -0.4 eV. The values of ratio were around 0.1 in REST AB / REST A and almost zero in REST BA / REST B. In Arg92 with positive charge the distributions of REST AA, REST AB, REST BA and REST BB were quite similar with those in Asp 40. The values of REST A and REST B distributed at around -0.6 eV, which were both lower than those in Asp40 by 0.1 eV. The distribution of REST A displayed a shoulder at around -0.8 eV. The values of REST AB / REST A were almost zero while those of REST BA / REST B varied around 0.1 ± 0.05 eV.



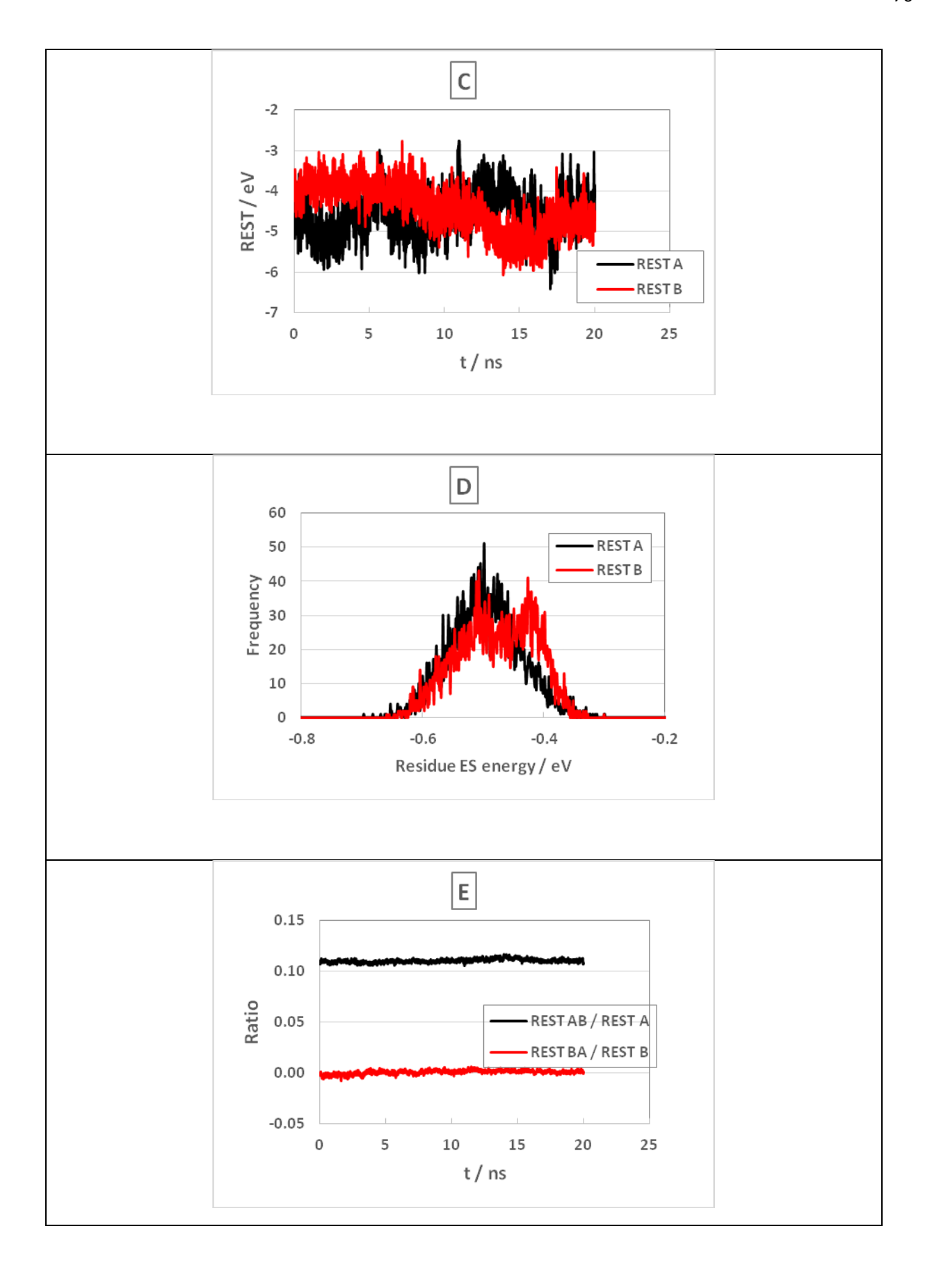
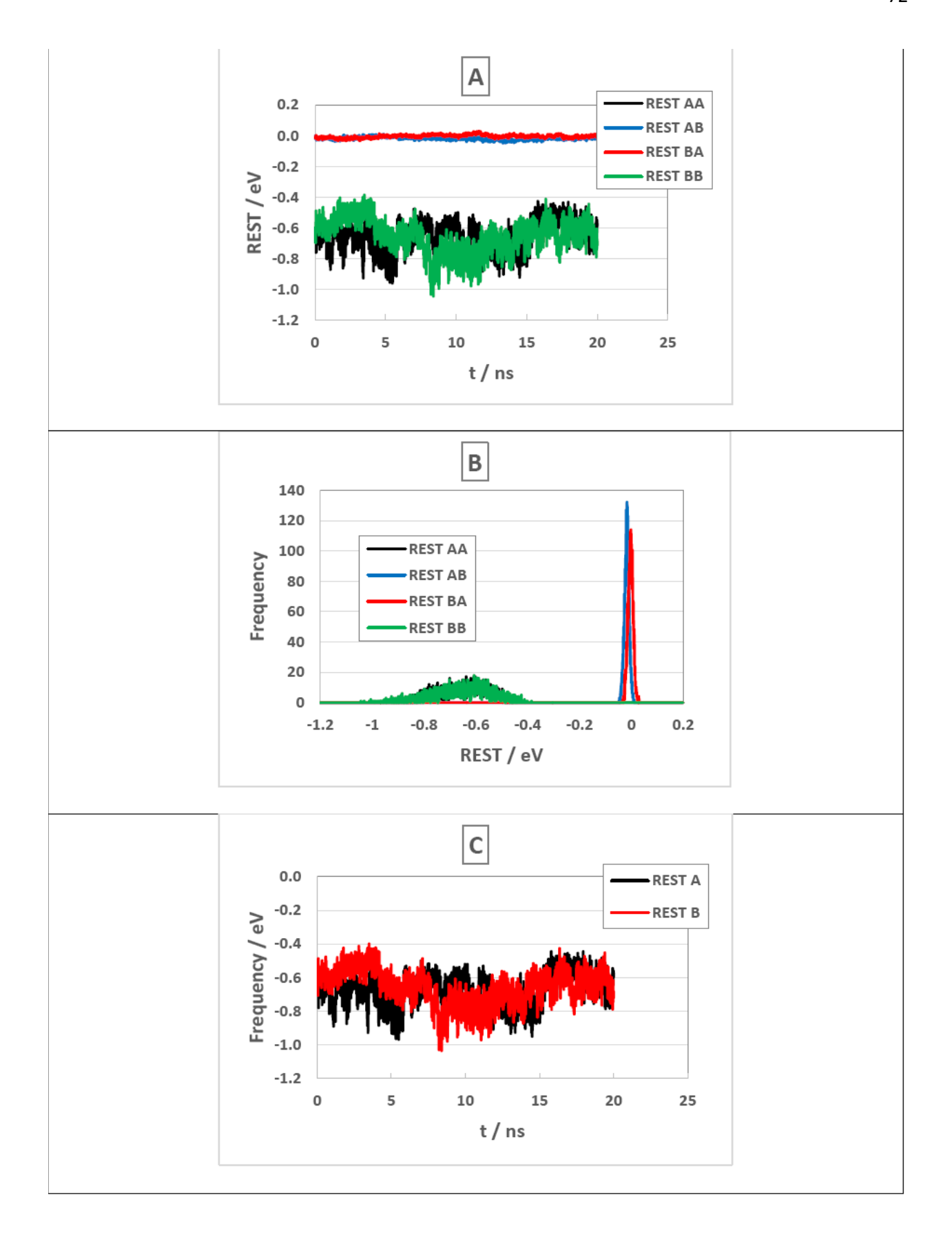
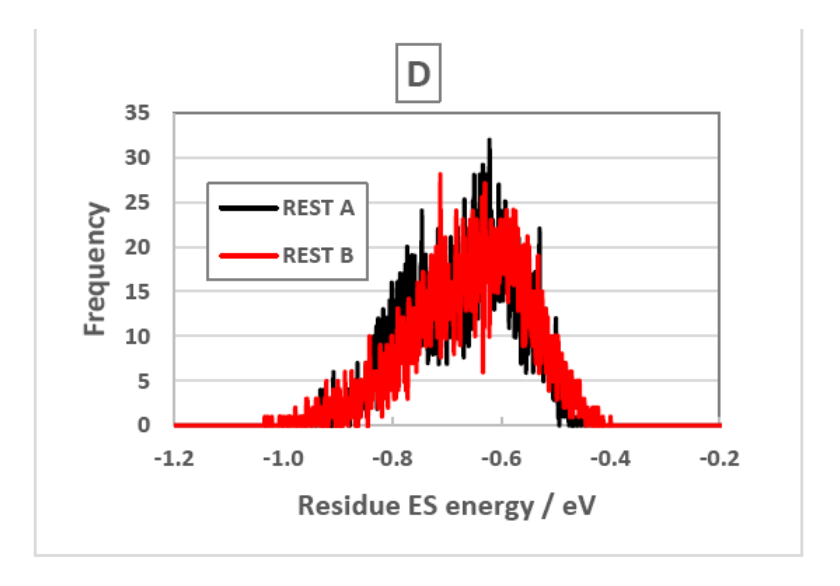


Figure 4.17 Dynamics and Distribution of REST in Asp40

The notations in inserts are described in the caption of Figure 4.13 in text.





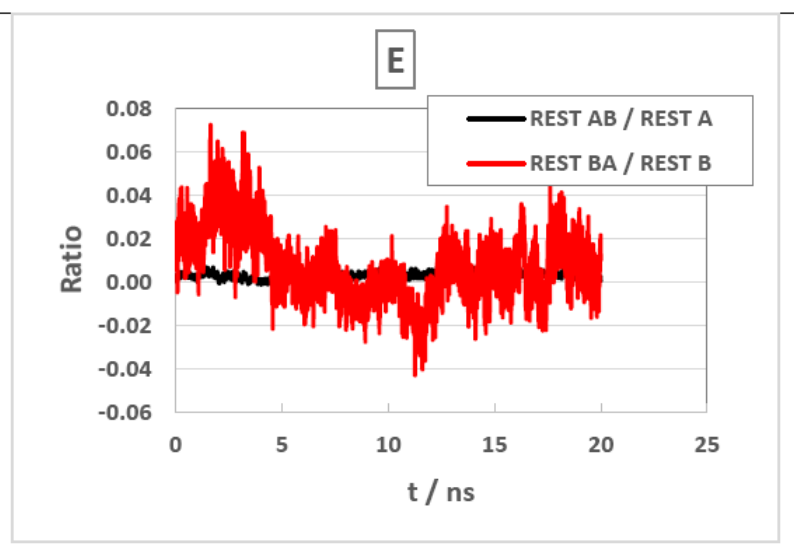


Figure 4.18 Dynamics and distribution in Arg 92

The notations in inserts are described in the caption of Figure 4.13 in text.

#### 4.2.2 RES of all residues

Figure 4.19 shows RES AA and RES BB along with the residue numbers, which denote RES values of a residue interacting with atoms within Sub A and Sub B, respectively. All residues displayed negative values of RESs within each subunit. The residues with great magnitude were mostly ionic. The RES values of FMN with Residue No. 123 (last residue No.) in both Sub A and Sub B were highest in magnitude among all residues, which contains two negative charges at phosphate oxygens. Figure 4.20 shows changes of RES AB and REST BA values with the Residue No., which denote RES between a residue in Sub A and all atoms in Sub B, and RES between a residue in Sub B and all atoms in Sub A. The magnitudes were mostly negligible. However, in some residues the values were quite high. The values of RES AB and BA displayed both positive and negative, which were in contrast with RES AA and RES BB with always negative values. Figure 4.21 shows changes of RES A and RES B with the residue Nos. The values of RES A were obtained as sum of RES AA and RES B were all negative and greatest in FMN in magnitude. In many residues the magnitudes of RESs displayed quite different between Sub A and Sub B.

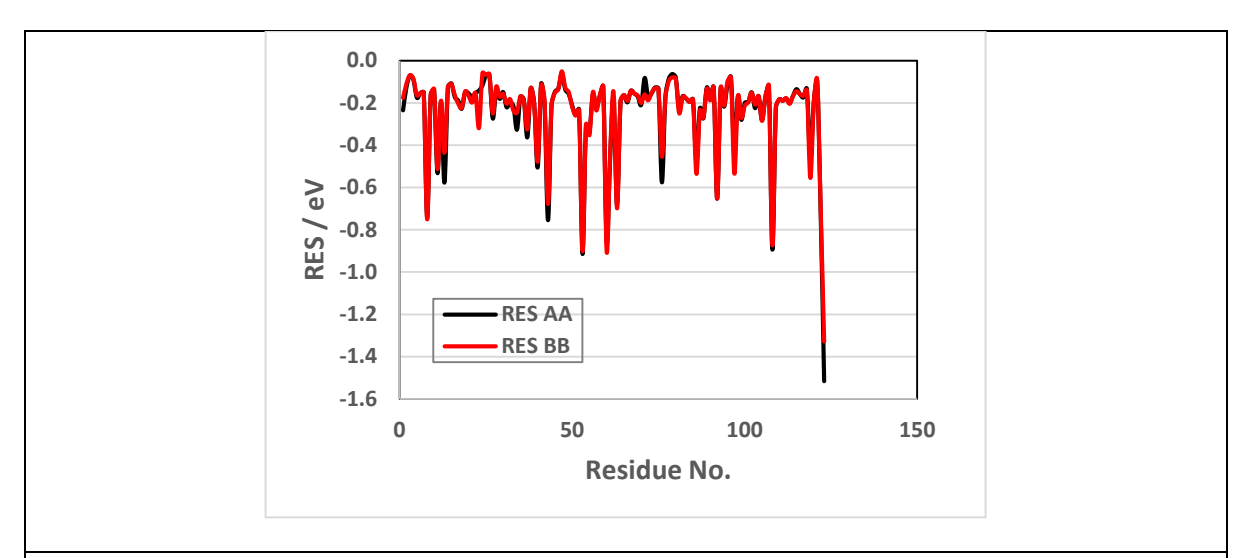


Figure 4.19 RES with residue number in RES AA and RES BB

The RES values were obtained by Eq (3.20). RES AA and RES BB denote RESs of a residue in Sub A interacting with atoms in Sub A, and in Sub B interacting with atoms in Sub B.

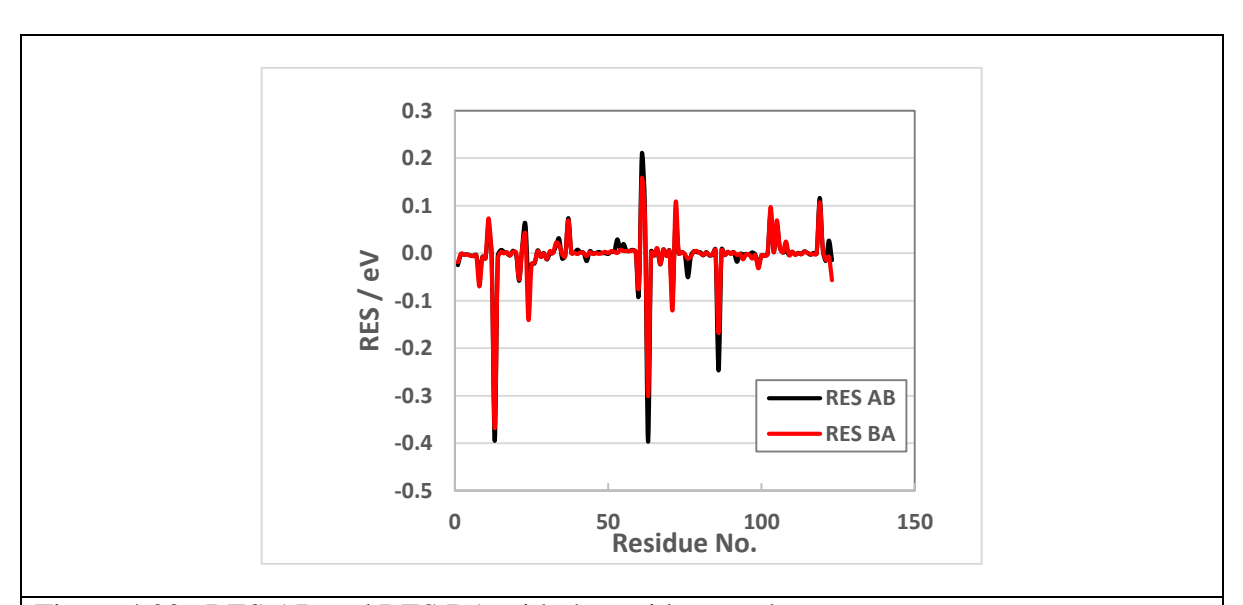


Figure 4.20 RES AB and RES BA with the residue number.

The RES AB and RES BA denote RES of a residues in Sub A interacting with atoms in Sub B, and a residue in Sub B interacting with atoms in Sub A.

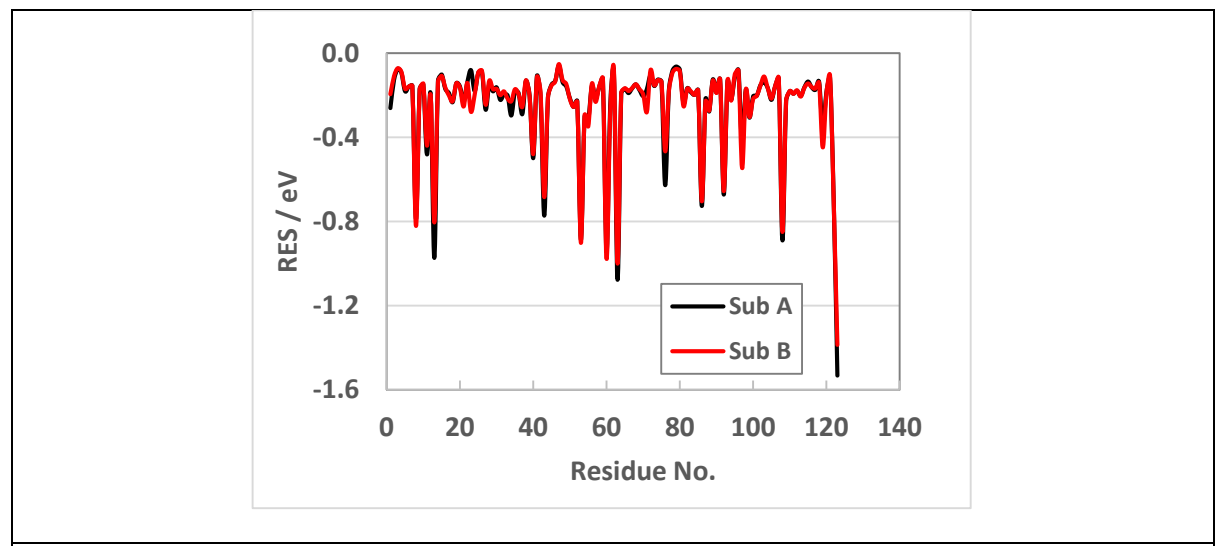


Figure 4.21 RES A and RES B with the residue numbers in FBP dimer The RES values were obtained with Eq (3.20).

#### 4.2.3 Differences between RES A and RES B

The ratios of RES A and RES B were examined, which measure the differences in the RES between Sub A and Sub B. Table 4.5 list ten residues with the highest and least values of the ratios. The ratio in Arg76 was highest, followed by Met1, Ser34, Lys72 and Arg103. In these residues, RES A values were quite high compared to those of RES B. The ratio of Glu23 was least, followed by Arg71, Glu119, Glu97 and Pro79. In these residues RES B values were quite high compared to those of RES A. In Glu23, the values of RES in Sub A were only 23 % of that in Sub B.

Table 4.5 Ten residues with highest and least values of the ratio RES A / RES Ba

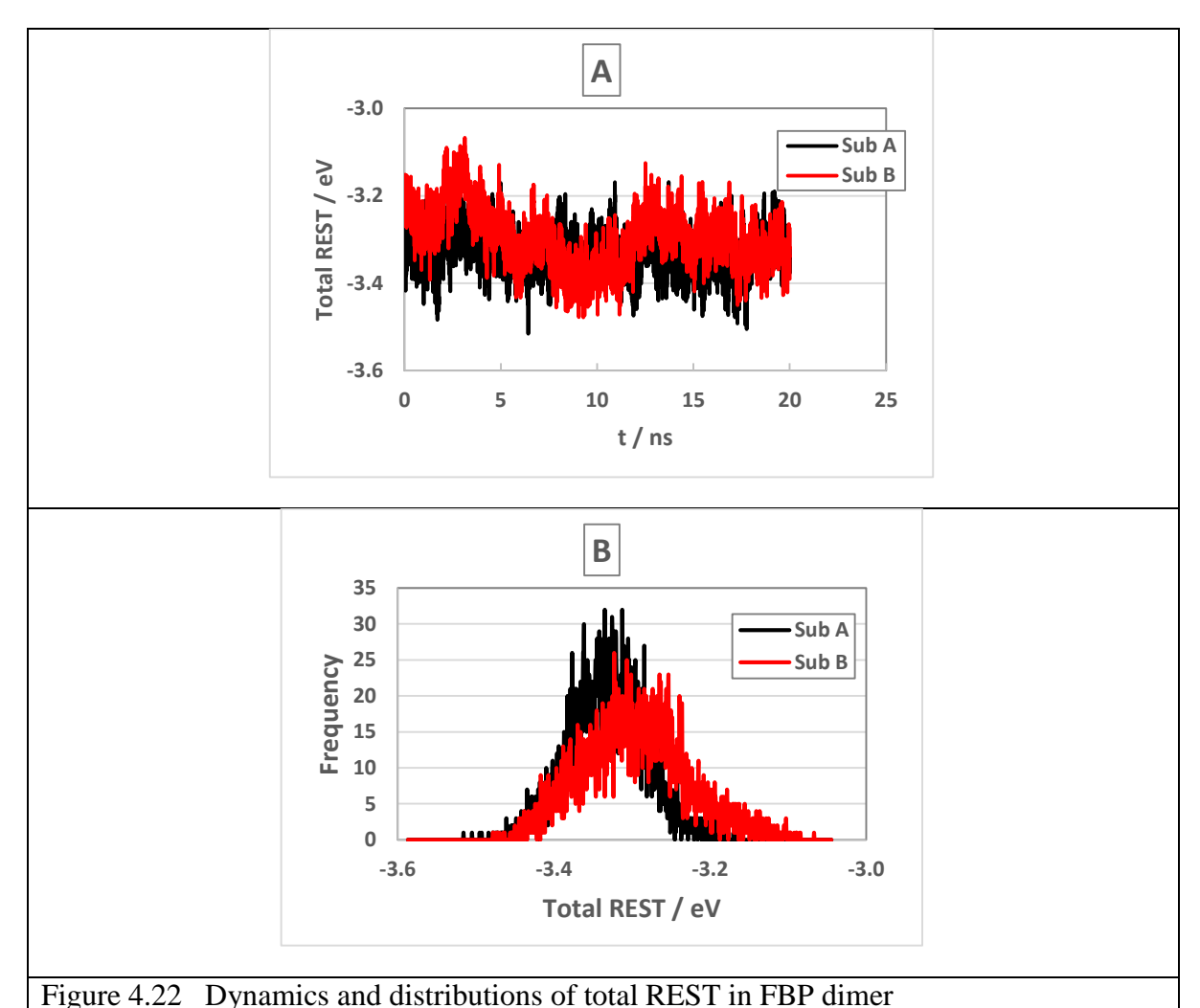
Residue	Residue	RES A / RES B	Residue	Residue	RES A/ RES B	
	No.			No.		
ARG	76	1.34	GLU	23	0.29	
MET	1	1.33	ARG	71	0.61	
SER	34	1.29	GLU	119	0.79	
LYS	72	1.28	GLU	97	0.80	
ARG	103	1.24	PRO	79	0.84	
GLU	13	1.21	ASP	61	0.88	
GLU	62	1.18	GLY	78	0.89	
LEU	2	1.15	ASP	24	0.90	
GLY	95	1.15	GLN	21	0.91	
LYS	37	1.13	GLU	55	0.91	

a The notations of amino acids and FMN are taken from PDB file.

#### 4.2.4 Dynamics and distributions of Total REST

The values of total REST were obtained as sums of REST values over all residues at each snapshot. Figure 4.22 shows dynamics and distributions of the total REST A, total REST B, total REST AB and total REST BA. Figure 4.22A shows time-evolutions of the total REST A and total REST B, which varied between -3.1 and -3.5 eV. Figure 4.22B shows time-evolutions of total REST AB and total REST BA. The values of total REST AB completely coincided with those of total REST BA at any instant. Accordingly, both total REST AB and total RESBA are considered

to be total ES interaction energy between the two subunits, so that they should be equal. It is noted that the interaction energies were always negative, despite that many residues displayed positive RES AB and RES BA (Figure 4.20). This implies that the formation of the dimer stabilizes the entire protein. The values of the total REST AB and total REST BA varied from -0.2 to -1.2 eV. The amplitude of the variation in total REST AB and total REST BA were much greater than those in the total REST A and total REST B. Figure 4.22 C shows distributions of the total RESTs. The peak distributions of in the total REST A and total REST B were at -3.32 eV and -3.26 eV. The distributions of the total REST AB and total REST BA completely coincided again, of which peak distribution was at -0.7 eV.



Total REST was obtained as sum of RESTs over all residues in Sub A and Sub B at each snapshot.

The ES energy of individual residue inside a protein have never been quantitatively evaluated, despite of its importance not only in ET phenomena, but also in binding energy of a ligand to a protein. Among interaction energies in a protein hydrogen bonding (H-Bond) energy is one of greatest energies, which is typically 10 kcal / mol (0.43 eV / pair). The RESs of most ionic groups are also very important, because they mostly displayed more than 0.43 eV. Dynamic behavior of ES energy of individual residue was clarified with REST. The REST values were

highly dependent on the residues. The RES values were obtained as mean values of REST over MDS snapshots. RES values of any residues with positive, negative and neutral charges displayed negative sign, which reveals that the ES energies of any residue contributes to stabilize the protein structure. The values of RES in FMN were most in magnitude both in Sub A and Sub B, which implies that the binding of FMN to the FBP stabilizes most the protein structure within each subunit among all residues. The residues with ionic groups displayed high RES values in magnitude. Non-ionic residues as Pro, Gly, Ala and Val displayed least RES values in magnitude, but some of ionic residues also displayed low values.

Total REST AB and total REST BA over all residues completely coincided at any MDS time with negative sign. Accordingly the total REST AB (or total REST BA) is considered to be whole interaction ES energy between the two subunits. It was found with RES AB and RES BA which residues attractively contribute most to the subunit binding. Arg63 and Glu13 among the residues displayed the highest interaction energy between the two subunits. The values of RES AB and RES BA in FMN were not much as Arg63 or Glu13, despite of the greatest values of RES A and RES B. This suggests that FMN greatly stabilizes the protein structure within a subunit, but does not contribute much to the Sub A - Sub B binding.

A static dielectric constant of a material is expressed with dipole-dipole interaction energies among molecules in the material. The RES of a residue is considered to relate with a microscopic dielectric constant at the location of a residue, which is extremely heterogeneous unlike in a bulk solution. The total RES A and total RES B values shown in Figure 4.22 should be also related to a dielectric constant of entire subunits, though it was time-dependent. The ET rates from aromatic amino acids to Iso\* in FBP dimer have been obtained assuming the static

dielectric constants are time-independent. If a time-dependent dielectric constant is introduced into the ET rate, the obtained physical quantities related to the ET rates should be more accurate.

#### 5. Conclusions

MDSs of four different single mutated FBP isomers (E13K, E13R, E13T, and E13Q) were carried out and their ET rates were calculated. The NetES energies in the four mutated FBP isomers with respect to the charged amino acids at 13 locations were dominant among the terms in the total free energy gap, so the ln Rate vs Rc relations were strongly dependent on the NetES. In Trp32KB, Trp32QA and Trp32QB, the ln Rate vs Rc profiles were separated into two groups, which are thought to have been brought about by conformational changes in the entire FBP dimers.

Moreover, the ES energies of each individual residue of the FBP dimer whose atomic coordinates were obtained from MDS were quantitatively evaluated. The negative RES values reveal their contributions to stabilize protein structure. Among all residues, both Arg63 and Glu13 mainly contribute to Sub A–Sub B binding, while the FMN molecule greatly stabilizes the protein structure within a subunit. The present work reveals that the ES energy not only plays an important role on ET phenomena but also in the protein stabilization in general.

#### 6. Suggestions for future works:

Applying the same protocols as utilized in this work to study the PET of other flavoproteins

#### REFERENCES

- [1]J. Jortner, M. Bixon, Electron Transfer-from Isolated Molecules to Biomolecules, in Advances in Chemical Physics: Electron Transfer - from Isolated Molecules to Biomolecules., in, Part 1. John Wiley & Sons, Inc., ISBN 9780471252924, Hoboken, NJ, U.S.A., 1999.
- [2]R.E. Blankenship, Molecular Mechanisms of Photosynthesis, in, Wiley-Blackwell, ISBN 0632043210, Oxford, UK, 2002.
- [3]S. Crosson, K. Moffat, Structure of a flavin-binding plant photoreceptor domain: insights into light-mediated signal transduction. Proc. Natl. Acad. Sci. U.S.A 98 (2001) 2995-3000.
- [4]B. Giovani, M. Byrdin, M. Ahmad, K. Brettel, Light-induced electron transfer in a cryptochrome blue-light photoreceptor. Nat Struct Biol. 10 (2003) 489-490.
- [5]S. Masuda, C.E. Bauer, AppA is a blue light photoreceptor that antirepresses photosynthesis gene expression in Rhodobacter sphaeroides. Cell 110 (2002) 613-623.
- [6]R.A. Marcus, On the Theory of Oxidation-Reduction Reactions Involving Electron Transfer. J. Chem. Phys. 24 (1956) 966-978.
- [7]R.A. Marcus, Electrostatic Free Energy and Other Properties of States Having Nonequilibrium Polarization. J. Chem. Phys. 24 (1956) 979-989.
- [8]H. Sumi, R.A. Marcus, Dynamical effects in electron transfer reactions. J. Chem. Phys. 84 (1986) 4894-4914.
- [9]M. Bixon, J. Jortner, Non-Arrhenius temperature dependence of electron-transfer rates. J. Phys. Chem. 95 (1991) 1941-1944.
- [10]M. Bixon, J. Jortner, J. Cortes, H. Heitele, M.E. Michel-Beyerle, Energy-Gap Law for Nonradiative and Radiative Charge-Transfer in Isolated and in Solvated Supermolecules. J. Phys. Chem. 98 (1994) 7289-7299.

- [11]T. Kakitani, A. Yoshimori, N. Mataga, Effects of the donor-acceptor distance distribution on the energy gap laws of charge separation and charge recombination reactions in polar solutions. J. Phys. Chem. 96 (1992) 5385-5392.
- [12]T. Kakitani, N. Matsuda, A. Yoshimori, N. Mataga, Present and future perspectives of theoretical aspects of photoinduced charge separation and charge recombination reactions in solution. Prog. React. Kinet 20 (1995) 347-381.
- [13]J.R. Miller, J.V. Beitz, R. K. Huddeston, Effect of free energy on rates of electron transfer between molecules. J. Am. Chem. Soc. 106 (1984) 5057-5068.
- [14]T. Asahi, M. Ohkohchi, R. Matsusaka, N. Mataga, R.P. Zhang, A. Osuka, K. Maruyama, Intramolecular photoinduced charge separation and charge recombination of the product ion pair states of a series of fixed-distance dyads of porphyrins and quinones: energy gap and temperature dependences of the rate constants. J. Am. Chem. Soc. 115 (1993) 5665-5674.
- [15]R.A. Marcus, N. Sutin, Electron transfers in chemistry and biology. Biochim. Biophys. Acta 811 (1985) 265-322.
- [16]C.C. Moser, J.M. Keske, K. Warncke, R.S. Farid, P.L. Dutton, Nature of biological electron transfer. Nature 335 (1992) 796-802.
- [17]D.N. Silverman, Marcus rate theory applied to enzymatic proton transfer. Biochim Biophys Acta. 1458 (2000) 88-103.
- [18]N. Mataga, H. Chosrowjan, S. Taniguchi, Ultrafast charge transfer in excited electronic states and investigations into fundamental problems of exciplex chemistry: Our early studies and recent developments. J. Photochem. Photobiol. C 6 (2005) 37-79.

- [19]H.B. Gray, J.R. Winkler, Electron Transfer in Proteins. Annu. Rev. Biochem 65 (1996) 537-561.
- [20]J. Sancho, Flavodoxins: sequence, folding, binding, function and beyond. Cell. Mol. Life Sci. 63 (2006) 855-864.
- [21]N. Cremades, A. Velázquez-Campoy, M. Martínez-Júlvez, J.L. Neira, I. Pérez-Dorado, J. Hermoso, P. Jiménez, A. Lanas, P.S. Hoffman, J. Sancho, Discovery of Specific Flavodoxin Inhibitors as Potential Therapeutic Agents against Helicobacter pylori Infection. ACS Chem. Biol. 4 (2009) 928-938.
- [22]M.L. Ludwig, C.L. Luschinsky, General properties of flavodoxins, in Chemistry and biochemistry of flavoenzymes (in, Boca Raton, Florida: CRC Press, 1992.
- [23]S. Crosson, K. Moffat, Structure of a flavin-binding plant photoreceptor domain: insights into light-mediated signal transduction. Proc. Natl. Acad. Sci. U.S.A. 98 (2001) 2995-3000.
- [24]N. Mataga, H. Chosrowjan, S. Taniguchi, Femtosecond fluorescence dynamics of flavoproteins: Comparative studies on flavodoxin, its site-directed mutants, and riboflavin binding protein regarding ultrafast electron transfer in protein nanospaces. J. Phys. Chem. B. 106 (2002) 8917-8920.
- [25]D.P. Zhong, A.H. Zewail, Femtosecond dynamics of flavoproteins: Charge separation and recombination in riboflavine (vitamin B-2)-binding protein and in glucose oxidase enzyme. Proc. Natl. Acad. Sci. U.S.A 98 (2001) 11867-11872.
- [26]J. Pan, M. Byrdin, C. Aubert, A.P.M. Eker, K. Brettel, M.H. Vos, Excited-state properties of flavin radicals in flavoproteins: Femtosecond spectroscopy of DNA photolyase, glucose oxidase, and flavodoxin. J. Phys. Chem. B. 108 (2004) 10160-10167.

- [27]H. Chosrowjan, S. Taniguchi, N. Mataga, F. Tanaka, D. Todoroki, M. Kitamura, Ultrafast fluorescence dynamics of FMN-binding protein from Desulfovibrio vulgaris (Miyazaki F) and its site-directed mutated proteins. Chem. Phys. Lett. 462 (2008) 121-124.
- [28]F. Tanaka, H. Chosrowjan, S. Taniguchi, N. Mataga, K. Sato, Y. Nishina, K. Shiga, Donor-acceptor distance-dependence of photoinduced electron-transfer rate in flavoproteins. J. Phys. Chem. B. 111 (2007) 5694-5699.
- [29]E.R. Henry, R.M. Hochstrasser, Molecular dynamics simulations of fluorescence polarization of tryptophans in myoglobin. Proc. Natl. Acad. Sci. U.S.A 84 (1987) 6142-6146.
- [30]M. Kitamura, S. Kojima, K. Ogasawara, T. Nakaya, T. Sagara, K. Niki, K. Miura, H. Akutsu, I. Kumagai, Novel FMN-binding protein from Desulfovibrio vulgaris (Miyazaki F). Cloning and expression of its gene in Escherichia coli, J. Biol. Chem 269 (1994) 5566-5573.
- [31]E. Liepinsh, M. Kitamura, T. Murakami, T. Nakaya, G. Otting, Pathway of chymotrypsin evolution suggested by the structure of the FMN-binding protein from Desulfovibrio vulgaris (Miyazaki F),. Nat. Struct. Biol. 4 (1997) 795-797.
- [32]K. Suto, K. Kawagoe, N. Shibata, Y. Morimoto, Y. Higuchi, M. Kitamura, T. Nakaya, N. Yasuoka, How do the x-ray structure and the NMR structure of FMN-binding protein differ? Acta Crystallogr. Sect. D- Biol. Crystallogr 56 (2000) 368-371.
- [33]C. Sengupta, M.K. Sarangi, A. Sau, D. Mandal, S. Basu, A case study of photo induced electron transfer between aliphatic amine: Deciphering different mechanisms from femtosecond to microsecond time domain. J. Photochem. Photobiol. A 296 (2015) 25-34.
- [34]A. Karen, N. Ikeda, N. Mataga, F. Tanaka, Picosecond laser photolysis studies of fluorescence quenching mechanisms of flavin: a direct observation of indole-flavin singlet charge

- transfer state formation in solutions and flavoenzymes,. Photochem. Photobiol. 37 (1983) 495-502.
- [35]J.R. Lakowitz, Principles of Fluorescence Spectroscopy (3rd Edition), in, Springer, New York, 2006.
- [36]B. Valeur, Molecular Fluorescence, Principles and Applications, in, WILEY VCH Verlag, Weihaim, 2002.
- [37]G. Weber, Fluorescence of riboflavin and flavin-adenine dinucleotide. Biochem J. 47 (1950) 114-121.
- [38]D.B. McCormick, Interactions of flavins with amino acid residues: assessments from spectral and photochemical studies. Photochem. Photobiol. 26 (1977) 169-182.
- [39]P.A. vanderBerg, A.J.W.G. Visser, In New Trends in Fluorescence Spectroscopy Applications to Chemical and Life Sciences, in, Springer: Berlin, 2001.
- [40]P.A. vandenBerg, A.v. Hoek, C.D. Walentas, R.N. Perham, A.J. Visser, Flavin fluorescence dynamics and photoinduced electron transfer in Escherichia coli glutathione reductase. Biophys J. 74 (1998) 2046-2058.
- [41]N. Mataga, H. Chosrowjan, Y. Shibata, F. Tanaka, Ultrafast fluorescence quenching dynamics of flavin chromophores in protein nanospace. J. Phys. Chem. B. 102 (1998) 7081-7084.
- [42]N. Mataga, H. Chosrowjan, Y. Shibata, F. Tanaka, Y. Nishina, K. Shiga, Dynamics and mechanisms of ultrafast fluorescence quenching reactions of flavin chromophores in protein nanospace. J. Phys. Chem. B. 104 (2000) 10667-10677.
- [43]A. Karen, M.T. Sawada, F. Tanaka, N. Mataga, Dynamics of excited flavoproteins-picosecond laser photolysis studies. Photochem. Photobiol. 45 (1987) 49-54.

- [44]H. Chosrowjan, S. Taniguchi, N. Mataga, F. Tanaka, D. Todoroki, M. Kitamura, Comparison between ultrafast fluorescence dynamics of FMN binding protein from Desulfovibrio vulgaris, strain miyazaki, in solution vs crystal phases. J. Phys. Chem. B. 111 (2007) 8695-8697.
- [45]F. Tanaka, R. Rujkorakarn, H. Chosrowjan, S. Taniguchi, N. Mataga, Analyses of donor-acceptor distance-dependent rates of photo-induced electron transfer in flavoproteins with three kinds of electron transfer theories. Chem. Phys. 348 (2008) 237-241.
- [46]D.A. Case, T.A. Darden, T.E. Cheatham, C.L. Simmerling, J. Wang, R.E. Duke, R. Luo, M. Crowley, R.C. Walker, W. Zhang, K.M. Merz, B. Wang, S. Hayik, A. Roitberg, G. Seabra, I. Kolossváry, K.F. Wong, F. Paesan, J. Vanicek, X. Wu, S.R. Brozell, T. Steinbrecher, H. Gohlke, L. Yang, C. Tan, J. Mongan, V. Hornak, G. Cui, H.D. Mathews, M.G. Seetin, C. Sagui, V. Babin, P.A. Kollman, AMBER 10. University of California, San Francisco (2008).
- [47]J. Wang, P. Cieplak, P.A. Kollman, How well does a restrained electrostatic potential (RESP) model perform in calculating conformational energies of organic and biological molecules.
  J. Comput. Chem. 21 (2000) 1049-1074.
- [48]C. Schneider, J. Suhnel, A molecular dynamics simulation of the flavin mononucleotide-RNA aptamer complex. Biopolymers 50 (1999) 287-302.
- [49]U. Essmann, L. Perera, M.L. Berkowitz, T. Darden, H. Lee, L.G. Pedersen, A smooth particle mesh Ewald method. J. Chem. Phys. 103 (1995) 8577-8593.
- [50]J.P. Ryckaert, G. Ciccotti, H.J.C. Berendsen, Numerical integration of the cartesian equations of motion of a system with constraints: molecular dynamics of n-alkanes. J. Comput. Phys. 23 (1977) 327-341.

- [51]T. Kakitani, N. Mataga, New energy gap laws for the charge separation process in the fluorescence quenching reaction and the charge recombination process of ion pairs produced in polar solvents. J. Phys. Chem. 89 (1985) 8-10.
- [52]N. Nunthaboot, F. Tanaka, S. Kokpol, H. Chosrowjan, S. Taniguchi, N. Mataga, Simultaneous analysis of ultrafast fluorescence decays of FMN binding protein and its mutated proteins by molecular dynamic simulation and electron transfer theory. J. Phys. Chem. B. 112 (2008) 13121-13127.
- [53]N. Nunthaboot, S. Pianwanit, S. Kokpol, F. Tanaka, Simultaneous analyses of photoinduced electron transfer in the wild type and four single substitution isomers of the FMN binding protein from Desulfovibrio vulgaris, Miyazaki F. Phys. Chem. Chem. Phys. 13 (2011) 6085-6097.
- [54]K. Lugsanangarm, S. Pianwanit, S. Kokpol, F. Tanaka, H. Chosrowjan, S. Taniguchi, N. Mataga, Photoinduced electron transfer in wild type and mutated flavodoxin from Desulfovibrio vulgaris, strain Miyazaki F.: Energy gap law. J. Photochem. Photobiol. A 219 (2011) 32-41.
- [55]N. Nunthaboot, N. Kido, F. Tanaka, K. Lugsanangarm, A. Nueangaudom, S. Pianwanit, S. Kokpol, Relationship between rate of photoinduced electron transfer and hydrogen bonding chain of tyrosine–glutamine–flavin in flavin photoreceptors: global analyses among four TePixDs and three AppAs. J. Photochem. Photobiol. A: Chem. 252 (2013) 14-24.
- [56]H. Chosrowjan, S. Taniguchi, N. Mataga, T. Nakanishi, Y. Haruyama, S. Sato, M. Kitamura, F. Tanaka, Effects of the disappearance of one charge on ultrafast fluorescence dynamics of the FMN binding protein. J. Phys. Chem. B. 114 (2010) 6175-6182.

- [57]A. Nueangaudom, K. Lugsanangarm, S. Pianwanit, S. Kokpol, N. Nunthaboot, F. Tanaka, Structural basis for the temperature-induced transition of D-amino acid oxidase from pig kidney revealed by molecular dynamic simulation and photo-induced electron transfer. Phys. Chem. Chem. Phys. 14 (2012) 2567-2578.
- [58]V. Vorsa, T. Kono, K.F. Willey, N. Winograd, Femtosecond photoionization of ion beam desorbed aliphatic and aromatic amino acids: Fragmentation via α-cleavage reactions. J. Phys. Chem. B. 103 (1999) 7889-7895.
- [59]N. Nunthaboot, K. Lugsanangarm, S. Pianwanit, S. Kokpol, F. Tanaka, T. Nakanishi, M. Kitamura, Conformational difference between two subunits in flavin mononucleotide binding protein dimers from Desulfovibrio vulgaris (MF): molecular dynamics simulation. Comp. Biol. Chem 64 (2016) 113-125.
- [60]S. Taniguchi, H. Chosrowjan, F. Tanaka, T. Nakanishi, S. Sato, Y. Haruyama, M. Kitamura, A key factor for ultrafast rates of photoinduced electron transfer among five flavin mononucleotide binding proteins: effect of negative, positive, and neutral charges at residue 13 on the rate. Bull. Chem. Soc. Jpn. 86 (2013) 339-350.
- [61]N. Nunthaboot, K. Lugsanangarm, A. Nueangaudom, S. Pianwanit, S. Kokpol, F. Tanaka, Role of the electrostatic energy between the photo-products and ionic groups on the photoinduced electron transfer rates from aromatic amino acids to the excited flavin in five single-point substitution isoforms of the charged amino acid residue-13 in the FMN-binding protein,. Mol. Sim. 41 (2015) 580-591.
- [62]N. Nunthaboot, K. Lugsanangarm, A. Nueangaudom, S. Pianwanit, S. Kokpol, F. Tanaka, S. Taniguchi, H. Chosrowjan, T. Nakanishi, M. Kitamura, Photoinduced electron transfer from aromatic amino acids to the excited isoalloxazine in flavin mononucleotide binding

- protein. Is the rate in the inverted region of donor-acceptor distance not real?,. J. Photochem. Photobiol. A 326 (2016) 60-68.
- [63]N. Nunthaboot, K. Lugsanangarm, S. Pianwanit, S. Kokpol, F. Tanaka, S. Taniguchi, H. Chosrowjan, T. Nakanishi, M. Kitamura, Bell-shaped dependence of the rate of ultrafast photoinduced electron transfer from aromatic amino acids to the excited flavin on the donor–acceptor distance in FMN binding proteins. Comp. Theor. Chem. 1030 (2014) 9-16.
- [64]A. Nueangaudom, K. Lugsanangarm, S. Pianwanit, S. Kokpol, N. Nunthaboot, F. Tanaka, S. Taniguchi, H. Chosrowjan, Theoretical analyses of the fluorescence lifetimes of the D-amino acid oxidase-benzoate complex dimer from porcine kidney: Molecular dynamics simulation and photoinduced electron transfer. RSC. Adv. 4 (2014) 54096-54108.
- [65]K. Lugsanangarm, A. Nueangaudom, S. Kokpol, S. Pianwanit, N. Nunthaboot, F. Tanaka, S. Taniguchi, H. Chosrowjan, Heterogeneous subunit structures in the pyranose 2-oxidase homotetramer revealed by theoretical analysis of the rates of photoinduced electron transfer from a tryptophan to the excited flavin, . J. Photochem. Photobiol. A 306 (2015) 66-79.
- [66] V.V. Yudanov, V.A. Mikhailova, A.I. Ivanov, Reorganization of intramolecular high frequency vibrational modes and dynamic solvent effect in electron transfer reactions. J. Phys. Chem. A 116 (2012) 4010-4019.
- [67]L.D. Zusman, Outer-sphere electron transfer in polar solvents. Chem. Phys. 49 (1980) 295-304.

#### **Appendices**

### สรุป Output จากโครงการวิจัยที่ได้รับทุนจาก สกว.

- 1. ผลงานตีพิมพ์ในวารสารวิชาการนานาชาติ 2 ฉบับ
- Nadtanet Nunthaboot, Kiattisak Lugsanangarm, Arthit Nueangaudom, Somsak Pianwanit, Sirirat Kokpol, Fumio Tanaka, Seiji Taniguchi, Haik Chosrowjan, Takeshi Nakanishi, Masaya Kitamura. Photoinduced electron transfer from aromatic amino acids to the excited isoalloxazine in single mutated flavin mononucleotide binding proteins. Effect of the dimer formation on the rate and the electrostatic energy inside the proteins. Computational and Theoretical Chemistry. 1108 (2017) 1-9. (ISI, Impact factor 1.403)
- Nadtanet Nunthaboot, Arthit Nueangaudom, Kiattisak Lugsanangarm, Somsak Pianwanit,
   Sirirat Kokpol, Fumio Tanaka. A novel physical quantity of residue electrostatic energy in flavin mononucleotide binding protein dimer. Submitted.
  - 2. การนำผลงานวิจัยไปใช้ประโยชน์

ได้มีการนำข้อมูลที่ได้จากงานวิจัยดังกล่าวไปใช้ประโยชน์ในแง่

- เชิงวิชาการ ได้มีการนำเนื้อหาบางส่วนของงานวิจัยมาประยุกต์ใช้ในการเรียน การสอน โดยเฉพาะวิชาทางเคมีคำนวณ เพื่อให้นักศึกษามีความรู้ความเข้าใจและสามารถ ประยุกต์ใช้หลักการหรือทฤษฎีทางเคมีได้
- 3. อื่นๆ

\_

FISEVIER

Contents lists available at ScienceDirect

### Computational and Theoretical Chemistry

journal homepage: www.elsevier.com/locate/comptc



# Photoinduced electron transfer from aromatic amino acids to the excited isoalloxazine in single mutated flavin mononucleotide binding proteins: Effect of the dimer formation on the rate and the electrostatic energy inside the proteins



Nadtanet Nunthaboot <sup>a,\*</sup>, Kiattisak Lugsanangarm <sup>b</sup>, Arthit Nueangaudom <sup>c</sup>, Somsak Pianwanit <sup>c</sup>, Sirirat Kokpol <sup>c</sup>, Fumio Tanaka <sup>c,d,\*</sup>, Seiji Taniguchi <sup>d</sup>, Haik Chosrowjan <sup>d</sup>, Takeshi Nakanishi <sup>e</sup>, Masaya Kitamura <sup>e</sup>

- <sup>a</sup> Department of Chemistry and Center of Excellence for Innovation in Chemistry, Faculty of Science, Mahasarakham University, Mahasarakham 44150, Thailand
- <sup>b</sup> Program of Science, Faculty of Education, Bansomdejchaopraya Rajabhat University, Bangkok 10600, Thailand
- <sup>c</sup> Department of Chemistry, Faculty of Science, Chulalongkorn University, Bangkok 10330, Thailand
- <sup>d</sup> Division of Laser Biochemistry, Institute for Laser Technology, Osaka 550-0004, Japan
- <sup>e</sup> Department of Applied Chemistry and Bioengineering, Graduate School of Engineering, Osaka City University, Osaka 558-8585, Japan

#### ARTICLE INFO

# Article history: Received 15 October 2016 Received in revised form 14 January 2017 Accepted 3 March 2017 Available online 7 March 2017

Keywords:
Photoinduced electron transfer
Flavin mononucleotide binding protein
FBP
Logarithmic ET rate and donor-acceptor
distance relation
Bell shape
Net electrostatic energy
Ultrafast fluorescence dynamics
Conformational changes
Kakitani and Mataga theory

#### ABSTRACT

Conformational changes in the single mutated flavin mononucleotide binding proteins (FBP), E13K (Glu13 of wild type FBP is replaced by Lys), E13R (Glu13 replaced by Arg), E13T (Glu13 replaced by Thr) and E13Q (Glu13 replaced by Gln) upon dimer formations were studied through the phenomena of photoinduced electron transfer (ET) from tryptophan 32 (Trp32) and tryptophan 106 (Trp106) to the excited isoalloxazine (Iso\*). The ET rates were obtained with atomic coordinates of the proteins determined by a method of molecular dynamics simulation (MDS) and an ET theory using the reported experimental fluorescence decays of the FBPs. The value of the net electrostatic energy (NetES) between the photo-products and ionic groups inside the proteins increased in magnitude upon the dimer formation in every mutated FBP. Dependencies in the logarithmic ET rate (In Rate) on the donor-acceptor distances (Rc) could not be approximated with simple linear nor parabolic functions in most ET donors, which are ascribed to the relatively greater values of the NetES in the dimers compared to the energy terms of the standard free energy gap (SFEG), solvent reorganization energy (SROE) and the electrostatic energy between the photo-products (ESDA) in total free energy gap (GT) in the ET rates. The NetES vs Rc relations displayed two distinct groups in Trp32KB, Trp32QA and Trp32QB. The In Rate vs Rc relations in these donors displayed different behaviors between the two groups.

© 2017 Elsevier B.V. All rights reserved.

#### 1. Introduction

In the last few decades, the mechanism of photoinduced electron transfer (ET) has been intensively studied in small molecules and proteins [1–5]. However, the details of the mechanism have not been obtained, because any theoretical ET rates contain several unknown parameters, which cannot be determined by any experimental or theoretical methods. In flavoproteins, the ET easily takes place from aromatic amino acids, such as tryptophan (Trp) and

tyrosine (Tyr), to the excited state isoalloxazine (Iso\*), so flavoproteins are suitable for the investigation of the ET mechanism with their fluorescence dynamics [6–15].

Flavin mononucleotide binding protein (FBP) is a small flavoprotein (Mw 13 kDa with 122 amino acids) that contains a flavin mononucleotide as a cofactor [16]. The protein structure of the wild type FBP (WT) was initially determined by means of NMR spectroscopy in solution as a monomeric form [17] and X-ray diffraction method in crystal as a dimeric form [18]. It was believed that FBP is monomer in solution but forms a dimer in crystal. In previous work, the rates of ET from Trp32, Tyr35 and Trp106 to Iso\* in FBP have been analyzed with atomic coordinates obtained with a molecular dynamics simulation (MDS) and Kakitani and Mataga (KM) rate as the monomer [17,18]. Now it is recognized

<sup>\*</sup> Corresponding authors at: Department of Chemistry, Faculty of Science, Chulalongkorn University, Bangkok 10330, Thailand (F. Tanaka).

E-mail addresses: nadtanet.n@msu.ac.th, nadtanet@gmail.com (N. Nunthaboot), fumio.tanaka@yahoo.com (F. Tanaka).

that FBP is also a dimer in solution [21]. The crystal structures of single mutated FBPs, E13K (Glu13 of WT is replaced by Lys), E13R (Glu13 replaced by Arg), E13T (Glu13 replaced by Thr) and E13Q (Glu13 replaced by Gln) have been also determined [22].

In the present work, we have numerically examined the effects of dimer formation on the ET rates and related physical quantities in the mutated FBP dimers.

#### 2. Methods

#### 2.1. ET analyses

The atomic coordinates of the four (E13K, E13R, E13R, E13Q) mutated FBP dimers obtained by MDS [23] were used for the ET rate calculation using the KM theory. Since the ET rates from Tyr35 were negligibly slow compared to those of Trps, only Trp32 and Trp106 were taken into account as ET donors [24]. The net electrostatic energies (NetES) between the photoproducts and ionic groups inside the proteins were computed and included in the ET rate calculation as expressed in Eq. (S1) in Supporting Materials (SM). The full procedures for the ET analyses along with their related parameters are described in SM.

#### 2.2. ET rates and related physical quantities

The original Marcus theory [25,26] of the ET rate has been modified in various ways [2,3,27–32]. In the present analysis, the KM rate [30–32] was used because it is applicable for non-adiabatic ET processes in addition to adiabatic processes, and has been found to provide satisfactory results for both static [15,33] and dynamic ET analyses [34–36]. FBP contains two Trps (Trp32 and Trp106) and one Tyr (Tyr35) in each subunit. The logarithmic ET rate (In Rate) may be decomposed into three terms as in Eq. (1).

$$\ln Rate = \ln EC + \ln SQ - GTLAM \tag{1}$$

Here.

$$\ln \text{Rate} = \ln k_M^{jk} \tag{2}$$

$$\ln EC = \ln \frac{v_0}{1 + \exp \left\{ \beta \left( R_{jk}^M - R_0 \right) \right\}}$$
 (3)

$$\ln SQ = \ln \sqrt{\frac{k_B T}{4\pi \lambda_{jk}^M}} \tag{4}$$

$$GTLAM = -\frac{\left\{GT\right\}^2}{4\lambda_{ik}^M k_B T} \tag{5}$$

The total free energy gap (GT) in Eq. (5) is expressed as Eq. (6).

$$GT = SFEG + ESDA + SROE + NetES$$
 (6)

Here, SFEG =  $\Delta G_M^0$ , ESDA =  $\frac{-e^2}{c_0^k R_{jk}^M}$ , SROE =  $\lambda_{jk}^M$ , and NetES =  $E_{Net}^{Mk}(j)$  (see below Eq. (S1) for the notations in the SM). Likewise, the quantity GP is defined by Eq. (7), which eliminates the NetES term from GT.

$$GP = SFEG + ESDA + SROE \tag{7}$$

#### 3. Results

#### 3.1. Theoretical fluorescence dynamics of mutated FBP dimers

Fig. S1 in the SM shows the MDS snapshots of the four mutated FBP dimers, where FMN, Trp32 and amino acids at position 13 are indicated with one letter notations for the amino acids in addition

to the peptide backbone [23]. The mean values of Rc over 10,000 snapshots are listed in Table S1 in the SM. The Rc values of Trp32 were 1.19 nm and 1.22 nm in Sub A and in Sub B of E13K; 1.20 nm in both Sub A and Sub B of E13R; 0.89 nm in both Sub A and Sub B of E13T; 1.11 nm in Sub A and 1.13 nm in Sub B of E13Q; and 0.70 and 0.99 nm in Sub A and Sub B of WT [23]. In the crystal structure, the Rc values were always shorter than those from solution.

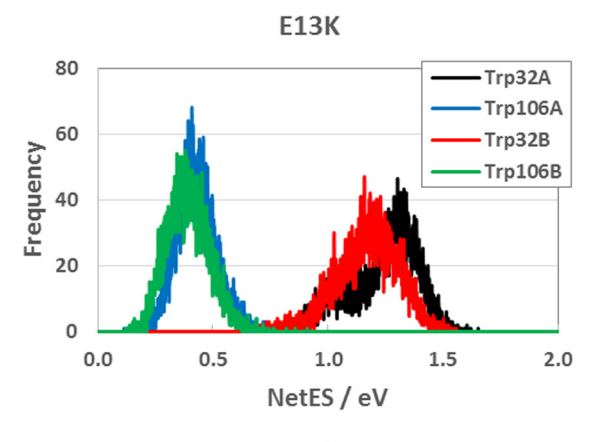
The reported experimental fluorescence lifetimes of the wild-type and four mutated FBP dimers are listed in Table S2 in the SM [22]. The experimental and theoretical fluorescence decays are shown in Fig. S2 (SM). The deviations between the two decays (see Eq. (S9) in the SM) are illustrated in the upper panels of the decays. The agreement between the experimental and calculated decays in all FBP dimers was much better than those with the FBP monomers [20]. The best-fit ET parameters together with the chi-squared values are also listed in Table S3 (SM).

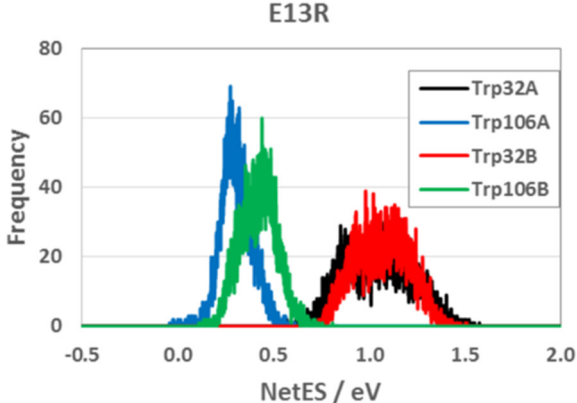
#### 3.2. Dynamics and distributions of NetES

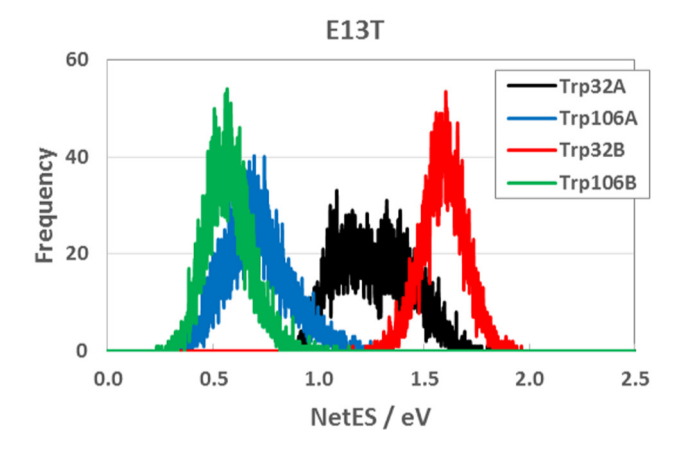
The time-evolutions of NetES are shown in Fig. S3 in the SM. In E13K, the NetES fluctuated within 0.7–1.5 eV in Trp32 and 0.2–0.6 eV in Trp106. In E13R, the NetES varied in the ranges of 0.6–1.5 eV in Trp32 and 0–0.7 eV in Trp106. In E13T, the values varied in the ranges of 0.9–1.9 eV in Trp32 and 0.3–1.2 eV in Trp106. In E13Q, the values varied in the ranges of 0.6–1.7 eV in Trp32 and 0.3–1.7 eV. The values of NetES in the WT fluctuated around 0.05–0.4 eV with time [24].

The distributions of the NetES are shown in Fig. 1. In E13K, the distribution of Trp32KA (Trp32 in Sub A of E13K dimer) displayed double maxima with a minor peak at ca. 1.0 eV. In both Trp32KB (Trp32 in Sub B of E13K) and Trp106KB (Trp106 in Sub B of E13K) the distributions were not symmetric along with Rc. The distribution of Trp32RA (Trp32 in Sub A of E13R) also displayed broad and double maxima at ca. 1.0 and 1.3 eV, though it was not as clear as Trp32KA. The distribution of Trp32RB (Trp32 in Sub B of E13R) was also broad with a single peak. The distributions of Trp106RA (Trp106 in Sub A of E13R) and Trp106RB (Trp106 in Sub B of E13R) displayed relatively sharp peaks at around 0.3 and 0.5 eV. The distributions in E13T displayed double maxima at ca.1.2 and 1.4 eV in Trp32TA (Trp32 in Sub A of E13T) and a single peak at ca. 1.7 eV in Trp32 TB (Trp32 in Sub B of E13T). The distributions in Trp32QB (Trp32 in Sub B of E13Q) displayed clear double peaks at around 0.9 and 1.3 eV, while Trp32QA (Trp32 in Sub A of E13Q) showed a single peak. In the WT, the distributions display almost symmetrical single peaks, including Trp106WTB (Trp106 in Sub B of WT) where the Rc values displayed a discontinuous change at around 15 ns of MDS time [24].

The mean values of NetES are listed in Table 1. The values in E13K were 1.24 and 1.17 eV in Trp32KA and Trp32KB as well as 0.43 and 0.39 eV in Trp106KA and Trp106KB, respectively. The values in E13R were 1.05 and 1.07 eV in Trp32RA and Trp32RB as well as 0.31 and 0.42 eV in Trp106RA and Trp106RB. The values in E13T were 1.26 and 1.59 eV in Trp32TA and Trp32TB as well as 0.70 and 0.57 eV in Trp106TA and Trp106 TB. The values in E13Q were 1.32 and 1.08 eV in Trp32QA and Trp32QB as well as 0.55 and 0.46 eV in Trp106QA and Trp106QB. The average values of Trp32WTA (Trp32 in Sub A of WT) and Trp32WTB (Trp32 in Sub B of WT) were 0.22 eV, and that of Trp106WTA (Trp106 in Sub A of WT) and Trp106WTB was 0.16 eV in the WT with a negative charge of Glu13. In E13K and E13R with a positive charge at amino acid-13, the average value among Trp32KA, Trp32KB, Trp32RA and Trp32RB was 1.13 eV, and that of Trp106KA, Trp106KB, Trp106RA and Trp106RB was 0.39 eV. In E13T and E13Q with neutral charge at amino acid-13, the average value among the four Trp32 residues was 1.31 eV and the average value among the four Trp106 residues







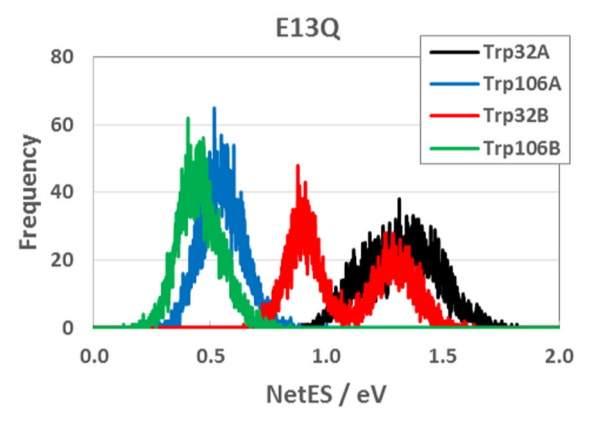


**Fig. 1.** Distribution of NetES in the FBP dimers. The NetES is given by Eq. (S5) in SM. Trp32A, Trp32B, Trp106A and Trp106B denote Trp32 in Sub A and Sub B, and Trp106 in Sub A and Sub B, respectively.

was 0.57 eV. In both Trp32 and Trp106, the average values of NetES were the least in the WT and the greatest in E13T and E13Q with the neutral charge while the second was in E13K and E13R with the positive charge. In the WT dimer, the values were 0.2 eV in Trp32A, 0.23 eV in Trp32B, 0.14 eV in Trp106A and 0.18 eV in Trp106B [24].

#### 3.3. Mean values of SROE and ESDA over MDS times

The mean values of SROE and ESDA are also listed in Table 1. These values did not vary much among the FBP dimers and subunits. The values of SROE were always lower in Trp32 compared to Trp106 because of the shorter donor-acceptor distances in Trp32. The ESDA also depended on the Rc as SROE. The variations in ESDA were not as remarkable as those in NetES. The values of ESDA were always lower in Trp32 than those in Trp106 because of the shorter Rc in Trp32 than that in Trp106, as in SROE.

#### 3.4. ET rates

Time-evolutions of the ln Rate are shown in Fig. S4 in the SM. In every mutated FBP dimer, the values of the In Rate in Trp106 greatly fluctuated with time, but not so much in Trp32. Fig. 2 shows the distributions of the In Rate. The In Rate values at the peak distributions of Trp32 were always greater than those of Trp106 in the mutated FBP dimers, where the Rc of Trp32 was always shorter than that of Trp106. All rates display an upperlimit because of the GTLAM terms, which always are negative and reduce the rates. The mean values of the ET rates over all snapshots are listed in Table 1. In E13K, the ET rates of Trp32KA and Trp32KB were 9.17 and  $8.58 \text{ ps}^{-1}$ , while they were 0.30 and 0.12 ps<sup>-1</sup> in Trp106KA and Trp106KB. In E13R, the ET rates of Trp32RA and Trp32RB were 8.31 and 9.21 ps<sup>-1</sup>, while they were 0.16 and 0.37 ps<sup>-1</sup> in Trp106AR and Trp106RB. In E13T, the ET rates of Trp32TA and Trp32 TB were 5.48 and 11.0 ps<sup>-1</sup>, while they were 0.48 and 0.03 ps<sup>-1</sup> in Trp106TA and Trp106 TB. In E13Q, the ET rates of Trp32QA and Trp32QB were 8.61 and 6.60 ps<sup>-1</sup>, while they were 1.17 and 0.32 ps<sup>-1</sup> in Trp106QA and Trp106QB. For the WT FBP dimer, the ET rates and related physical quantities are shown in Table 1 for comparison [24].

#### 3.5. Dependence of NetES on Rc

Fig. S5 in the SM shows the relationship of NetES vs Rc for some donors, which were not uniform. The relations in Trp32KA and Trp32KB seemed to display two groups of NetES at higher and lower parts, as shown in the top and second panels. The distinction of the NetES into two groups was more pronounced in Trp32KB than in Trp32KA.

The correlation was not clear between the NetES vs Rc relation (Fig. S5) and the distribution of the NetES with time (Fig. 1). The distributions of Trp32KA, Trp32RA, Trp32TA and Trp32QB displayed double maxima (Fig. 1). However, the NetES vs Rc relationship did not show much heterogeneity with Trp32KA, Trp32RA and Trp32TA. The distribution of NetES in Trp32KA displayed clear double maxima, but the heterogeneity in the NetES vs Rc relation was not as pronounced as in the second panel of Fig. S5. Further the distribution in Trp32QB did not show any double maxima, but the NetES and Rc relation displayed two distinct groups as in the bottom panel of Fig. S5, though its distribution was broad. In Trp32QB the distribution of NetES displayed clear double maxima, and the NetES vs Rc relation also displayed two distinct groups.

**Table 1** ET rate and related physical quantity<sup>a</sup>.

FBP	Donor	Subunit	ET rate <sup>b</sup> (ps <sup>-1</sup> )	SROE <sup>c</sup> (eV)	ESDA <sup>d</sup> (eV)	NetES <sup>e</sup> (eV)	GP <sup>f</sup> (eV)
E13K	Trp32	Α	9.17	0.65	-0.74	1.24	-1.21
		В	8.58	0.61	-0.79	1.17	-1.29
		Monomer <sup>g</sup>	14.0	0.468	-0.830	0.268	-0.528
	Trp106	Α	0.30	0.72	-0.55	0.43	-0.94
		В	0.12	0.69	-0.55	0.39	-0.98
		Monomer <sup>g</sup>	$2.86 \times 10^{-4}$	0.518	-0.621	-0.472	-0.269
E13R	Trp32	Α	8.31	0.66	-0.72	1.05	-1.11
		В	9.21	0.63	-0.73	1.07	-1.15
		Monomer <sup>g</sup>	11.5	0.457	-0.875	0.306	-0.113
	Trp106	A	0.16	0.72	-0.56	0.31	-0.88
		В	0.37	0.70	-0.53	0.42	-0.88
		Monomer <sup>g</sup>	$2.27\times10^{-3}$	0.518	-0.623	-0.347	0.200
E13T	Trp32	Α	5.48	0.65	-0.75	1.26	-1.51
		В	11.0	0.62	-0.77	1.59	-1.56
		Monomer <sup>g</sup>	9.77	0.474	-0.803	0.822	-0.749
	Trp106	Α	0.48	0.72	-0.55	0.70	-1.24
		В	0.03	0.70	-0.55	0.57	-1.27
		Monomer <sup>g</sup>	$5.07\times10^{-7}$	0.515	-0.636	-0.949	-0.541
E13Q	Trp32	Α	8.61	0.65	-0.75	1.32	-1.21
		В	6.60	0.62	-0.77	1.08	-1.26
		Monomer <sup>g</sup>	7.05	0.481	-0.777	0.873	-0.776
	Trp106	Α	1.17	0.72	-0.55	0.55	-0.93
		В	0.32	0.69	-0.55	0.46	-0.96
		Monomer <sup>g</sup>	$9.70\times10^{-8}$	0.519	-0.619	-0.846	-0.580

<sup>&</sup>lt;sup>a</sup> ET rates and related physical quantities were obtained with the best-fit ET parameters listed in Table SIII in SM. The mean values are listed over 10,000 snapshots with 2 ps intervals.

#### 3.6. Dependence of ln Rate on Rc

The linear relation of the ln Rate with Rc is called the Dutton rule [2], which was experimentally demonstrated in photosynthetic proteins. Fig. 3 shows the relationships of the ln Rate and Rc in FBP dimers in some donors. In any donors in this figure, the relationships of ln Rate and Rc were not linear nor simply parabolic [19,36,37]. In these donors, the mean values of NetES were quite great, and further, the NetES vs Rc relation displayed at least two distinct groups. The ln Rate in these donors exhibited much more complicated functions of Rc, which are ascribed to heterogeneity in the NetES vs Rc relations, as shown in Fig. S5 in the SM.

#### 3.7. Relative magnitude of GP and NetES

The mean values of the GP as defined by Eq. (7) are listed in Table 1. When the NetES was not negligible compared to the GP, the ET rates were strongly dependent on NetES. The relations of the In Rate vs Rc in FBP dimers were very much influenced by the NetES vs Rc relations. The mean values of GP in Trp32A were -1.21 in E13K, -1.11 in E13R, -1.51 in E13T and -1.21 eV in E13Q. The values of GP in Trp32B were -1.29 in E13K, -1.15 in E13R, -1.56 in E13T and -1.26 eV in E13Q. The values did not differ much between Trp32A and Trp32B in all the dimers. The values of GP in Trp106A were -0.94 in E13K, -0.88 in E13R, -1.24 in E13T and -0.93 eV in E13Q. The values of GP in Trp106B were -0.98 in E13K, -0.88 in E13R, -1.27 in E13T and -0.96 eV in E13Q. In the WT, the absolute values of the GP are higher than those of NetES in all donors [24]. However, the absolute values of the GP were comparable or lower than those of NetES in any donors in E13K, E13R, E13T and E13Q.

#### 3.8. Comparison of NetES and ET rates between dimer and monomer

The ET rates and related quantities for the FBP monomer are listed in Table 1 for comparison. The data in Table 1 for the monomers were revised from the reported values [19,20] where the  $G_M^0$ is given by Eq. (S3) in the SM and was common in all FBP monomers, and different among the dimers in the present work [24]. Using different values of  $G_M^0$  for each dimer, the fittings between the experimental and calculated decays were much improved [24]. The values of NetES remarkably increased in the dimers compared to those in the monomers. This should be ascribed to the formation of the dimer, and thus the NetES of a donor in Sub A was influenced by the ionic groups in Sub B, and vice versa. In the monomers, the absolute values of NetES were always smaller than GP (Table 1), while those in the dimers were not negligible compared to the GP. The ET rates of Trp106 in the dimers increased more than 1000 times compared to those of the corresponding monomers, while the rates of Trp32 in any dimers did not differ much from those in the monomers.

#### 3.9. Separation of NetES and In Rate into two groups

Fig. 4 shows two groups of NetES vs Rc and ln Rate vs Rc relations in Trp32KB. The NetES and Rc relation was separated with a straight line determined by the coordinates (Rc = 0.596 nm, NetE-S = 0.776 eV) and (Rc = 0.801 nm, NetES = 1.25 eV). The upper group denotes an ensemble of the NetES data above this straight line and lower group below the straight line. The top panel of Fig. 4 shows the relationship of NetES and Rc in the upper group. The values of NetES displayed a tendency to increase with Rc, though the data scattered a lot. The approximate linear function

<sup>&</sup>lt;sup>b</sup> ET rate given by Eq. (S1) in SM.

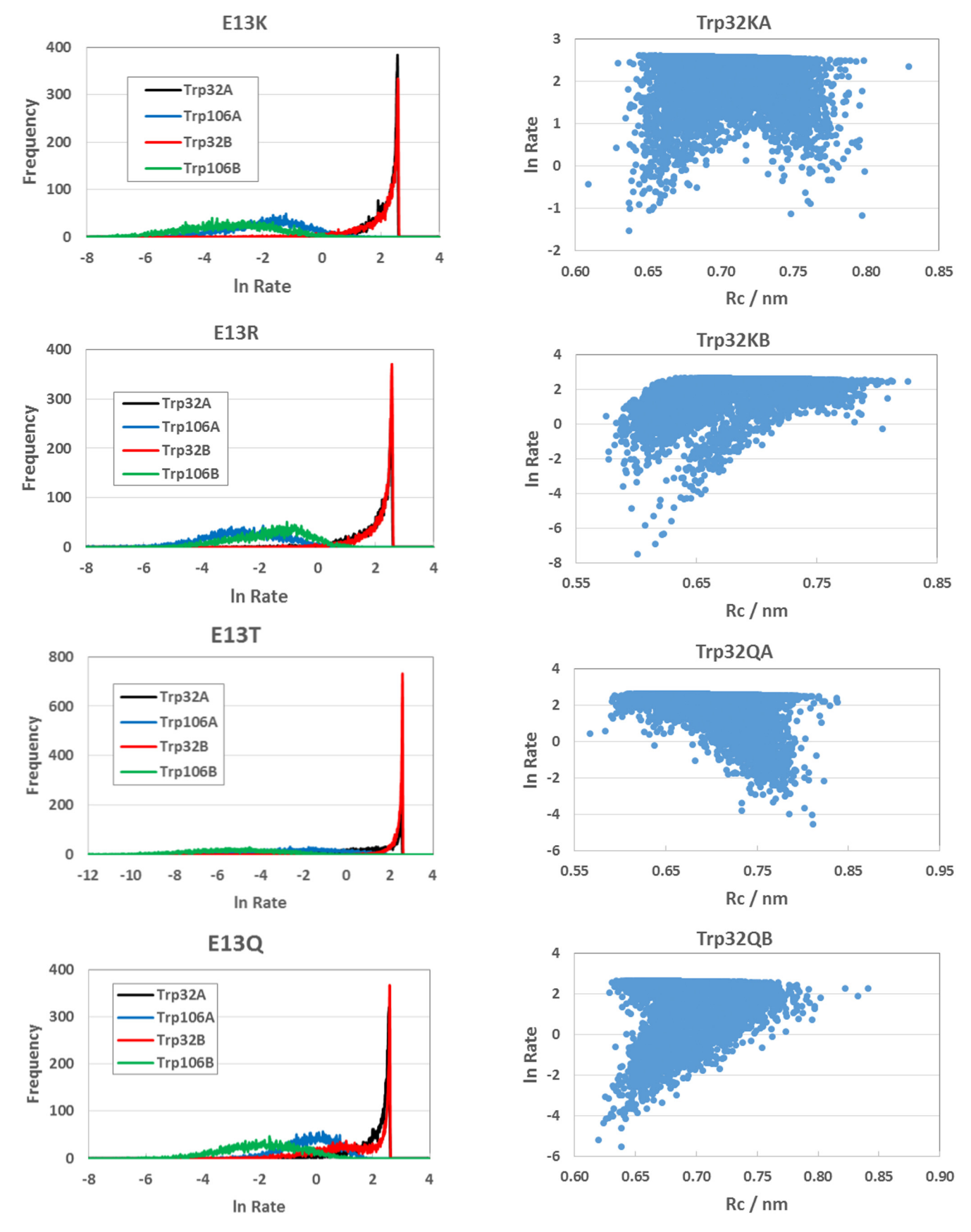
Solvent reorganization energy given by Eq. (S2) in SM.

<sup>&</sup>lt;sup>d</sup> ES energy between photo-products, ESDA =  $-e^2/\varepsilon_0^k R_{ik}^M$  in Eq. (S1) in SM.

e Net ES energy given by Eq. (S5) in SM.

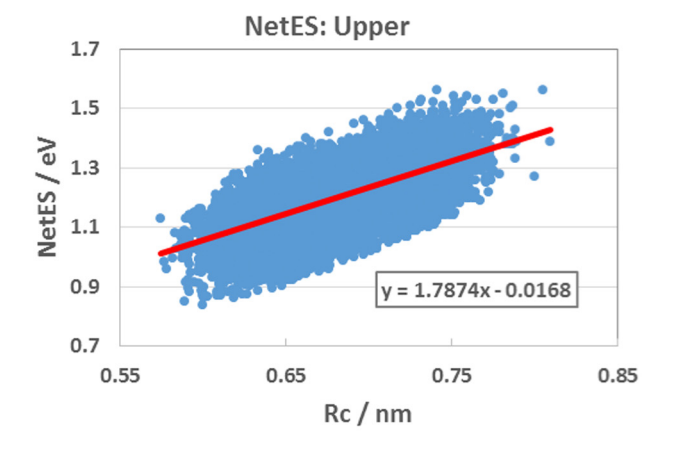
f GP is defined by Eq. (7) in text.

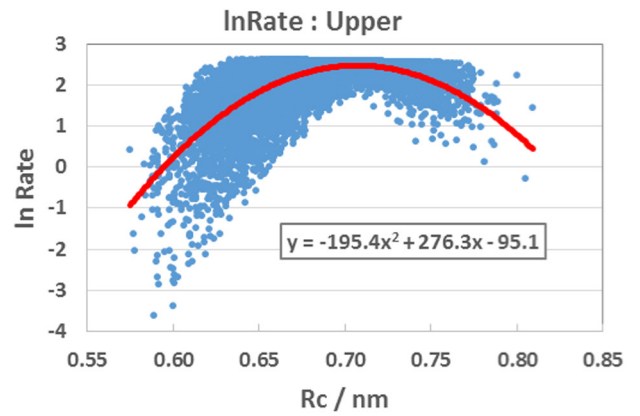
g Data for Monomer were obtained with the same method as for the dimers [24].

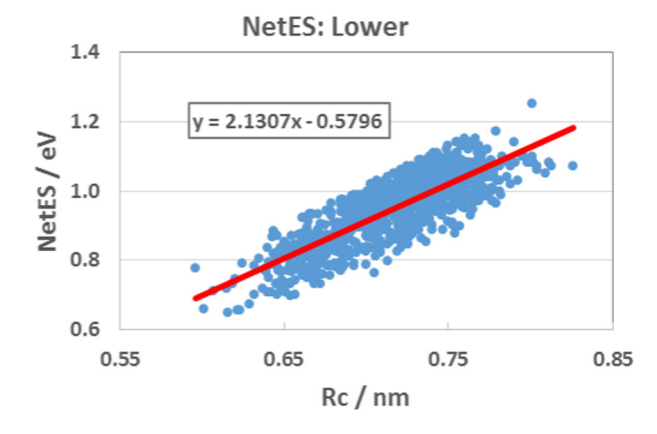


**Fig. 2.** Distribution of logarithmic ET rate. The ln Rate denotes logarithmic ET rate, which was obtained by Eq. (S1) in SM. Trp32A and Trp32B in inserts denote Trp32 in Sub A and Sub B respectively. ET rates are expressed in  $ps^{-1}$  unit.

**Fig. 3.** Relationships between In Rate and Rc in Trp32KA, Trp32KB, Trp32QA and Trp32QB. The values of In Rate were obtained by Eq. (1) in text with ET parameters listed in Table S3 in SM. Trp32KA, Trp32KB, Trp32QA and Trp32QB denote Trp32 in Sub A and Sub of E13K, and Trp32 in Sub A and Sub B of E13Q, respectively.







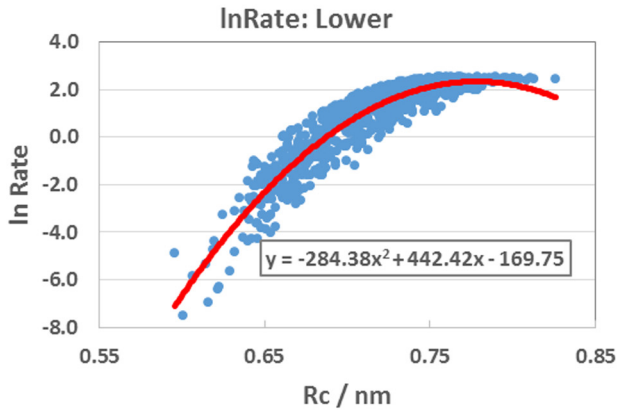


**Fig. 4.** Separation of NetES and In Rate into two components in Trp32KB. Inserts show approximate functions of NetES or In Rate (y) with Rc (x). The data of NetES in Fig. S5 in SM were divided with a straight line determined by Rc = 0.569 nm and NetES = 0.776 eV, and Rc = 0.801 nm and NetES = 1.25 eV. Upper and Lower denote upper and lower groups of the NetES above and below the straight line.

was y = 1.787 x - 0.017 (y, NetES; x, Rc). The second panel shows the ln Rate vs Rc relation in the upper group. The values of the ln Rate displayed an approximate parabolic function,  $y = -195.4 \text{ x}^2 + 276.3 \text{ x} - 95.1$ . The third panel shows the relationship of NetES vs Rc in the lower group. The values of NetES increased with Rc, for which the approximate function was y = 2.131 x - 0.580. The slope of the NetES vs Rc functions was y = 2.131 x - 0.580. The slope of the upper group. The relationship of ln Rate ys Rc in the lower group displayed a parabolic function,  $y = -284.4 \text{ x}^2 + 442.4 \text{ x} - 169.8$ , in which the data were less scattered when compared to those in the upper group.

Fig. 5 shows the relations of NetES vs Rc and ln Rate vs Rc in Trp32QA. The top panel shows the dependence of NetES on Rc. The values of NetES linearly increased with Rc, for which the approximate function was y = 2.040 x - 0.039. The second panel shows the ln Rate and Rc relation in the upper group. The values of the ln Rate changed with an approximate parabolic function,  $y = -191 \text{ x}^2 + 248 \text{ x} - 77.9$ . The third panel shows the NetES vs Rc relation in the lower group, for which the values of NetES increased with a linear function of Rc, y = 0.838 x + 0.534. The slope of the linear function was 0.84 in the lower group, while it was 2.04 in the upper group. The bottom panel shows the ln Rate vs Rc relation in the lower group. The approximate function was  $-81.9 \text{ x}^2 + 121 \text{ x} - 42.2$ .

Fig. 6 shows the relations in Trp32QB. The NetES vs Rc relation in the upper group shown in the top panel approximately increased with a linear function of Rc,  $y = 1.36 \times + 0.36$ , though the linearity was much poorer than the other donors. The ln Rate vs Rc relation is shown in the second panel. The ln Rate values were more scattered with the Rc. The values of the ln Rate were approximated with a parabolic function of Rc,  $y = -127 \times^2 + 171 \times -55.3$ . The NetES and Rc relation in the lower group is shown in the third panel. The values of NetES were more scattered with Rc, as in the upper group. The approximate function of NetES with Rc was  $y = 1.06 \times + 0.16$ . The bottom panel shows the ln Rate and Rc in the lower group. The approximate function of the ln Rate with Rc was  $y = -233 \times^2 + 358 \times -136$ .

The complex profiles of the ln Rate vs Rc relationship became much clearer when the NetESs were separated into two groups. This suggests that the proteins hold at least two conformations, which were especially clear in Sub B of E13K and in both Sub A and Sub B of E13Q. The heterogeneity in Sub B of E13K and in the Sub A and Sub B of E13Q are considered to be brought about by conformational changes in the entire proteins, because NetES is related to all charged groups inside the dimer proteins.

#### 4. Discussion

The donor-acceptor distance is one of the most important index determining ET rates not only in flavoproteins [19,36,37], but also in ET phenomena in general [2]. The ET mechanism from aromatic amino acids to Iso\* in flavoproteins has been categorized into four groups with sub-groups of adiabatic and non-adiabatic processes, through the relationship of the In Rate and Rc [37]. The criteria of the classification were the relative magnitudes of NetES against GP. When the absolute value of the GP is greater than that of NetES, the In Rate displays a clear parabolic or linear function of Rc. When the NetES is dominant compared to the GP, the In Rate *vs* Rc does not display any clear function. It was believed that NetES does not display any relations with Rc [19,37]. The present work, however, has demonstrated that sometimes the NetES displays a weak relation with Rc.

The dependencies of the ET rates, NetES, SROE and ESDA on Rc were examined for the donors of Trp32 and Trp106 in both subunits in the four mutated FBP dimers. Explicit relations between

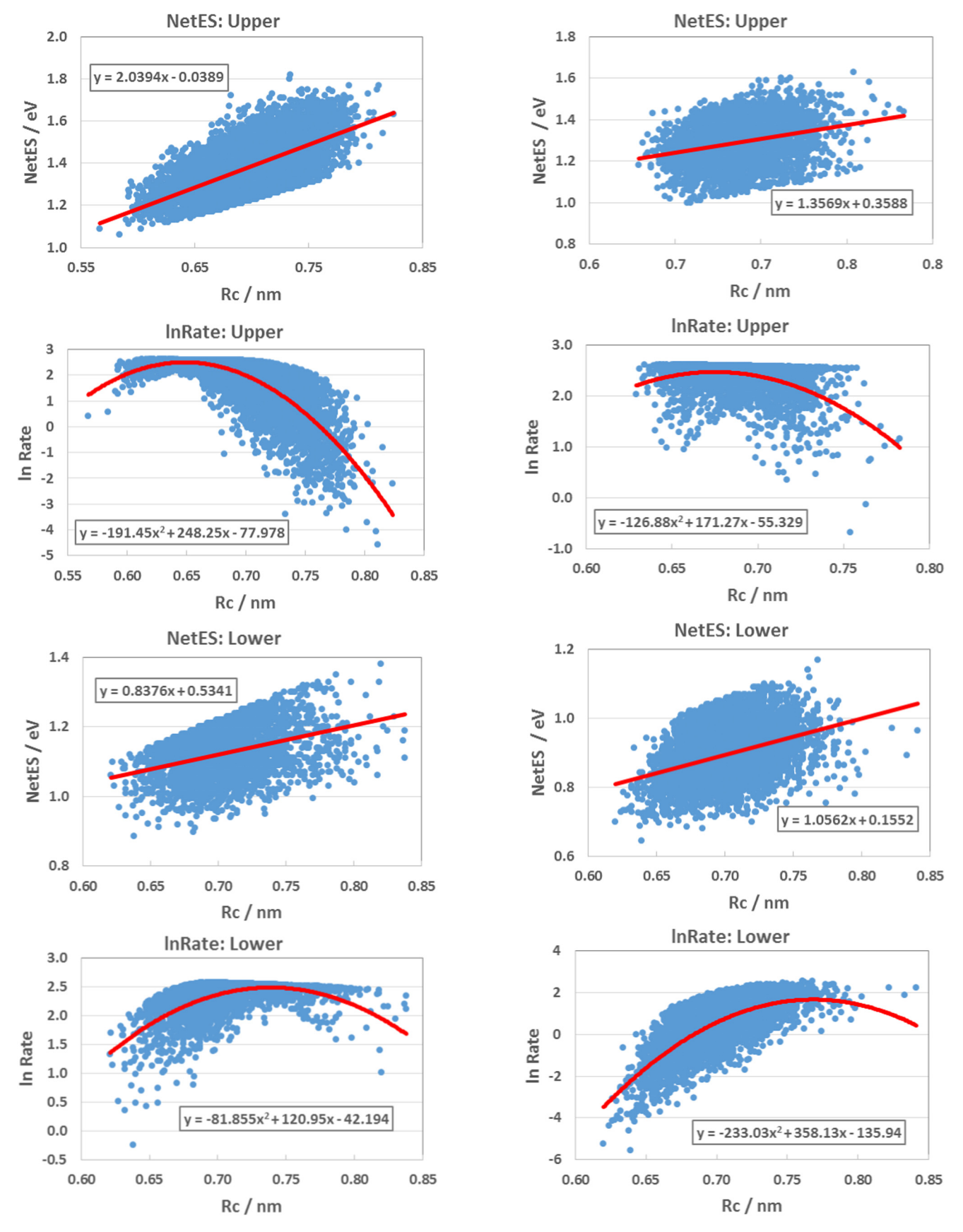


**Fig. 5.** Separation of NetES and In Rate into two components in Trp32QA. Inserts show approximate functions of NetES or In Rate (y) with Rc (x). The NetES data in Fig. S5 in SM were divided with a straight line determined by Rc = 0.622 nm and NetES = 1.10 eV, and Rc = 0.798 nm and NetES = 1.33 eV. Upper and Lower denote the data above and below the line.

**Fig. 6.** Separation of NetES and In Rate into two groups in Trp32QB. Inserts show approximate functions of NetES or In Rate (y) with Rc (x). The NetES data in Fig. S5 in SM were divided by a straight line determined with Rc = 0.647 nm and NetES = 1.02 eV, and Rc = 0.768 nm and NetES = 1.17 nm. Upper and Lower denote the data above and below the line.

the ET rate and Rc were given for SROE and ESDA in Marcus [2,25,26] and KM rates [37], but not for NetES. In FBP dimers other than the WT, the absolute values of NetES were quite large and comparable to or even greater than those of the GP, as shown in Table 1. In the WT, the most remarkable difference between the dimer and monomer was SFEG [24], while the values of NetES were not so much different between the WT dimer and monomer in Trp32 as in the mutated FBP dimers. The greater values of NetES were ascribed to the formation of a dimer, in which the NetES of a donor in Sub A is influenced by Sub B, and vice versa as in the d-amino acid oxidase dimer [38,39] and pyranose 2-oxidase tetramer [36]. In some cases, the ln Rate vs Rc relations were determined by the NetES and Rc relations as in Trp32KB, Trp32OA and Trp32QB. In these donors, the values of NetES could be divided into two groups, and accordingly the ln Rate and Rc relation displayed two kinds of profile.

It is believed that the NetES is a useful index for the detection of conformational changes in the entire protein. The two groups in the NetES of Trp32KB, Trp32QA and Trp32QB could be due to two different conformations of the entire subunits. Similar behaviors for the NetES vs Rc relation were also found in other donors, though they were not so clear as in Trp32KB, Trp32QA and Trp32QB. The conformational change revealed that Trp106B of the WT FBP dimer may be local [23,24] because it is brought about by a discontinuous change in the Rc. The relationship between the heterogeneous distribution of the NetES and heterogeneity in the NetES vs Rc relation is of interest, though it is not clear at the moment.

Recently, Ivanov's group has reported theoretical work on the ET rate in small molecules, and they emphasized the importance of a solvent reorganization from high-frequency vibrational modes and dynamical solvent effect on the ET rate [40], based on Zusman's ET theory [27]. In flavoproteins the medium surrounding the ET donors and accepter is not uniform, as in a bulk solution. The terms of SROE plus NetES in the present systems are considered to correspond to the solvent reorganization energy in the ET processes in a bulk solution. Accordingly, the dynamic solvent effect is already taken into account through the time-dependent changes of Rc and the NetES. In flavoproteins, the ET takes place from Trp or Tyr in the ground state to Iso\*, so the population of the vibrational modes should be mostly in the lowest vibrational-energy level at room temperature. It is conceivable that the ET takes place from the donors in the ground states to higher vibration states of Iso\*. The effects of the higher vibrational modes on the ET rate have been already reported by Bixon and Jortner (BJ theory) [28]. In our earlier work [41], the non-exponential fluorescence decay of the WT was analyzed with the Marcus and Huch (MH) theory [2], BJ theory [3,28,29] and KM theory [30], and the values of  $\chi^2$  between the experimental and calculated decays were compared among these theories. The values of  $\chi^2$  were 1.83  $\times$   $10^{-4}$ with the MH theory,  $4.31 \times 10^{-4}$  with the BJ theory and  $1.47 \times 10^{-4}$  with the KM theory. The vibrational relaxation from the higher states to the fluorescent state in Iso\* in flavoproteins should be much faster than the solvent relaxation time of the amino acids near to the donors and acceptor, which is because the amino acids are covalently linked by peptide bonds, and further free water molecules do not exist near Iso in FBP dimers, as in other flavoenzymes [23,24].

Currently, satisfactory results on the ET phenomena in flavoproteins have been obtained with the present method with relation to the following points: (1) the structure of each subunit is not equivalent: the flavoproteins consist of two subunits in a complex dimer of d-amino acid oxidase with benzoate [39] or four subunits in pyranose 2-oxidase [36], which have been verified by the experimental fluorescence dynamics [11,42,43]. (2) A temperature

induced transition of the protein structure in d-amino acid oxidase, as experimentally found in earlier work [44–46], was satisfactorily elucidated with ET parameters [33]. (3) The static dielectric constants near ET donors and acceptor obtained by the present method have been elucidated with the presence of water molecules near Iso obtained by MDS as discussed in previous work [23,24]. (4) The Dutton rule [2] has been demonstrated in the ET processes with relatively slow rates in FBP [19,37] and d-amino acid oxidase dimer [38].

#### 5. Conclusions

The NetES energies in the four mutated FBP isomers with respect to the charged amino acids at 13 locations were dominant among the terms in the total free energy gap, so the ln Rate vs Rc relations were strongly dependent on the NetES. In Trp32KB, Trp32QA and Trp32QB, the ln Rate vs Rc profiles were separated into two groups, which are thought to have been brought about by conformational changes in the entire FBP dimers.

#### Acknowledgements

N.N. would like to acknowledge financial support from the Thailand Research Fund (MRG5380255) and the Center of Excellence for Innovation in Chemistry (PERCH-CIC), Office of the Higher Education Commission, Ministry of Education. F.T. is thankful for financial support from the Ratchadaphiseksomphot Endowment Fund of Chulalongkorn University and a short-term visit grant from Chulalongkorn University. S.T. was also supported by the Japan Society for the Promotion of Science (Grant-in-Aid for Scientific Research No. 26410029). Thanks also to The National e-Science Infrastructure Consortium Project for computing facilities.

#### Appendix A. Supplementary material

Supplementary data associated with this article can be found, in the online version, at http://dx.doi.org/10.1016/j.comptc.2017.03.005.

#### References

- [1] R.A. Marcus, N. Sutin, Electron transfers in chemistry and biology, Biochim. Biophys. Acta 811 (1985) 265–322.
- [2] C.C. Moser, J.M. Keske, K. Warncke, R.S. Farid, P.L. Dutton, Nature of biological electron transfer, Nature 355 (1992) 796–802.
- [3] M. Bixon, J. Jortner, Electron transfer-from isolated molecules to biomolecules, Advances in Chemical Physics, John Wiley & Sons Inc, 1999, pp. 35–202.
- [4] D.N. Silverman, Marcus rate theory applied to enzymatic proton transfer, Biochim. Biophys. Acta 1458 (2000) 88–103.
- [5] N. Mataga, H. Chosrowjan, S. Taniguchi, Ultrafast charge transfer in excited electronic states and investigations into fundamental problems of exciplex chemistry: our early studies and recent developments, J. Photochem. Photobiol., C 6 (2005) 37–79.
- [6] C. Sengupta, M.K. Sarangi, A. Sau, D. Mandal, S. Basu, A case study of photo induced electron transfer between aliphatic amine: deciphering different mechanisms from femtosecond to microsecond time domain, J. Photochem. Photobiol., A 296 (2015) 25–34.
- [7] A. Karen, N. Ikeda, N. Mataga, F. Tanaka, Picosecond laser photolysis studies of fluorescence quenching mechanisms of flavin: a direct observation of indoleflavin singlet charge transfer state formation in solutions and flavoenzymes, Photochem. Photobiol. 37 (1983) 495–502.
- [8] A. Karen, M.T. Sawada, F. Tanaka, N. Mataga, Dynamics of excited flavoproteins-picosecond laser photolysis studies, Photochem. Photobiol. 45 (1987) 49–53.
- [9] D. Zhong, A.H. Zewail, Femtosecond dynamics of flavoproteins: charge separation and recombination in riboflavine (vitamin B2)-binding protein and in glucose oxidase enzyme, Proc. Natl. Acad. Sci. U.S.A. 98 (2001) 11867– 11872
- [10] N. Mataga, H. Chosrowjan, Y. Shibata, F. Tanaka, Ultrafast fluorescence quenching dynamics of flavin chromophores in protein nanospace, J. Phys. Chem. B 102 (1998) 7081–7084.

- [11] N. Mataga, H. Chosrowjan, Y. Shibata, F. Tanaka, Y. Nishina, K. Shiga, Dynamics and mechanisms of ultrafast fluorescence quenching reactions of flavin chromophores in protein nanospace, J. Phys. Chem. B 104 (2000) 10667– 10677
- [12] N. Mataga, H. Chosrowjan, S. Taniguchi, F. Tanaka, N. Kido, M. Kitamura, Femtosecond fluorescence dynamics of flavoproteins: comparative studies on flavodoxin, its site-directed mutants, and riboflavin binding protein regarding ultrafast electron transfer in protein nanospaces, J. Phys. Chem. B 106 (2002) 8917–8920.
- [13] H. Chosrowjan, S. Taniguchi, N. Mataga, F. Tanaka, D. Todoroki, M. Kitamura, Comparison between ultrafast fluorescence dynamics of fmn binding protein from *Desulfovibrio vulgaris*, strain miyazaki, in solution vs crystal phases, J. Phys. Chem. B 111 (2007) 8695–8697.
- [14] H. Chosrowjan, S. Taniguchi, N. Mataga, F. Tanaka, D. Todoroki, M. Kitamura, Ultrafast fluorescence dynamics of FMN-binding protein from *Desulfovibrio vulgaris* (Miyazaki F) and its site-directed mutated proteins, Chem. Phys. Lett. 462 (2008) 121–124.
- [15] H. Chosrowjan, S. Taniguchi, N. Mataga, T. Nakanishi, Y. Haruyama, S. Sato, M. Kitamura, F. Tanaka, Effects of the disappearance of one charge on ultrafast fluorescence dynamics of the FMN binding protein, J. Phys. Chem. B 114 (2010) 6175–6182.
- [16] M. Kitamura, S. Kojima, K. Ogasawara, T. Nakaya, T. Sagara, K. Niki, K. Miura, H. Akutsu, I. Kumagai, Novel FMN-binding protein from *Desulfovibrio vulgaris* (Miyazaki F). Cloning and expression of its gene in Escherichia coli, J. Biol. Chem. 269 (1994) 5566–5573.
- [17] E. Liepinsh, M. Kitamura, T. Murakami, T. Nakaya, G. Otting, Pathway of chymotrypsin evolution suggested by the structure of the FMN-binding protein from Desulfovibrio vulgaris (Miyazaki F), Nat. Struct. Biol. 4 (1997) 975-979
- [18] K. Suto, K. Kawagoe, N. Shibata, Y. Morimoto, Y. Higuchi, M. Kitamura, T. Nakaya, N. Yasuoka, How do the X-ray structure and the NMR structure of FMN-binding protein differ?, Acta Crystallogr Sect. D Biol. Crystallogr. 56 (2000) 368–371.
- [19] N. Nunthaboot, K. Lugsanangarm, S. Pianwanit, S. Kokpol, F. Tanaka, S. Taniguchi, H. Chosrowjan, T. Nakanishi, M. Kitamura, Bell-shaped dependence of the rate of ultrafast photoinduced electron transfer from aromatic amino acids to the excited flavin on the donor-acceptor distance in FMN binding proteins, Comput. Theor. Chem. 1030 (2014) 9–16.
- [20] N. Nunthaboot, K. Lugsanangarm, A. Nueangaudom, S. Pianwanit, S. Kokpol, F. Tanaka, Role of the electrostatic energy between the photo-products and ionic groups on the photoinduced electron transfer rates from aromatic amino acids to the excited flavin in five single-point substitution isoforms of the charged amino acid residue-13 in the FMN-binding protein, Mol. Sim. 41 (2015) 580-591
- [21] M. Kitamura, K. Terakawa, H. Inoue, T. Hayashida, K. Suto, Y. Morimoto, N. Yasuoka, N. Shibata, Y. Higuchi, Determination of the role of the Carboxylterminal leucine-122 in FMN-binding protein by mutational and structural analysis, J. Biochem. (Tokyo) 141 (2007) 459-468.
- [22] S. Taniguchi, H. Chosrowjan, F. Tanaka, T. Nakanishi, S. Sato, Y. Haruyama, M. Kitamura, A key factor for ultrafast rates of photoinduced electron transfer among five flavin mononucleotide binding proteins: effect of negative, positive, and neutral charges at residue 13 on the rate, Bull. Chem. Soc. Jpn. 86 (2013) 339–350.
- [23] N. Nunthaboot, K. Lugsanangarm, S. Pianwanit, S. Kokpol, F. Tanaka, T. Nakanishi, M. Kitamura, Conformational difference between two subunits in flavin mononucleotide binding protein dimers from Desulfovibrio vulgaris (MF): molecular dynamics simulation, Comput. Biol. Chem. 64 (2016) 113–125.
- [24] N. Nunthaboot, K. Lugsanangarm, A. Nueangaudom, S. Pianwanit, S. Kokpol, F. Tanaka, S. Taniguchi, H. Chosrowjan, T. Nakanishi, M. Kitamura, Photoinduced electron transfer from aromatic amino acids to the excited isoalloxazine in flavin mononucleotide binding protein. Is the rate in the inverted region of donor-acceptor distance not real?, J Photochem. Photobiol., A 326 (2016) 60–68
- [25] R.A. Marcus, On the theory of oxidation-reduction reactions involving electron transfer. I, J. Chem. Phys. 24 (1956) 966–978.
- [26] R.A. Marcus, Electrostatic free energy and other properties of states having nonequilibrium polarization. I, J. Chem. Phys. 24 (1956) 979–989.
- [27] L.D. Zusman, Outer-sphere electron transfer in polar solvents, Chem. Phys. 49 (1980) 295–304.
- [28] M. Bixon, J. Jortner, Non-Arrhenius temperature dependence of electron-transfer rates, J. Chem. Phys. 95 (1991) 1941–1944.

- [29] M. Bixon, J. Jortner, J. Cortes, H. Heitele, M.E. Michel-Beyerle, Energy gap law for nonradiative and radiative charge transfer in isolated and in solvated supermolecules, J. Chem. Phys. 98 (1994) 7289–7299.
- [30] T. Kakitani, N. Mataga, New energy gap laws for the charge separation process in the fluorescence quenching reaction and the charge recombination process of ion pairs produced in polar solvents, J. Chem. Phys. 89 (1985) 8–10.
- [31] A. Yoshimori, T. Kakitani, Y. Enomoto, N. Mataga, Shapes of the electron-transfer rate vs energy gap relations in polar solutions, J. Chem. Phys. 93 (1989) 8316–8323.
- [32] N. Matsuda, T. Kakitani, T. Denda, N. Mataga, Examination of the viability of the Collins-Kimball model and numerical calculation of the time-dependent energy gap law of photoinduced charge separation in polar solution, Chem. Phys. 190 (1995) 83–95.
- [33] A. Nueangaudom, K. Lugsanangarm, S. Pianwanit, S. Kokpol, N. Nunthaboot, F. Tanaka, Structural basis for the temperature-induced transition of d-amino acid oxidase from pig kidney revealed by molecular dynamic simulation and photo-induced electron transfer, Phys. Chem. Chem. Phys. 14 (2012) 2567–2578.
- [34] K. Lugsanangarm, S. Pianwanit, S. Kokpol, F. Tanaka, H. Chosrowjan, S. Taniguchi, N. Mataga, Photoinduced electron transfer in wild type and mutated flavodoxin from Desulfovibrio vulgaris, strain Miyazaki F.: energy gap law, J. Photochem. Photobiol., A 219 (2011) 32–41.
- [35] K. Lugsanangarm, S. Pianwanit, A. Nueangaudom, S. Kokpol, F. Tanakaa, N. Nunthaboot, K. Ogino, R. Takagi, T. Nakanishic, M. Kitamura, S. Taniguchi, H. Chosrowjan, Mechanism of photoinduced electron transfer from tyrosine to theexcited flavin in the flavodoxin from Helicobacter pylori. Acomparative study with the flavodoxin and flavin mononucleotidebinding protein from Desulfovibrio vulgaris (miyazaki f), J. Photochem. Photobiol., A 268 (2013) 58–66
- [36] K. Lugsanangarm, A. Nueangaudom, S. Kokpol, S. Pianwanit, N. Nunthaboot, F. Tanaka, S. Taniguchi, H. Chosrowjan, Heterogeneous subunit structures in the pyranose 2-oxidase homotetramer revealed by theoretical analysis of the rates of photoinduced electron transfer from a tryptophan to the excited flavin, J. Photochem. Photobiol., A 306 (2015) 66–79.
- [37] F. Tanaka, K. Lugsanangarm, N. Nunthaboot, A. Nueangaudom, S. Pianwanit, S. Kokpol, S. Taniguchi, H. Chosrowjan, Classification of the mechanisms of photoinduced electron transfer from aromatic amino acids to the excited flavins in flavoproteins, Phys. Chem. Chem. Phys. 17 (2015) 16813–16825.
- [38] A. Nueangaudom, K. Lugsanangarm, S. Pianwanit, S. Kokpol, N. Nunthaboot, F. Tanaka, Non-equivalent conformations of d-amino acid oxidase dimer from porcine kidney between the two subunits. Molecular dynamics simulation and photoinduced electron transfer, Phys. Chem. Chem. Phys. 16 (2014) 1930–1944.
- [39] A. Nueangaudom, K. Lugsanangarm, S. Pianwanit, S. Kokpol, N. Nunthaboot, F. Tanaka, S. Taniguchi, H. Chosrowjan, Theoretical analyses of the fluorescence lifetimes of the d-amino acid oxidase-benzoate complex dimer from porcine kidney: molecular dynamics simulation and photoinduced electron transfer, RSC Adv. 4 (2014) 54096–54108.
- [40] V.V. Yudanov, V.A. Mikhailova, A.I. Ivanov, Reorganization of intramolecular high frequency vibrational modes and dynamic solvent effect in electron transfer reactions, J. Phys. Chem. A 116 (2012) 4010–4019.
- [41] N. Nunthaboot, F. Tanaka, S. Kokpol, H. Chosrowjan, S. Taniguchi, N. Mataga, Simulation of ultrafast non-exponential fluorescence decay induced by electron transfer in FMN binding protein, J. Photochem. Photobiol., A 201 (2009) 191–196.
- [42] H. Chosrowjan, S. Taniguchi, T. Wongnate, J. Sucharitakul, P. Chaiyen, F. Tanaka, Conformational heterogeneity in pyranose 2-oxidase from Trametes multicolor revealed by ultrafast fluorescence dynamics, J. Photochem. Photobiol., A 234 (2012) 44–48.
- [43] S. Taniguchi, H. Chosrowjan, T. Wongnate, J. Sucharitakul, P. Chaiyen, F. Tanaka, Ultrafast fluorescence dynamics of flavin adenine dinucleotide in pyranose 2-oxidases variants and their complexes with acetate: conformational heterogeneity with different dielectric constants, J. Photochem. Photobiol., A 245 (2012) 33–42.
  [44] V. Massey, B. Curti, H. Ganther, A temperature-dependent conformational
- [44] V. Massey, B. Curti, H. Ganther, A temperature-dependent conformational change in d-amino acid oxidase and its effect on catalysis, J. Biol. Chem. 241 (1966) 2347–2357.
- [45] J.F. Koster, C. Veeger, The relation between temperature-inducible allosteric effects and the activation energies of amino-acid oxidases, Biochim. Biophys. Acta 167 (1968) 48–63.
- [46] K. Shiga, T. Shiga, The kinetic features of monomers and dimers in high- and low-temperature conformational states of d-amino acid oxidase, Biochim. Biophys. Acta 263 (1972) 294–303.

## A novel physical quantity of residue electrostatic energy in flavin mononucleotide binding protein dimer

Nadtanet Nunthaboot<sup>a\*</sup>, Arthit Nueangaudom<sup>b</sup>, Kiattisak Lugsanangarm<sup>c</sup>, Somsak Pianwanit<sup>b</sup>, Sirirat Kokpol<sup>b</sup>, Fumio Tanaka<sup>b,d</sup>

<sup>a</sup>Department of Chemistry and Center of Excellence for Innovation in Chemistry,
Faculty of Science, Mahasarakham University, Mahasarakham, 44150 Thailand
<sup>b</sup>Department of Chemistry, Faculty of Science, Chulalongkorn University, Bangkok
10330, Thailand

<sup>c</sup>Program of Chemistry, Faculty of Science and Technology, Bansomdej Chaopraya Rajabhat University, Bangkok 10600, Thailand

<sup>d</sup>Division of Laser Biochemistry, Institute for Laser Technology, Osaka 550-0004, Japan

Corresponding authors:

Nadtanet Nunthaboot:nadtanet.n@msu.ac.th, nadtanet@gmail.com

#### **Abstract**

Electrostatic (ES) energy of each residue was first time quantitatively evaluated in flavin mononucleotide binding protein (FBP). A residue electrostatic energy (RES) was obtained as the sum of ES energies between atoms in each residue and all other atoms in FBP dimer, using atomic coordinates obtained by molecular dynamic simulation (MDS). The ES is one of the most important energies among the interaction energies in a protein. It was judged from the RES which residues mainly contribute to stabilize the structure of each subunits and the binding energy between the two subunits were estimated. The RES of all residues in subunit A (Sub A) and subunit B (Sub B) were negative, even though the residues contain the net negative or positive charges. This reveals that ES energies of any residues contribute to stabilize the protein structure. The total binding ES energy over all residues among the subunits distributes between -0.2 to -1.2 eV (mean = -0.67 eV) with MDS time.

Keywords: Electrostatic energy; FMN, FBP; Protein stabilization